UNIVERSITY OF HELSINKI

Investigation of Atmospheric Gas-Phase Reactions Using Multireference Electronic Structure Methods

Vili-Taneli Salo

University of Helsinki

Faculty of Science

Department of Chemistry

A.I. Virtasen aukio 1 (P.O. Box 55)

Helsinki 00014, Finland

ACADEMIC DISSERTATION

To be presented, with the permission of the Faculty of Science, University of Helsinki, for public discussion in Auditorium E204, Department of Physics, on the 10th of January 2025, at 12:15 o'clock.

Helsinki 2025

Helsingin yliopisto (University of Helsinki)
Dissertationes Universitatis Helsingiensis 11/2025

Julkaisija (Publisher): Helsingin yliopisto
Sarja (Series): Dissertationes Universitatis Helsingiensis 11/2025
ISBN 978-952-84-0478-1 (print)
ISBN 978-952-84-0477-4 (online)
ISSN 2954-2898 (print)
ISSN 2954-2952 (online)
PunaMusta, Joensuu 2025

Supervised by:

Theo Kurtén, Professor, PhD
Department of Chemistry
University of Helsinki
Helsinki, Finland

Rashid Valiev, PhD
Department of Chemistry
University of Helsinki
Helsinki, Finland

Reviewed by:

Juha Vaara, Professor, PhD
NMR Research Unit
University of Oulu
Oulu, Finland

Michelle L. Coote, Professor, PhD
Institute for Nanoscale Science and Technology
College of Science and Engineering
Flinders University
Adelaide, Australia

Custos:

Theo Kurtén, Professor, PhD

Opponent:

Anna Novelli, Senior Scientist, PhD
Forschungszentrum Jülich GmbH
Jülich, Germany

If all this damned quantum jumping
were really here to stay,
I should be sorry
I ever got involved with quantum theory.

ERWIN SCHRÖDINGER

Abstract

This dissertation deals with the chemical reactions between radicals in the atmosphere, and the reaction mechanisms related to these reactions. Radical molecules are key species in many different atmospheric processes, but the focus of this dissertation is on reactions that involve peroxyl radicals, which are common reaction intermediates in atmospheric oxidation reactions.

In this thesis, these reactions were studied by modeling them with theoretical methods, which enabled to zoom into the elementary reactions, mechanisms, and intermediate reaction products that all in tandem help to determine, what kind of reaction products are formed and in what magnitude. Precise understanding of the details of these reactions is central for predicting what kind of chemical transformations occur in atmospheric reaction conditions, and what impact these would have on the atmosphere, air-quality, and climate.

However, reactions between radicals are difficult to model because of the involvement of complicated electronic states. Accurate assessments of these electronic states require multireference electronic structure methods, whose accuracy and applicability depend on many variables.

This thesis explores these variables in the context of self- and cross-reactions of peroxyl radicals, and in the atmospheric oxidation of ammonia, which are both important processes in the atmosphere, but for which the current understanding is lacking. Choosing these reactions as model systems for multireference calculations proved to be extremely successful – they provided a challenging framework to optimize the multireference methodologies for, but the application of the optimized methods for these systems also brought renewed insight into these reactions.

In terms of the peroxyl radical self- and cross-reactions, the results show that the propagation of these reactions through the tetroxide intermediate is energetically favorable across multiple studied primary- and secondary peroxyl radicals. A more rigorous

inspection of the $MeO_2 + MeO_2$ reaction revealed that both the formation and decomposition reactions of the tetroxide intermediate occur on barrierless potential energy surfaces. It is currently unknown whether this result is generalizable to all tetroxide intermediates.

As for the atmospheric oxidation of ammonia, based on the results the reaction between the aminyl radical and molecular oxygen is much faster than previously thought, which means that part of the atmospheric oxidation reactions of ammonia possibly goes through the aminoperoxyl intermediate formed in the aforementioned reaction, which potentially leads to different product distributions than what is currently understood.

In addition to the discussion of the specific results in the original publications, this thesis provides a thorough literature review of past published works on these reactions, as well as broader context to why these reactions are important and impactful. Lastly, many chemists find the multireference methods intimidating. This thesis aims to make it easier to start using these methods by highlighting important theoretical aspects of these methods, clearly communicating their limitations, and offering practical guidelines for carrying out multireference calculations.

List of Publications

Original Publications Related to the Thesis

I **Salo, V.-T.**, Valiev, R. R., Lehtola, S., Kurtén, T., Gas-Phase Peroxyl Radical Recombination Reactions: A Computational Study of Formation and Decomposition of Tetroxides, *The Journal of Physical Chemistry A* **2022**, 126, 4046–4056.

II **Salo, V.-T.**, Chen, J., Runeberg, N., Kjaergaard, H. G., Kurtén, T., Multireference and Coupled-Cluster Study of Dimethyltetroxide (MeO_4Me) Formation and Decomposition, *The Journal of Physical Chemistry A* **2024**, 128, 10, 1825–1836.

III **Salo, V.-T.**, Chen J., Kjaergaard, H. G., The Aminoperoxyl Radical is an Important Intermediate in Atmospheric Oxidation of Ammonia, *Manuscript submitted to Environmental Science: Atmospheres*.

The author of this thesis was responsible for writing the manuscripts for all publications **I**, **II**, and **III**, with contributions from all co-authors. Apart from the ASCI-SCF and ASCI-SCF(PT2) calculations in publication **I** by Susi Lehtola, and the W2X and W3X-L composite method calculations in publication **II** by Nino Runeberg, all quantum chemical calculations, analysis and visualizations thereof, were solely done by the author of this thesis. The research ideas underlying each publication were planned in collaboration with all the associated authors. Throughout the thesis, the original publications are referred to with their respective roman numerals as shown above.

Other Publications Not Included in the Thesis

IV Valiev, R. R., Hasan, G., **Salo, V.-T.**, Kubečka, J., Kurtén, T., Intersystem Crossings Drive Atmospheric Gas-Phase Dimer Formation, *The Journal of Physical Chemistry A* **2019**, 123, 30, 6596–6604.

V Hasan, G., **Salo, V.-T.**, Valiev, R. R., Kubečka, J., Kurtén, T., Comparing Reaction Routes for ^{3}(RO$\cdot\cdot\cdot$OR') Intermediates Formed in Peroxy Radical Self- and Cross-Reactions, *The Journal of Physical Chemistry A* **2020**, 124, 40, 8305–8320.

VI Hasan, G., Valiev, R. R., **Salo, V.-T.**, Kurtén, T., Computational Investigation of the Formation of Peroxide (ROOR) Accretion Products in the OH- and NO_3-Initiated Oxidation of α-Pinene, *The Journal of Physical Chemistry A* **2021**, 125, 50, 10632–10639.

VII Daub, C. D., Zakai, I., Valiev, R., **Salo, V.-T.**, Gerber, R. B., Kurtén, T., Energy Transfer, Pre-Reactive Complex Formation and Recombination Reactions During the Collision of Peroxy Radicals, *Physical Chemistry Chemical Physics* **2022**, 24, 10033–10043.

VIII Daub, C. D., Valiev, R., **Salo, V.-T.**, Zakai, I., Gerber, R. B., Kurtén, T., Computed Pre-Reactive Complex Association Lifetimes Explain Trends in Experimental Reaction Rates for Peroxy Radical Recombinations, *ACS Earth and Space Chemistry* **2022**, 6, 10, 2446–2452.

IX Hasan, G., **Salo, V.-T.**, Golin Almeida, T., Valiev, R. R. Kurtén, T., Computational Investigation of Substituent Effects on the Alcohol + Carbonyl Channel of Peroxy Radical Self- and Cross-Reactions, *The Journal of Physical Chemistry A* **2023**, 127, 7, 1686–1696.

Acknowledgements

Firstly, I want to thank my supervisors, Prof. Theo Kurtén and Dr. Rashid Valiev. Theo, thank you for letting me join the group and getting me into atmospheric chemistry, computational chemistry, and everything else that comes with it. Thank you for understanding that sometimes science takes time and patience – I hope I was worth every penny that you have paid me, as you like to say. I'm extremely grateful for Rashid for teaching me to run all those multireference calculations. I would have probably ended taking another course in my PhD if you had not been there to help me out.

Science tends to be better and more fun, when you get to do it in collaboration with other people. Thank you Dr. Susi Lehtola for helping me out with my first publication, I am especially grateful for all that red pen I found in my manuscript drafts. I hope I have become a bit better at scientific writing at this point so that you don't need to use the red pen as much, if you choose to read this book. Thank you Nino Runeberg, whom I got to know as the contact person in the CSC – IT Center for Science, and later during his sabbatical in our research group. Your help was invaluable in both of your roles, and collaborating with you was fun and inspiring.

I want to express my utmost thanks and respect to Galib Hasan and Thomas Golin Almeida, who started their PhD studies at the same time as I did, and with whom I've been delighted to share an office and experience most of the highs and lows that come with scientific progress. You are both exceptional people and scientists, thanks for all the help and friendship, in the words of Aragorn: You bow to no one. That same office later attracted other exceptional minds in the form of Lauri Franzon and Robert Skog – you guys have a bright future ahead of yourselves. I also want to thank Noora Hyttinen and Siddharth Iyer who were both just about to finish their PhDs, when I joined the group. Thanks for teaching the ropes around using supercomputers and showing examples of what becoming a pioneering computational chemist would require. I also want to extend

my gratitude to everyone else in the Atmospheric Computational Chemistry Group and in the other closely-affiliated groups in the 4th floor of Chemicum, you know who you are, thank you.

I have been privileged much to my delight to spend the last leg of my PhD journey in Copenhagen, Denmark. Prof. Henrik Kjaergaard was kind enough to allow my presence in the University of Copenhagen premises, and already since the first day I arrived here, I have felt very welcomed and integrated into the wonderful and inspiring Kjaergaard Group. In addition to giving me an office corner, Henrik provided me a lot of invaluable guidance and help – I could not have wished for a better step-supervisor and a colleague. I want to thank Dr. Jing Chen for being an irreplaceable collaborator in my research projects and being another individual who understands that you lose part of your soul when you decide to open the Pandora's box of multireference methods. Thank you to the rest of my UCPH colleagues – Casper, Dhritabrata, Andras, and others – I am still unsure what you put into your morning porridge, but apparently it makes you driven, hard-working, and smart.

I will be forever indebted to Dr. Kjell Knapas and Prof. Timo Repo for sparking a genuine interest in chemistry and research and being the first ones to offer me jobs in chemistry – turns out you can have fun and get paid for doing it. The guidance and inspiration that you have provided is very likely the reason that I ever decided to continue to pursue a career as a chemist.

On the matter of getting paid for doing science, I am grateful for the Department of Chemistry, the Doctoral Programme in Chemistry and Molecular Sciences (CHEMS), and the Center of Excellence: Virtual Laboratory for Molecular Level Atmospheric Transformations (VILMA) for funding this thesis work.

I also want to thank all the other people with whom I have had the pleasure to work with during the University years before starting my PhD. Special thanks to Dr. Juha Keskiväli and Dr. Teemu Niemi for offering practical guidance and showing how to do science. By the way Juha; at the time of writing ManU has just lost 0-3 at home to Liverpool, and Teemu, American football is still not real football. I want to thank all the other cardsharks: Kalle, Jere, Otto, Fjor, Jussi, and all the other occasional reinforcements. I also want to remember those of you who are no longer with us. The band upstairs got a fantastic lead guitarist in you Erkki, thank you for all those hilarious

stories and for the uncontrollable laughs that they caused.

Talking of bands, greatest thanks to my brothers-in-metal: Antti, Lassi, Teemu, and Santeri, who have provided me a channel to express the less-scientific side of myself. I think we have made great music so everyone who reads this: do yourself and my wallet a favor and go buy some Void Cruiser LPs.

All my other dear friends outside the world of science and chemistry, thank you for being there and for sharing all those unforgettable moments with me – I hope there is many more to come.

Not a single word or even a letter would have made their way within the covers of this book, if you had not been there, Kajsa. Thank you for believing in me during all those moments I simply was not able to. To find a person that is both the best friend anyone could ever wish for, and an intellectual equal, is something that I consider the greatest achievement in my life. The chemistry that I share with you is of the sort that cannot be measured or modelled by any means.

Lastly, I thank everyone in my family: Mom and dad for raising an upstanding member of the society, my brother Santeri and sister Salli for being the same kind of goofs as I am, my parents-in-law Kata and Mika, and finally Kent, Byron, and Mauno. Yes, the last three are two dogs and a cat, they know what's up.

List of Abbreviations and Symbols

The list below explains several abbreviations and symbols used throughout the main body of the thesis

Abbreviations

AHP Alkenylhydroperoxide

ASCI Adaptive sampling configuration interaction

BO Born-Oppenheimer approximation

CAS Complete active space

CASCI Complete active space configuration interaction

CASPT2 Complete active space second-order pertubation theory

CASSCF Complete active space SCF

CBS Complete basis set

CC Coupled-cluster

CI Configuration interaction

CL Chemiluminescence

CSF Configuration state function

DFT Density functional theory

EA Electron affinity

FCI Full configuration interaction

FIC Fully internally contracted

FOD Fractional occupation number weighted electron density

FOIS First-order interacting space

GASSCF Generalized active space SCF

GGA Generalized gradient approximation

GTO Gaussian-type orbital

HAT Hydrogen atom transfer

HF Hartree-Fock

HK Hohenberg-Kohn

HOM Highly oxidized organic molecule

HOMO Highest occupied molecular orbital

IC Internally contracted

IP Ionization potential

IPEA Ionization potential-electron affinity shift

ISC Intersystem crossing

KS Kohn-Sham

LCAO-MO Linear combination of atomic orbitals – molecular orbitals

LUMO Lowest unoccupied molecular orbital

MC-PDFT Multiconfiguration pair-density functional theory

MCSCF Multiconfigurational SCF

MP Møller-Plesset perturbation theory

MR-MP2 Multireference Møller-Plesset second-order perturbation theory

MRCI Multireference configuration interaction

MS-CASPT2 Multi-state CASPT2

NEVPT2 N-electron valence state second-order perturbation theory

NO Natural orbital

PC Partially contracted

PES Potential energy surface

QD-NEVPT2 Quasi-degenerate NEVPT2

RASSCF Restriced active space SCF

RM Russell mechanism

RRHO Rigid-rotor harmonic oscillator

SA-MCSCF State-averaged multiconfigurational SCF

SCF Self-consistent field

SD Slater determinant

SE Schrödinger equation

SOA Secondary organic aerosol

SS-MCSCF State-specific multiconfigurational SCF

STO Slater-type orbital

TST Transition state theory

UC Uncontracted

VOC Volatile organic compound

XMC-QDPT2 Extended multiconfigurational quasi-degenerate second-order perturbation theory

XMS-CASPT2 Extended multi-state CASPT2

ZPVE Zero-point vibrational energy

Symbols

χ	Atomic orbital
$\hat{\mathcal{F}}$	Fock operator
$\hat{\mathcal{H}}$	Hamiltonian operator
$\hat{\mathcal{H}}_D$	Dyall Hamiltonian operator
$\hat{\mathcal{P}}$	Projection operator
$\hat{T}$	Kinetic energy operator
$\hat{U}$	Potential energy operator
$\mathcal{E}$	Energy of electronic state in configuration interaction
Φ	Determinant or configuration state function
ϕ	Spatial wavefunction / orbital
Ψ	The exact non-relativistic wavefunction
ψ	Spin-orbital
ψ^{HF}	Canonical Hartree-Fock spin-orbital
ψ_i^C	Canonical spin-orbital
σ	Spin-function
ε	Orbital energy
C_i	CI expansion coefficient
$c_{\mu i}$	Orbital expansion coefficient
M_{basis}	Total number of basis functions
G	Gibbs energy
H	Enthalpy
M	Number of virtual/unoccupied orbitals, $M = M_{\mathrm{basis}} - N$. Also reaction molecularity

N Total number of electrons

S Entropy

S Total spin angular momentum, related to spin multiplicity = 2S+1

U Internal energy

Contents

List of Figures

List of Tables

Chapter 1

Introduction

1.1 Motivation of the Work

The atmosphere can be thought of as a massive chemical reactor where countless chemical reactions are constantly taking place. These reactions form a complex network into which the compounds in the atmosphere enter, go through chemical transformations, and finally exit in one way or another. This network of reactions is enormous in size, and while researchers who study the atmosphere and its dynamics have unraveled parts of it, a complete understanding of how it works remains elusive.

What do we know about this network of reactions? The chemical composition of the atmosphere can guide us in understanding the general direction in which these chemical changes proceed. Earth has an exceptionally unique atmosphere in that it contains high concentration of gaseous oxygen. In fact, oxygen is the second most abundant compound in Earth's atmosphere, and out of the abundantly occurring compounds, it is by far the most reactive. This is why much of the atmospheric chemistry is chemistry with oxygen.

The chemistry with oxygen, also known as oxidation, combustion or burning, is a phenomenon familiar to everyone. But as we know, oxygen doesn't ignite things by itself. To initiate burning, external heat must be supplied. Just like a match is lit by applying frictional force against the matchbox, also the reactions of oxygen in the atmosphere require a little help to start. This initial push is provided by the sunlight, which activates various molecules in the atmosphere such that they start reacting with oxygen.

However, the compounds that react with oxygen – the volatile organic compounds (VOC) – are present in such minute amounts that the heat formed in these reactions

readily dissipates to the surroundings, and the fire is not able to keep itself alive; therefore, the atmospheric reactions with oxygen are often incomplete. To give a sense of how little VOCs there is in the atmosphere, 21% of the air is oxygen, while the VOCs constitute only around 0.0003% of the air mass. Imperfect burning means that in addition to the end products, such as carbon dioxide and water, various intermediate species are present as well. These intermediates are molecules to which the oxygen has been added, but for which the heat produced in the reaction has not been sufficient to break the molecule down further. Overall, these reactions produce molecules that are larger and heavier than they originally were before the oxidation.

This increase in size and mass is reflected also in other properties of these molecules. Importantly, the addition of oxygen into these molecules increases their polarity, which means that they start sticking easily to other polar molecules in the atmosphere, and ultimately these clusters of sticky molecules become so large that they cannot exist in the gaseous state anymore, and they phase-transition into aerosols — liquid or solid particles that are suspended in the gas phase.

These aerosols have a substantial impact on the climate. The moisture in the atmosphere is able to condense on the surfaces of aerosols, which leads to the formation of clouds. The clouds filter some of the incoming sunlight, which cools the planet's surface. In fact, without the cloud cover, Earth's surface temperature would be so high that biological life in the magnitude and diversity that we have today would not exist.

However, not all chemical compounds and particles entering the atmosphere have such a benign effect. Small aerosol particles at ground level are harmful to human health – exposure to these aerosols has been directly linked to, for example, increased risks of various respiratory and cardiovascular diseases. Additionally, some atmospheric compounds actually trap sunlight's heat in the lower atmosphere or partially destroy the sunlight filtering ability of the higher atmosphere, which has a net warming effect on Earth's surface. These compounds are collectively known as the greenhouse gases, and their elevated concentrations in the atmosphere are unfortunately largely caused by human activities.

The motivation of atmospheric sciences is to understand, how the various compounds that are emitted into the atmosphere, both from natural sources and from human-activities, affect the atmosphere, climate, and air-quality. In particular, it is important to know the effect of human caused emissions, because these we can adjust with our own choices.

However, we do not want to run experiments with the atmosphere to find out what it likes and what it does not. We have tried that before, for example, with the halocarbon compounds, which turned out to destroy the stratospheric ozone layer; therefore, it is necessary to know in advance how different compounds would react in the atmosphere, such that detrimental emissions could be either limited or banned with emission and climate policies. But, to convince politicians to act requires credible, accurate, and complete knowledge about the chemistry and dynamics of the atmosphere. The purpose of this dissertation and its underlying research is to contribute to the accumulation of this knowledge.

1.2 Preface and the Objectives of the Thesis

The rates of chemical reactions, reaction mechanisms, branching ratios of products formed, and how different structural properties affect reactivity are central to understanding how chemical reactions proceed. Usually chemical reactions are studied experimentally in the laboratory, and while conducting experiments is an irreplaceable method for studying reactions, experiments do not capture the full picture of chemical reactivity. Ideally, experiments tell how fast the reacting compounds are consumed and how fast stable reaction products are formed, and what kind of stable products are formed; however, information related to reaction intermediates or reaction mechanisms may not be easily deduced from experiments. Moreover, in the context of the atmosphere, the reactions are often between radicals, so also both the reactants and products are unstable and short-lived. Such reactions are particularly complicated to study with experimental methods, and these methods often require special conditions, which are far removed from the reaction conditions of the real atmosphere.

In addition to experiments, chemical reactions can be studied by modeling the interactions between atoms and molecules theoretically. The theoretical models can be applied for the individual reaction steps, intermediates, and reaction mechanisms – to capture all the information the experiments miss; thus, experimental observations and theoretical models complement each other.

However, the theoretical models have their limitations as well. Molecules are such a small objects that they do not obey the laws of classical physics, but the principles of

quantum mechanics instead. Quantum mechanics is a complex theory, whose application to systems even as small as molecules, let alone for chemical reactions between molecules, was for a long time an unattainable goal – waiting for the future, where powerful computers could process the massive amounts of underlying physics and mathematics. Fortunately, that future is now and these computers exist, and the modeling of chemical reactions with quantum mechanics has become a common tool in the chemists's toolkit. It is also the tool that I have chosen to conduct the research for this thesis.

This dissertation centers around quantum mechanical modeling of radical reactions that are central to atmospheric oxidation. Just like studying these reactions experimentally is particularly difficult, also their theoretical analysis is complicated, and requires specialized methods. This thesis aims to bring these methods into the attention of a wider audience of atmospheric scientists and computational chemists. The objectives of this thesis are:

- Find and optimize computational methodologies required for accurate descriptions of chemical reactions occurring on complex electronic states.
- Apply these methods to further the knowledge of atmospheric radical reactions. This is done specifically by studying:
  - The peroxyl radical self- and cross-reactions, with particular interest in the formation and decomposition mechanisms of the tetroxide intermediates formed in these reactions (publications **I** and **II**).
  - The formation and stability of the aminoperoxyl radical, which is a currently overlooked intermediate in the atmospheric oxidation of ammonia (manuscript **III**).
- Promote the use of multireference electronic structure methods as a tool for studying chemical reactions.

The thesis is structured as follows: Chapter 2 introduces atmospheric oxidation processes with the focus on the oxidation of hydrocarbon-derived compounds. Chapter 3 provides a closer look to the bimolecular reactions between peroxyl radicals, which has been the subject of the original publications **I** and **II**. Chapter 4 is an introduction to the atmospheric oxidation of amines, and more specifically to the oxidation of ammonia,

which is the subject of manuscript **III**. Chapter 5 presents an overview of the various theoretical methods used in this research, and the purpose of Chapter 6 is to give a more hands-on perspective of how to use multireference electronic structure methods, which have been the principal tools that I have conducted the research with. Chapter 7 is a discussion of the most important results of the original publications. Finally, Chapter 8 summarizes the thesis and presents a view of what kind of future research could be expected on the topics discussed in the thesis.

Chapter 2

Overview of Atmospheric Oxidation Reactions

Although the Earth's atmosphere is approximately 21% of molecular oxygen (O_2), its reactions with other molecules are rare, as most of these reactions are kinetically disfavored in atmospheric reaction conditions. From a biological viewpoint this is great news, because otherwise organic compounds under the influence of O_2 would spontaneously burn and Earth would not facilitate organic life at all. Then again, O_2, which is a biradical in its ground electronic state, is extremely reactive towards other radical compounds in the atmosphere, and is a central component of atmospheric chemistry through these reactions. This chapter is an introduction to how these various radical compounds are formed in the atmosphere, and how their reactions with O_2 affect the chemical diversity of the atmosphere.

The discussion begins with a review of how the most important compounds for initiating oxidation reactions – Ozone (O_3), hydroxyl radical (OH), and nitrate radical (NO_3) – are formed in the atmosphere. Afterward, their reactions with VOCs are discussed, along with the subsequent reactions with O_2, which lead to the formation of peroxyl radicals (RO_2). Then, various further reactions of the RO_2, namely their bimolecular reactions and autoxidation reactions, are reviewed. Thereafter, consequent reactions of the oxyl radicals (RO), which are formed as major products in the reactions of RO_2, are discussed.

Some comments on the focus and what has been excluded from the discussion are warranted: the following sections concentrate on reactions in the troposphere, since the oxidation of organic compounds predominantly occurs in the lowest part of the atmo-

sphere. Furthermore, from section 2.3 onwards, the oxidation chemistry is discussed exclusively from the perspective of oxidation of hydrocarbon-derived compounds, although other compound classes, such as amines, sulphur compounds, and halogens undergo atmospheric oxidation as well. This decision is based on the fact that two of the original publications for this thesis, **I** and **II**, relate to reactions of hydrocarbon-derived peroxyl radicals. Publication **III** relates to the atmospheric oxidation of ammonia, background and context for that process is given in Chapter 4.

2.1 Nitrogen Oxides (NO_x) – The Generators of Primary Tropospheric Radicals

The formation of a plethora of atmospheric radicals is closely related to the atmospheric chemistry of nitrogen oxides ($NO_x = NO + NO_2$). Naturally, these compounds are formed in extreme conditions such as lightning-induced combustion reactions between N_2 and O_2.[1] Anthropogenic sources include biomass and fossil fuel burning, and oxidation of ammonia. Nitrogen dioxide (NO_2) is one of the rare photolabile molecules in the troposphere,[2] and its photolysis to NO and ground-state triplet atomic oxygen $O(^3P)$ is the only known chemical source of tropospheric ozone:[3]

$$NO_2 \xrightarrow{h\nu} NO + O(^3P) \tag{2.1}$$

$$O_2 + O(^3P) + M \longrightarrow O_3 + M \tag{2.2}$$

The process occurs also in reverse, where NO_2 is regenerated and ozone destroyed in reaction between NO and O_3:

$$NO + O_3 \longrightarrow NO_2 + O_2 \tag{2.3}$$

NO_2 is also regenerated in other reactions of NO, such as in reactions with hydroperoxyl radical (HO_2) and other peroxyl radicals (RO_2):

$$HO_2 + NO \longrightarrow OH + NO_2 \tag{2.4}$$

$$RO_2 + NO \longrightarrow RO + NO_2 \tag{2.5}$$

Ozone reacts also with NO_2 to form nitrate radicals (NO_3),

$$NO_2 + O_3 \longrightarrow NO_3 + O_2 \tag{2.6}$$

which are important mediators of further oxidation chemistry due to their ability to abstract hydrogen atoms from various organic compounds, but such chemistry is limited to night-time, because NO_3 photolyzes easily in sunlight (420–640nm):[4]

$$NO_3 \xrightarrow{h\nu} NO_2 + O(^3P) \tag{2.7}$$

$$NO_3 \xrightarrow{h\nu} NO + O_2 \tag{2.8}$$

The NO_3 photolysis recycles NO and NO_2, thus the total effect is a catalytic destruction of O_3 during the daytime.

2.2 Photolysis of Ozone – Formation of OH Radicals

In addition to its reactions with NO_x, ozone also photolyzes in the troposphere, albeit less so than NO_2. The lesser photolysis is explained by drastically reduced solar actinic flux in the wavelength range where O_3 absorbs light. Most of the sunlight in this range is absorbed by ozone, but a different kind – the stratospheric ozone layer,[5] which with stratospheric molecular oxygen absorb most of the incoming short wavelength ultraviolet radiation (UV-C and UV-B, 100–315nm).

Ozone has various photolysis mechanisms.[2,6] Of these mechanisms, those leading to singlet atomic oxygen, $O(^1D)$, are especially impactful, because singlet oxygen reacts with water to form hydroxyl radicals, which are arguably the most reactive molecules in the atmosphere:

$$O_3 \xrightarrow{h\nu} O_2(a^1\Delta_g) + O(^1D), \qquad \lambda < 310\text{nm} \tag{2.9}$$

$$O_3 \xrightarrow{h\nu} O_2(^3\Sigma_g^-) + O(^1D), \qquad \lambda < 411\text{nm} \tag{2.10}$$

$$H_2O + O(^1D) \longrightarrow 2OH \tag{2.11}$$

For the most part, OH radicals are consumed in the oxidation of CO, and in the oxidation of methane (CH_4) and other hydrocarbons.[7] The oxidation of CO by OH is also the main source of HO_2 radicals in the atmosphere:[8]

$$CO + OH \longrightarrow HOCO\cdot \longrightarrow CO_2 + H \xrightarrow{O_2} CO_2 + HO_2 \tag{2.12}$$

2.3 Reactions of OH, O_3, and NO_3 With Organic Compounds – Formation of Peroxyl Radicals

OH, O_3, and NO_3 are unique compounds in the atmosphere in that they are able to initiate the oxidation of hydrocarbons.[9] OH and NO_3 react with hydrocarbons via two mechanisms: by hydrogen atom transfer (HAT), which yields carbon-centered radicals and H_2O/HNO_3 (Fig. 2.1a), or by radical addition to a C=C double bond, yielding β-OH/-NO_3 substituted carbon-centered radicals (Fig. 2.1b and c).[10–13] The carbon-centered radicals are very short-lived intermediates and react readily with molecular oxygen to form peroxyl radicals (RO_2). A minor fraction of the NO_3 derived carbon-centered radicals may also decompose to yield an epoxide and NO_2.[14]

The radical addition of OH and NO_3 to hydrocarbons, whenever possible, is generally faster than the corresponding H-abstraction reactions.[15,16] Unsaturated hydrocarbons, e.g. isoprene, oxidize a lot quicker in the atmosphere than saturated hydrocarbons, such as methane. This difference in reactivity is reflected in their atmospheric lifetimes, which is an hour for isoprene, but on the order of 10 years for methane.[17,18] Furthermore, the unsaturated hydrocarbons often undergo both the addition and H-abstraction reactions, and the availability of multiple oxidation mechanisms decrease their atmospheric lifetimes even further.

Ozone also takes part in the oxidation of hydrocarbons, albeit by a different mechanism than OH and NO_3. Ozone is unable to undergo direct H-abstraction reactions. Instead, it adds into a C=C double bond forming a primary ozonide intermediate that ultimately decomposes to a carbonyl oxide (Criegee intermediate) and a carbonyl compound (Fig. 2.2a).[19] The decomposition of the ozonide intermediate is very exothermic,[20] so further unimolecular decomposition reactions of the product fragments instantly follow, unless they are thermalized by collisions.[21] If the terminal oxygen of the carbonyl oxide points towards β-methylene group, isomerization of the carbonyl oxide by intramolecular HAT to alkenylhydroperoxide (AHP) is possible.[22] The AHPs decompose to OH and enoxyl radicals,[23] which tautomerize to β-oxo alkyl radicals that then react with molecular oxygen to form β-oxo alkyl peroxyl radicals (Fig. 2.2b).[24]

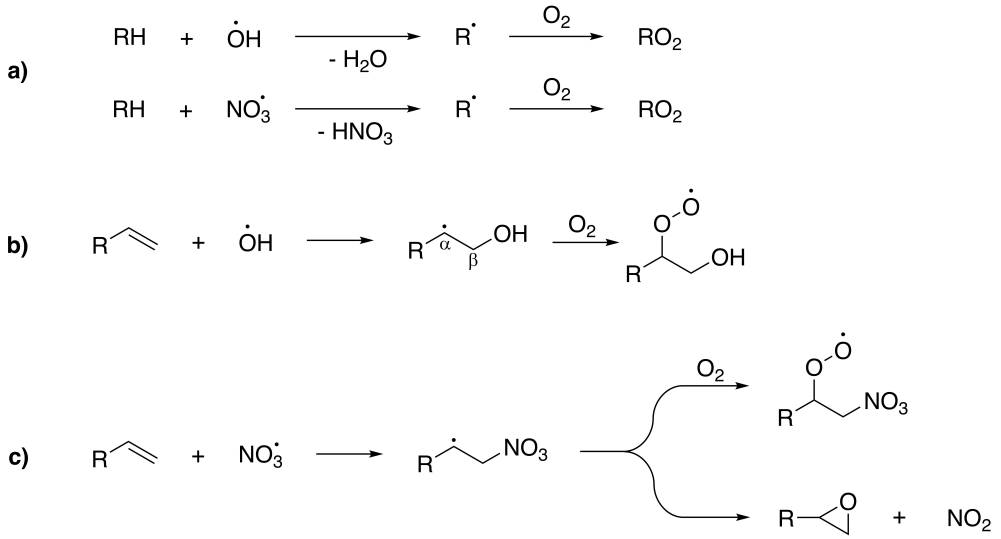

Fig. 2.1: First reaction steps in hydrocarbon oxidation. a) Hydrogen atom transfer by OH or NO_3, followed by the addition of O_2. b) Radical addition of OH into a C=C double bond, followed by addition of O_2, yielding β-hydroxy peroxyl radical. c) Radical addition of NO_3 into a C=C double bond, followed by either O_2 addition or unimolecular decomposition to an epoxide and NO_2.

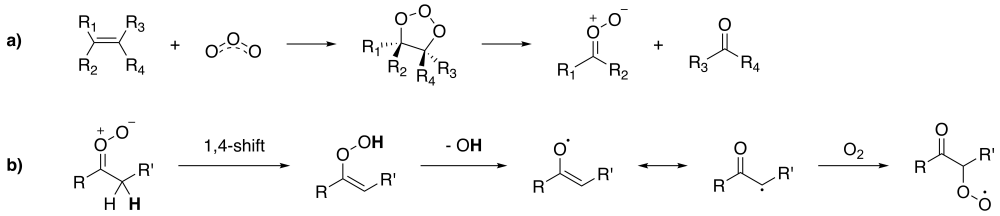

Fig. 2.2: Oxidation of alkenes by ozone. a) Formation of primary ozonide from the addition of ozone to alkene, followed decomposition to Criegee intermediate and carbonyl compound, b) isomerization of the Criegee intermediate to alkenylhydroperoxide (AHP), followed by its decomposition to OH and enoxyl radical / β-oxo alkyl radical, which adds oxygen to form β-oxo alkyl peroxyl radical.

2.4 Reactions of Peroxyl Radicals

The RO_2 radicals have a variety of further reactions in atmospheric conditions.[25–27] In general, and especially in polluted conditions, the bimolecular reactions with NO are the predominant fate of RO_2. In environments with low NO_x mixing ratios, the bimolecular reactions with HO_2 and RO_2 account for most of the bimolecular reactivity. Some RO_2 may also undergo unimolecular isomerization reactions,[28] potentially leading to autoxidation.[29,30] These various reactions will be discussed below. The self- and cross-reactions of RO_2 and HO_2 are only briefly introduced here to set them in context, but these reactions will be discussed in more detail in the following chapter, because these reactions are central to the Publications **I** and **II**.

2.4.1 RO_2 + NO_x

The reaction between RO_2 and NO occurs via a peroxynitrite (ROONO) intermediate,[27,31] which either dissociates into an oxyl radical (RO) and NO_2 or isomerizes to thermodynamically much more stable organic nitrate species $RONO_2$,[32,33] which acts as a long atmospheric lifetime sink for both the RO_2 and NO. For small peroxyl radicals the $RONO_2$ yields are negligible, but the fraction of $RONO_2$ increases with increasing system size and pressure and decreasing temperature, so the $RONO_2$ channel may even be the dominant pathway in certain conditions.[34] The $RO_2 + NO \longrightarrow RO + NO_2$ reaction contributes to tropospheric ozone production by forming NO_2 (eqns. 2.1 and 2.2), and the analogous reaction with HO_2 also regenerates OH (eqn. 2.4).

The $RO_2 + NO_2$ reaction does not follow the same pattern, as to yield RO and NO_3. Instead, for certain RO_2, mainly for acyl peroxyl radicals, the peroxynitrate ($ROONO_2$) addition product is stable in atmospheric conditions; however, the $ROONO_2$ is in thermal equilibrium with the $RO_2 + NO_2$. The dissociation back to reactants is favored in higher temperatures;[35] therefore, the $ROONO_2$ may form in colder regions and transport far from the emission source and later dissociate in warmer conditions.[36,37]

2.4.2 $RO_2 + HO_2$ and RO_2 + R'O_2

The $RO_2 + HO_2$ and $RO_2 + R'O_2$ reactions occur via different mechanisms.[31] While the first predominantly follows the mechanism of the RO_2 directly abstracting the hydrogen atom from HO_2, giving an organic hydroperoxide (ROOH) and O_2,[38,39] the latter occurs via an addition reaction, where the two peroxyl radicals form an intermediate with four oxygen atoms in a chain.[40,41] These intermediates, known as tetroxides (or tetraoxidanes, RO_4R'), are extremely unstable in the gas-phase and decompose to give three major product channels: dissociation to two oxyl radicals (RO + R'O), an alcohol and a carbonyl compound (R_{-H}=O + R'OH), and an organic peroxide (ROOR') by the addition of the two oxyl radicals. The ROOR' formation channel provides a mechanism of forming low-volatility high molecular mass accretion products,[42,43] contributing to secondary organic aerosol (SOA) mass in the troposphere.[44]

2.4.3 Unimolecular reactions of RO_2

In pristine environments, the RO_2 can have sufficiently long lifetimes with respect to bimolecular reactions that unimolecular rearrangement reactions can take place. The most important unimolecular reactions mediated by the peroxy moiety (Fig. 2.3) are intramolecular HAT reactions,[45–50] and endo cyclization reactions,[51–54] which both may also lead to autoxidation.[30]

The HAT reactions are limited to relatively large hydrocarbons, because mostly 1,N-HAT reactions, where N=5–7, are fast enough to compete with bimolecular reactions of RO_2.[50] Moreover, the HAT rates are largely structure dependent, such that functionalized hydrocarbons are much more reactive towards HAT reactions and autoxidation in general.[30,50]

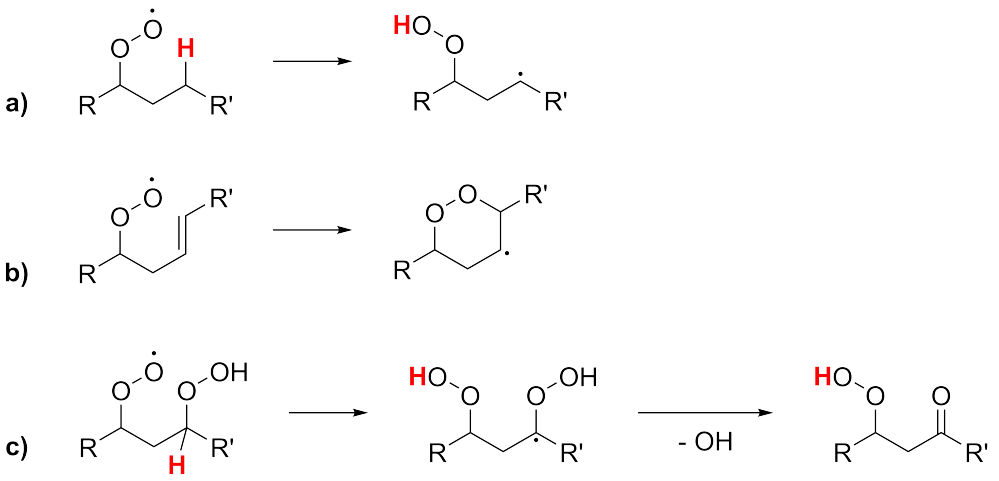

Fig. 2.3: Examples of unimolecular reactions of peroxyl radicals. a) intramolecular 1,5-HAT reaction, b) endo cyclization by intramolecular addition into a C=C double bond, c) hydrogen atom abstraction from hydroperoxyalkyl carbon leads to unstable QOOH radical, which decomposes to a carbonyl compound and an OH radical.

The autoxidation reactions may occur, when the intramolecular rearrangement reactions yield carbon-centered radicals, which readily add O_2 to form new peroxyl radicals, which then may repeat the unimolecular reactions shown in Fig. 2.3. These autoxidation reactions may continue as long as there are either reactive C-H groups or C=C double bonds, and for large hydrocarbons this process leads to a rapid increase in the oxygen content of the oxidizing molecule, giving rise to highly oxidized organic molecules (HOMs), which have a potential to contribute to tropospheric SOA.[55,56]

Autoxidation terminates when the RO_2 functionality no longer has accessible unimolecular reactions, or when the radical functionality is lost from the parent hydrocarbon molecule. Most probable terminating mechanisms are α-hydroperoxyalkyl radical (QOOH) decomposition, which yields OH and a carbonyl compound (Fig. 2.3c),[49,57] and epoxidation reactions, which may occur when the carbon-centered radical is formed vicinally to a hydroperoxide group (β-hydroperoxy alkyl radical).[58] The hydroperoxide eliminates OH radical and the remaining oxyl radical recombines with the adjacent alkyl radical to form an epoxide. For most β-hydroperoxy alkyl radical systems, the O_2 addition is still the dominating pathway, but for certain functionalized systems, the epoxidation reaction may be competitive even under high oxygen concentration.[59]

2.5 Reactions of Oxyl Radicals

The oxyl radicals (RO), which are major products in both the $RO_2 + NO$ and RO_2 + R'O_2 reactions, have three further competitive reaction pathways,[60–62] whose branching depends on the nature of the RO: intramolecular HAT reaction, β-C-C-scission, and α-H abstraction (Fig. 2.4). Similarly to the intramolecular HATs mediated by RO_2, the RO HATs are limited to relatively long hydrocarbons, where at least 1,5 HAT are possible. These reactions yield carbon-centered radicals susceptible to O_2 addition reactions, thus promoting autoxidation. Non-methyl alkyl oxyl radicals (alkoxyl) may also dissociate via β-C-C-scission reaction,[63,64] yielding carbonyl functionality in one fragment and a carbon-centered radical in the other. Primary and secondary alkoxyl radicals are prone to hydrogen abstraction reactions. These reactions are mostly mediated by molecular oxygen, where the O_2 abstracts the α-H, giving HO_2 and a closed-shell aldehyde or ketone compound.[65–67]

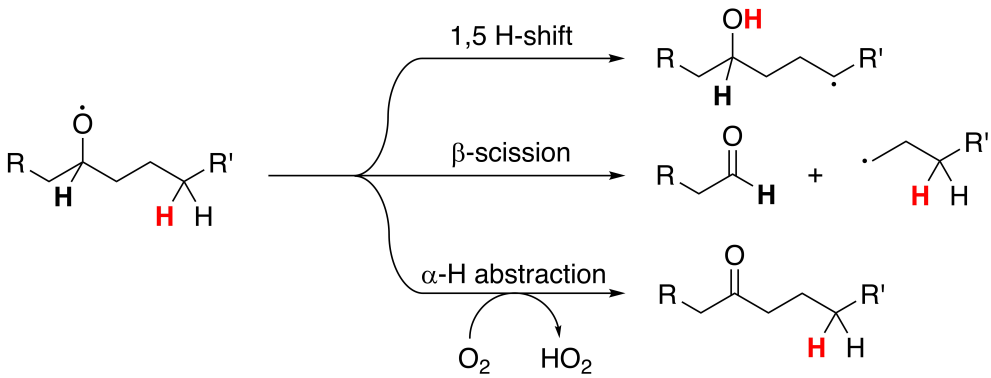

Fig. 2.4: Further reactions of oxyl radicals in the atmosphere: 1,5-HAT, which regenerates carbon-centered radicals, (cf. Fig. 2.3a), β-C-C scission reaction breaks the parent hydrocarbon to two fragments – a closed-shell carbonyl compound and a radical fragment, α-C-H abstraction by O_2 forming carbonyl and HO_2 radical.

The carbonyl products can then react with either OH radicals by H-abstraction (Fig. 2.5a) or photolyze at aldehydic-C-H or α-C-C sites via Norrish type I homolysis reactions (Fig. 2.5b). The aldehyde + OH, aldehydic-C-H photolysis, and ketonic α-C-C photolysis (Fig. 2.5c) are the most important sources of atmospheric acylperoxyl radicals (R(O)O_2). The formyl radical (HCO) formed in the aldehydic α-C-C photolysis predominantly reacts

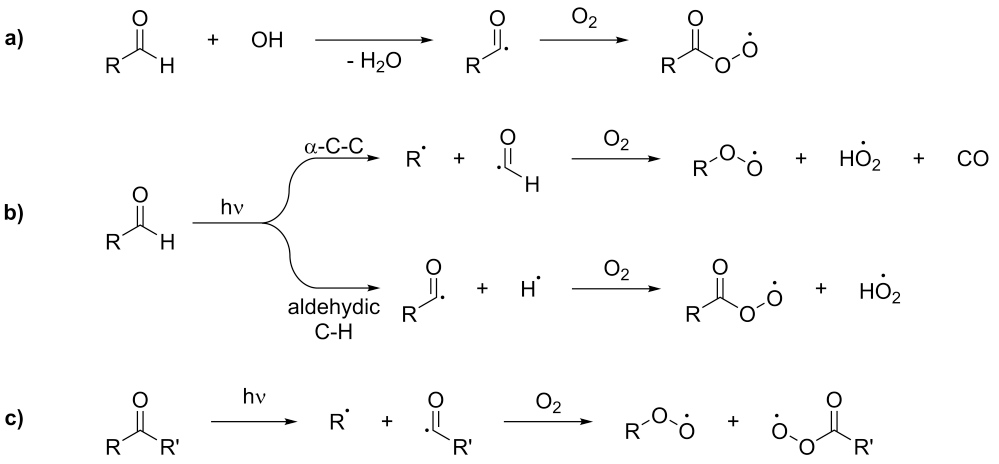

Fig. 2.5: Reactions of carbonyl compounds: a) aldehydes react with OH to give acyl radicals, which add O_2 to yield R(O)O_2 radicals, b) photolysis of aldehydes branches to α-C-C scission and aldehydic-C-H scission reactions that yield RO_2, HO_2, CO, and R(O)O_2, c) photolysis of ketones yields both RO_2 and R(O)O_2 radicals.

with O_2 to give CO and HO_2. Photolysis of formaldehyde yields both the homolysis products $H + HCO$, as well as $H_2 + CO$, which is the dominant photochemical source of molecular hydrogen in the atmosphere.[68]

Chapter 3

Bimolecular Reactions Between Peroxyl Radicals

This chapter provides a more detailed introduction to the $RO_2 + R'O_2$ reactions. The section begins with the discussion of the chemical mechanisms involved in these reactions, followed by discussion of the research done within this area so far and a summary of observed reactivity trends. The $RO_2 + R'O_2$ reactions are the main theme in publications **I** and **II**. Discussion of the research done in these publications is given in Chapter 7.

3.1 Association Reactions Between Peroxyl Radicals

The general reaction between two peroxyl radicals, $RO_2 + R'O_2$, is referred to as a self-reaction when R=R', and a cross-reaction when R≠R'. The association between two peroxyl radicals can in principle lead to three reactions (Fig. 3.1): direct bimolecular homolytic substitution (S_H2) reaction, intermolecular HAT, and "head-to-head" association reaction, where the terminal oxygen atoms of the peroxyl radicals form a bond, to yield a tetroxide (RO_4R'). The associating peroxyl radicals are doublets, so the overall coupled spin state of the system can be either a singlet or a triplet. The S_H2 and HAT reactions can occur on both spin states, but the RO_4R' formation is limited to the singlet state. Little is known about the plausibility of the first two mechanisms, apart from $RO_2 + HO_2$ reactions, which are known to predominantly react through the S_H2 mechanism. The S_H2-type reactions involve geometry inversion transition states with respect to the displacement center, but the $RO_2 + HO_2 \longrightarrow ROOH + O_2$ reactions do not

have the energy penalty associated with this inversion, because the displacement center is a single hydrogen atom. Both the S_H2 reactions and intermolecular HAT reactions between peroxyl radicals involve simultaneous breaking and forming of covalent bonds, thus the reactions are likely associated with significant energy barriers, but with the lack of knowledge about substituent effects and other contributing factors on these reactions, this assumption should be further investigated. Interestingly, if the intermolecular HAT reactions of the α-peroxyl hydrogen atoms were to be competitive, it would provide another mechanism for the formation of Criegee intermediates (Fig. 3.1b). The currently

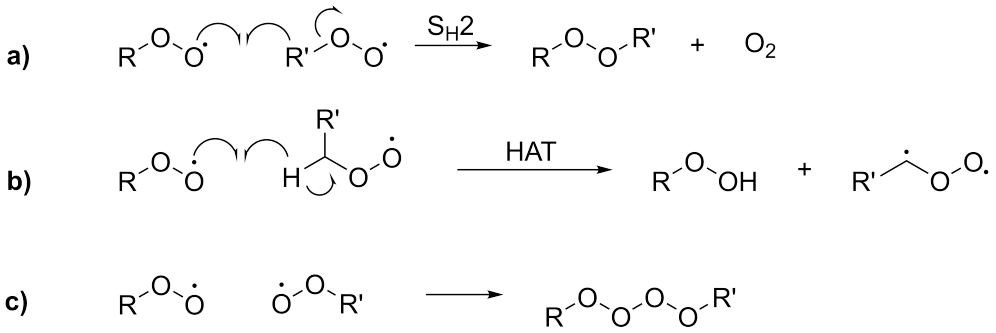

Fig. 3.1: The bimolecular peroxyl radical association reactions: a) bimolecular homolytic substitution, b) intermolecular HAT, and c) addition to form a tetroxide.

accepted hypothesis is that the vast majority if not all of these reactions occur through the RO_4R' forming pathway (when R≠H). The presence of the RO_4R' is based on two key observations. First one is from experiments, where self-reactions of isotopically labelled RO_2 – such that the reaction mixture contained both $R^{16}O^{16}O$ and $R^{18}O^{18}O$ isotopologues – produces molecular oxygen with isotopic composition of $^{16}O^{18}O$.[69,70] This result entails that RO_2 indeed react "head-to-head" such that the different oxygen isotopes form a bond, resulting in the postulated RO_4R', whose decomposition yields the $^{16}O^{18}O$ and other products. Second observation is that the tetroxides from methyl- and ethylperoxyl radical self-reactions have been identified in low-temperature matrix isolation experiments using IR spectroscopy,[71,72] and some larger tertiary tetroxides have also been observed in liquid-phase experiments.[73,74] In the gas phase and atmospherically relevant temperatures and pressures, RO_4R' have not been observed, and their decomposition in these conditions is thought to be rapid.

3.2 Decomposition of the Tetroxide Intermediate

The mechanism, by which the RO_4R' decomposes, has been a subject of many studies, including publications **I** and **II**. First study on the subject was done already in 1957,[40] suggesting a cyclic decomposition transition state, which in later literature has been referred to as the Russell mechanism (RM), named after the original author. This mechanism involves a concerted decomposition of the RO_4R' intermediate to molecular oxygen, alcohol, and carbonyl compound (Fig. 3.2). The mechanism provided a fitting explanation for the observed major product channel in their investigated RO_2 system, but has since been disputed due to several observations that contradict it. The RM also poses an interesting

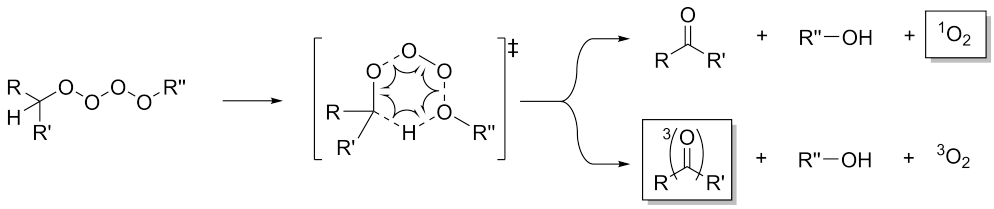

Fig. 3.2: Russell-type decomposition of the tetroxide intermediate. The concerted decomposition yields either the carbonyl product or the molecular oxygen in excited electronic state (molecules in brackets). This type of decomposition is only possible for systems with α-hydrogen atoms.

dilemma in that as the ground electronic state of RO_4R is a singlet, its decomposition directly to molecular products would give one of the product molecules in an excited electronic state, if the spin conservation rule is to be satisfied. This requires that either the dissociating molecular oxygen is formed as a singlet, or the carbonyl compound forms as a triplet.[a] While both these reactions are exothermic with respect to the free peroxyl radicals, the energy barrier for the singlet oxygen forming pathway has been found to be insurmountably high for ethyl peroxyl self-reaction.[75] On the other hand, some liquid-phase studies of $RO_2+R'O_2$ reactions have reported intense chemiluminescence (CL) from triplet carbonyl relaxation,[76,77] which is in line with the Russell-type decomposition.

Studies with large tertiary peroxyl radicals showed that the RO_2 decay follows second order kinetics and that at elevated temperatures (above -80 °C) the RO_4R' decomposes

[a] Alcohol formation in triplet state is very unlikely, because alcohol is not a chromophoric functional group.

irreversibly, which strongly suggests that it does not simply decompose back to peroxyl radicals.[73,74] However, tertiary RO_2 do not have α-peroxyl hydrogen atoms, which are required for the concerted RM, so the decomposition occurs with another mechanism. Also, the fastest experimentally observed $RO_2 + RO_2$ reaction is the self-reaction between two acetylperoxyl radicals, which also lack the α-peroxyl hydrogen atoms; therefore, there must be another competing decomposition mechanism.

The chemiluminescence from carbonyl triplet state may also originate from other decomposition mechanisms than the RM. For example, CL from carbonyl triplet state has been observed during thermal decomposition of *trans*-alkylhyponitrites (R-O-N=N-O-R'),[78] where the RM type cyclic decomposition is not possible, as the trans-hyponitrite functional group is strictly planar. The decomposition of these compounds yields molecular nitrogen and a pair of alkoxyl radicals. The only potential source of triplet carbonyl is from a reaction between the alkoxyl radical doublets, coupled in an overall triplet electronic state. The initial decomposition yields the alkoxyl radical doublets coupled in a singlet state, because the dissociating N_2 is a singlet. However, an intersystem crossing (ISC) within the alkoxyl radical pair, followed by HAT, yields a triplet carbonyl and an alcohol. The reactions between the alkoxyl radicals likely occur within a cage-like structure after the hyponitrite decomposition, because external radical scavengers do not significantly decrease the triplet carbonyl CL,[78] i.e. the reactions between alkoxyl radicals predominantly occur between those from the same hyponitrite.

This three-body dissociation mechanism is also the most likely decomposition mechanism for RO_4R'.[79] This reaction may either occur via a concerted mechanism or sequenctial mechanism. In the concerted mechanism, both the outer O-O bonds of the RO_4R' are cleaved simultaneously to give two alkoxyl radicals and triplet molecular oxygen. In the sequential decomposition, the dissociation first yields an alkoxyl radical $R'O$ and an unstable trioxyl (RO_3) intermediate, which then further dissociates into another alkoxyl radical and triplet molecular oxygen.[75] In the publication **II**, we found that at least for the studied MeO_4Me system, the concerted decomposition directly to two alkoxyl radicals and O_2 is the preferred mechanism.

The three-body decomposition yields a triplet molecular oxygen and a triplet pair of alkoxyl radicals, so the CL from triplet carbonyl is easily explained by the HAT reaction between the alkoxyl radicals, which yields the carbonyl compound in the triplet state.

Moreover, this mechanism explains all different observed reaction products (Fig. 3.3), as well as the reactivity of the RO_2 radicals that do not have α-peroxyl hydrogen atoms.

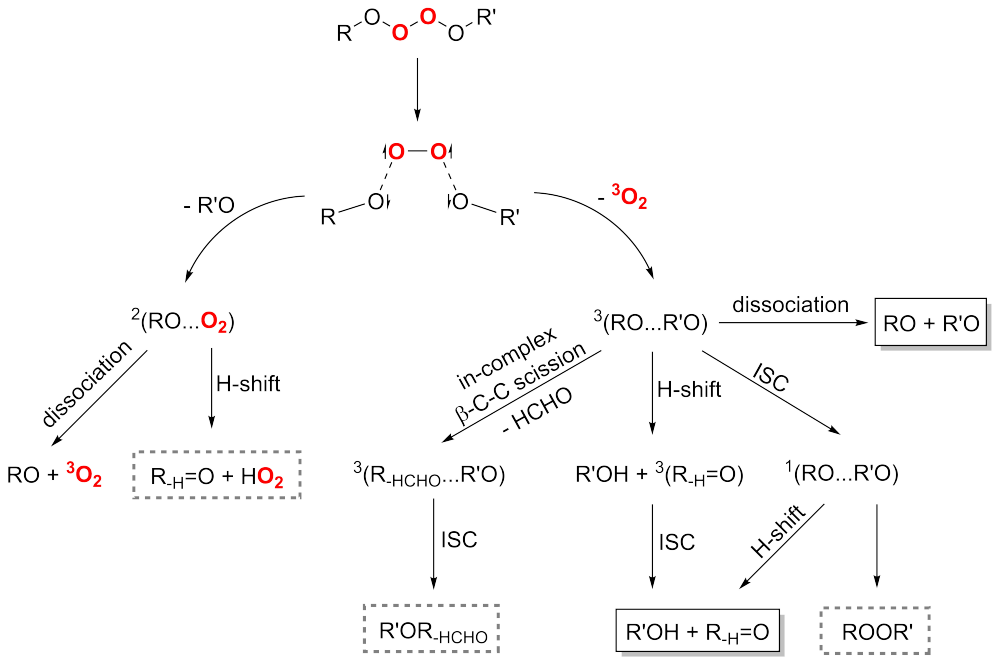

Fig. 3.3: The three-body decomposition mechanism of the RO_4R' and the possible product pathways. The products surrounded by solid boxes are the major products observed in RO_2 + $R'O_2$ reactions. The products in grey-shaded boxes are usually minor products for simple R.

3.3 Reactivity Trends and Product Distributions in RO_2+ $R'O_2$ Reactions

The reaction rates of RO_2 + $R'O_2$ are system dependent and affected by various factors. The ROO−OOR′ bond formation itself is likely a barrierless process, because radical-radical recombination reactions are electronically exoergic. Energy barriers may be present for other reasons, such as intermolecular binding between the peroxyl radicals that must be broken to form the tetroxides, or a free energy barrier caused by the entropic penalty of forming a single molecule from two reactants. However, the largest contributing factor to the reaction rate appears to be the energy difference between the free RO_2 radicals and the RO_4R' intermediate, i.e. the ROO−OOR′ bond enthalpy, which correlates

strongly with the experimentally obtained gas-phase RO_2+$R'O_2$ reaction rate coefficients, across multiple studied self- and cross-reaction systems.[80] This strongly suggests that the rate-limiting step in the gas phase $RO_2 + R'O_2$ reactions is the formation reaction of the RO_4R' intermediate, and not its decomposition. The $RO_2 + R'O_2$ reaction rates have also been found to correlate strongly with simulated lifetimes of the corresponding pre-reactive complexes RO_2...$R'O_2$, which further reinforces the picture that the association reaction is rate-limiting.[81–83]

The product distributions can be predicted similarly from binding energies to certain degree. The decomposition of the RO_4R' intermediate can be assumed to lead to intermediate product complexes RO...R'O, RO...O_2, and R'O...O_2. Apart from special cases (cf. publication **II**) the RO...R'O complexes are more stable than the RO...O_2 complexes. Then, the binding energy of the RO...R'O complex correlates with the branching between the dissociation channel (RO + R'O + O_2) and the molecular channels (R_{-H}=O + R'OH and ROOR'),[84–86] as well as with the novel product channels (ethers and esters, the $R'OR_{-HCHO}$ in Fig. 3.3), which have not yet received much attention apart from recent experimental observations,[87,88] and a theoretical structure-activity-relationship study that investigated in-complex C-C scission reactions for various model systems.[89] Weaker RO...R'O complexes are more prone to dissociation, while stronger complexes are more likely to react via the other pathways. The HAT pathway depends on the energy barrier height associated with the reaction.[84,85] The ROOR' formation requires an intersystem crossing (ISC) within the triplet alkoxyl radical complex to facilitate the peroxide formation. The ISC rate has been found to be both highly system and conformation dependent.[84,85,90]

Tables 3.1 to 3.3 summarize experimentally obtained bimolecular reaction rate coefficients (k) for atmospherically representative RO_2+$R'O_2$ self-reactions, along with product branching ratios (k_1/k = RO + R'O, k_2/k = R_{-H}=O + R'OH, and k_3/k = ROOR'). Experimental results of peroxyl radical cross-reactions and RO_2 + HO_2 reactions are not discussed further in this thesis, but available experimental data has been reviewed elsewhere.[27,91] The Table 3.1 shows the data for simple alkyl RO_2 (cf. Fig. 2.1a), Table 3.2 for β-hydroxo alkyl RO_2 (cf. Fig. 2.1b), and Table 3.3 for β-oxo alkyl RO_2 and acyl RO_2 (cf. Fig. 2.2b and Fig. 2.5).

Few important things to note before discussing the rate coefficients and branching

ratios further is that experimental RO_2 decay rates are sensitive to reactive impurities, such as residual NO_x, and feedback reactions with other $R'O_2$ that form in reactions with non-methyl alkyl peroxyl radicals. The alkoxyl radicals, which are formed in the tetroxide dissociation, decompose further by β-C-C scission reactions, producing alkyl radicals that readily add molecular oxygen to produce new peroxyl radicals, and increase the decay rate of the original RO_2 by cross-reactions. Well-designed experiments account for these feedback reactions, but the results from experiments with larger peroxyl radicals are inherently more uncertain due to the competing reactions. Another thing is that especially in the older studies, often only the radical channel (RO + R'O) formation rates are measured along with the total reaction rate, so the contribution of other products is indirectly determined, and the ROOR' channel is often completely neglected. Some of the newer studies report considerable branching to the ROOR' channel, likely because the mass-spectrometric measurements are able to detect the peroxide products directly.[43,92]

The experimental rate coefficients demonstrate clear trends in the reactivity. For the most part, the simple alkyl peroxyl radicals have the slowest reactions, where the reactivity notably decreases in order of primary > secondary > tertiary peroxyl radicals. The hydroxyl group at the β-position enhances the reaction rate by one to three orders of magnitude. Similar rate-enhancing effect is observed also with the β-oxo substitution, albeit the available data is limited to acetonyl peroxyl reactions. In addition, the ROOR' pathway appears to be competitive with the other channels, likely because of more strongly bound RO...RO product complex caused by stronger the intermolecular hydrogen bonds mediated by the polar side-groups. The acyl-RO_2 self-reactions are considerably faster compared to other systems, and demonstrate surprisingly system-independent reaction rates. None of the experimental studies with acyl-RO_2 report ROOR' product yields, but the corresponding tetroxide intermediate forms with extremely high excess energy (cf. publication **I**), so the complete dissociation likely outcompetes other available product pathways. The corresponding acyloxyl radical products easily decompose to CO_2 and alkyl radicals, decreasing the probability to form accretion products even further.

Table 3.1: Experimental peroxyl radical self-reaction rate coefficients (298 K) and product branching ratios, simple alkyl peroxyl radicals.

Author	Ref.	Year	k (cm^3 $molecule^{-1}$ s^{-1})	k_1/k	k_2/k	k_3/k
			$CH_3O_2 + CH_3O_2$			
IUPAC	93	2002	3.5×10^{-13}	0.35	0.65	n.a.
Tyndall et al.	94	1998	3.5×10^{-13}	0.42	0.58	< 0.06
Horie et al.	95	1990	n.a.	0.30	-	n.a.
Lightfoot et al.	96	1990	4.5×10^{-13}	0.29–0.82[b]	0.71–0.18[b]	n.a.
			$C_2H_5O_2 + C_2H_5O_2$			
IUPAC[a]	93	2022	9.7×10^{-14}	0.3	0.7	n.a.
Shamas et al.	97	2022	1.0×10^{-13}	0.31	0.69	n.a.
Noell et al.	98	2010	1.2×10^{-13}	0.28	-	n.a.
Sander et al.	99	2006	6.8×10^{-14}	0.60	0.40	n.a.
			$n-C_3H_7O_2 + n-C_3H_7O_2$			
IUPAC	93	2002	3.0×10^{-13}	n.a.	n.a.	n.a.
Adachi et al.	100	1982	3.65×10^{-13}	n.a.	n.a.	n.a.
			$n-C_5H_{11}O_2 + n-C_5H_{11}O_2$			
Boyd et al.	101	1999	3.9×10^{-13}	n.a.	n.a.	n.a.
			$i-C_3H_7O_2 + i-C_3H_7O_2$			
IUPAC	93	2002	1.0×10^{-15}	0.56	0.44	n.a.
Kirsch et al.	102	1979	8.6×10^{-16}	0.58	0.42	n.a.
Cowley et al.	103	1982	n.a.	0.58–0.74[b]	0.42–0.26[b]	n.a.
			$t-C_4H_9O_2 + t-C_4H_9O_2$			
IUPAC[a]	93	2011	2.1×10^{-17}	1.0	-	n.a.
Lightfoot et al.	96	1990	$1.7. \times 10^{-17}$	1.0	-	n.a.
Osborne et al.	104	1984	$0.4–8.8 \times 10^{-16}$	n.a.	-	n.a.
Kirsch et al.	105	1981	n.a.	0.88		0.12

[a] The IUPAC recommendation for this reaction has been updated since the 2006 evaluation.[93] Up-to-date information can be found at `https://iupac.aeris-data.fr` (accessed 22.08.2024).

[b] Determined for a temperature range, branching ratio range corresponds from lower to higher temperature experiments.

Table 3.2: Experimental peroxyl radical self-reaction rate coefficients (298 K) and product branching ratios, β-hydroxo alkyl peroxyl radicals.

Author	Ref.	Year	k (cm^3 $molecule^{-1}$ s^{-1})	k_1/k	k_2/k	k_3/k
$HOCH_2CH_2O_2 + HOCH_2CH_2O_2$						
Murphy et al.	92	2023	2.4×10^{-12}	0.37	0.40	0.23
IUPAC[a]	93	2022	2.2×10^{-12}	0.5	0.5	<0.02
Boyd et al.	106	1997	2.3×10^{-12}	0.5	0.5	n.a.
$CH_3CH(OH)CH(CH_3)O_2 + CH_3CH(OH)CH(CH_3)O_2$						
IUPAC[a]	93	2011	6.7×10^{-13}	0.18	0.88	n.a.
Boyd et al.	106	1997	6.8×10^{-13}	0.18	0.88	n.a.
$(CH_3)_2C(OH)C(CH_3)_2O_2 + (CH_3)_2C(OH)C(CH_3)_2O_2$						
Boyd et al.	106	1997	4.0×10^{-15}	1.0	-	n.a.
cyclo$-C_6H_{10}(OH)O_2 +$ *cyclo*$-C_6H_{10}(OH)O_2$						
Boyd et al.	107	2003	1.6×10^{-12}	n.a.	n.a.	n.a.
cyclo$-C_6H_8(CH_3)_2(OH)O_2 +$ *cyclo*$-C_6H_8(CH_3)_2(OH)O_2$						
Boyd et al.	107	2003	2.0×10^{-14}	1.0	-	n.a.

[a] The IUPAC recommendation for this reaction has been updated since the 2006 evaluation.[93] Up-to-date information can be found at `https://iupac.aeris-data.fr` (accessed 22.08.2024).

Table 3.3: Experimental peroxyl radical self-reaction rate coefficients (298 K) and product branching ratios, β-oxo alkyl peroxyl radicals and acyl peroxyl radicals.

Author	Ref.	Year	k (cm^3 $molecule^{-1}$ s^{-1})	k_1/k	k_2/k	k_3/k
β-oxo peroxyl radicals						
$CH_3C(O)CH_2O_2 + CH_3C(O)CH_2O_2$						
Zuraski et al.	108	2023	4.2×10^{-12}	0.27	-	-
Assali et al.	109	2022	5.4×10^{-12}	0.60	-	-
Zuraski et al.	110	2020	4.8×10^{-12}	0.33	0.37	0.30
Berndt et al.	43	2018	IUPAC2005 rate	n.a.	n.a.	0.16
IUPAC	93	2005	8.0×10^{-12}	0.63	0.37	n.a.
Bridier et al.	111	1993	8.0×10^{-12}	0.75	0.25	n.a.
Acyl peroxyl radicals						
$CH_3C(O)O_2 + CH_3C(O)O_2$						
Assali et al.	112	2022	1.3×10^{-11}	1.0	-	n.a.
IUPAC	93	2002	1.6×10^{-11}	1.0	-	n.a.
Roehl et al.	113	1996	1.4×10^{-11}	1.0	-	n.a.
Moortgat et al.	114	1989	1.7×10^{-11}	1.0	-	n.a.
$CH_3CH_2C(O)O_2 + CH_3CH_2C(O)O_2$						
IUPAC[a]	93	2009	1.7×10^{-11}	1.0	-	n.a.
Crâne et al.	115	2005	1.7×10^{-11}	1.0	-	n.a.
$(CH_3)_2CHC(O)O_2 + (CH_3)_2CHC(O)O_2$						
Tomas et al.	116	2000	1.4×10^{-11}	1.0	-	n.a.
$(CH_3)_3C(O)O_2 + (CH_3)_3C(O)O_2$						
Tomas et al.	116	2000	1.4×10^{-11}	1.0	-	n.a.

[a] The IUPAC recommendation for this reaction has been updated since the 2006 evaluation.[93] Up-to-date information can be found at `https://iupac.aeris-data.fr` (accessed 22.08.2024).

Chapter 4

Atmospheric Oxidation of Ammonia

Unlike hydrocarbons, whose predominant fate in the atmosphere is to undergo oxidation reactions, the atmospheric chemistry of ammonia and other amines is more diverse. Amines are Brønsted bases, which means that they react easily with acidic compounds and are much more soluble in water than hydrocarbons. For this reason, most of the atmospheric reactions of amines are either liquid phase reactions within water droplets, or clustering reactions with acid molecules, such as sulphuric acid or nitric acid; however, a small but non-negligible fraction of the amines undergo oxidation reactions. These oxidation reactions are especially impactful for larger amines, due to their lower water-solubility, but the oxidation is a significant loss mechanism also for ammonia and other smaller amines. From here on, the reactions of aminyl radicals are discussed only from the perspective of NH_2 radical, which is formed in ammonia oxidation.

The oxidation of ammonia begins with a hydrogen atom abstraction reaction by OH radical, or Cl radical, which leads to the formation of aminyl radical (NH_2). The subsequent reactions of the aminyl radical are bimolecular association reactions with other radicals, most likely reactions being with NO_x, O_3, O_2. The current understanding of the relative importance of these reactions is that the reactions with NO_x/O_3 dominate, and that the reaction with O_2 is too slow to compete in atmospheric conditions.

The association of NH_2 with NO is a highly exothermic reaction, which yields a nitrosamine (NH_2NO) intermediate. Theoretical calculations show that nitrosamines are photolabile, and may photodissociate back into aminyl radicals and NO.[117] However, the NH_2NO is formed with high excess energy, so other unimolecular reactions are also possible, and the thermodynamically most stable products are $N_2 + H_2O$,[118] which are also

major products observed in experiments.[119] The reaction of NH_2 with NO is a so-called deNO_x reaction, because the reaction consumes NO_x from atmosphere.

The reaction between NH_2 and NO_2 branches to two product channels: aminonitrite (NH_2ONO) and nitroamine (NH_2NO_2), which is the lower energy product.[120] The aminonitrite decomposes to NO and aminoxyl radical (H_2NO). Thermalized nitroamine is relatively stable towards unimolecular decomposition in the gas phase, but if it forms with high excess energy, it decomposes to water and nitrous oxide (N_2O). The formation of N_2O is very harmful to the atmosphere because it acts as a reservoir for NO, and when it reaches the stratosphere it reacts with atomic oxygen to form NO, which destroys stratospheric ozone.

Although the nitroamine is the lower energy product, the formation of aminonitrite is statistically favored, because both reactions are barrierless, and the probability of NH_2 to collide with one of the oxygen atoms in NO_2 is higher than with the nitrogen atom. This is also reflected in the experimental branching of the end products (75% of $H_2NO + NO$, 25% of $H_2O + N_2O$).[121]

The reaction of O_3 with NH_2 is thought to occur only via single reaction pathway, where the ozone transfers one of its terminal oxygen atom to NH_2 to form NH_2O and O_2.[122] Further reactions of the NH_2O radical, which forms in both $NH_2 + NO_2$ and $NH_2 + O_3$ reactions, are still uncertain, and require further investigations. The most competitive reactions are likely HAT reactions to form HNO and, ultimately NO (Fig. 4.1). The oxidation of ammonia has an effect on the tropospheric NO_x budget. The

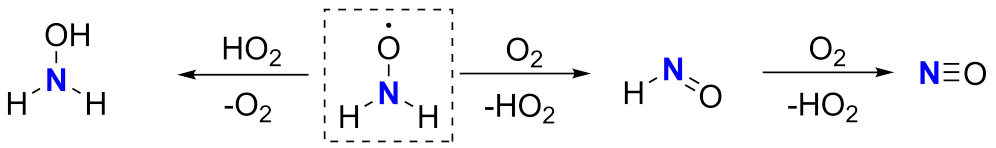

Fig. 4.1: Further reactions of the aminoxyl radical in the atmosphere.

various bimolecular reactions of NH_2 can be categorized into either NO_x consuming or producing reactions (Fig. 4.2). The overall effect depends on the relative concentrations of NO, NO_2, and O_3.

The results in manuscript **III** show that also the $NH_2 + O_2$ reaction may be competitive in atmospheric conditions. If the association product, aminoperoxyl radical (NH_2O_2), is sufficiently stable, then the current understanding about the effect of NH_3 oxidation on the

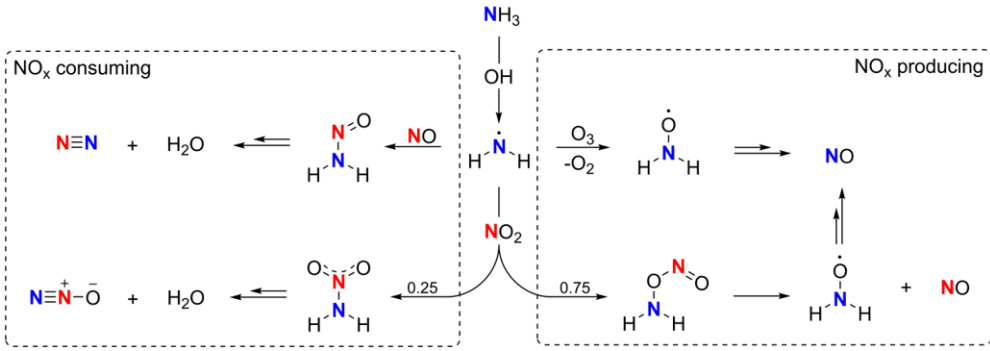

Fig. 4.2: Current understanding on the reactions involved in the atmospheric oxidation of ammonia.

NO_x budget changes considerably. This is because the further bimolecular reactions of the NH_2O_2 radical with NO, NO_2, and O_3 all have a NO_x-producing effect (Fig. 4.3); however, the thermodynamics and kinetics related to these reactions are currently unknown, and should be investigated further to assess their importance.

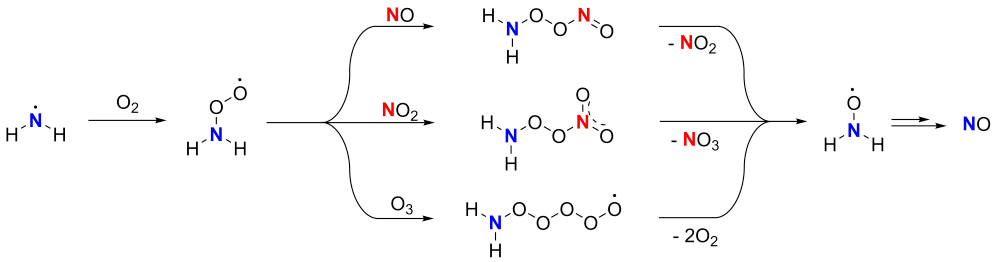

Fig. 4.3: Possible further bimolecular reactions of NH_2O_2 with NO, NO_2, and O_3.

Chapter 5

Theoretical Methods

5.1 Non-Relativistic Time-Independent Quantum Mechanics

In quantum mechanics, all properties of a quantum system are described with a wavefunction Ψ.[a] The energy of the wavefunction is calculated by solving the time-independent Schrödinger equation (SE):

$$\hat{\mathcal{H}} |\Psi\rangle = E |\Psi\rangle \tag{5.1}$$

where $|\Psi\rangle$ is the exact wavefunction, E is the exact energy of state described by wavefunction $|\Psi\rangle$, and the $\hat{\mathcal{H}}$ is the exact time-independent non-relativistic Hamiltonian operator:

$$\hat{\mathcal{H}} = \hat{T}_n + \hat{T}_e + \hat{U}_{en} + \hat{U}_{ee} + \hat{U}_{nn} \tag{5.2}$$

In general, the exact form of the wavefunction is unknown and it has to be approximated, and also the form of the Hamiltonian operator is often simplified. The accuracy of the energy in SE thus depends on these approximations.

In practice, the total wavefunction of the system is assumed to be separable to nuclear and electronic wavefunctions, as per Born-Oppenheimer -approximation (BO). This approximation leads to electronic SE:

$$\hat{\mathcal{H}}_e |\Psi_e\rangle = E_e |\Psi_e\rangle \tag{5.3}$$

[a] Ground electronic states can also be described in terms of electron density, c.f. Section 5.7 for details.

where the nuclear kinetic energy is assumed to be zero and the Hamiltonian is reduced to the "clamped nucleus Hamiltonian" $\hat{\mathcal{H}}_e$. The solution of the electronic SE, the electronic energy E_e, depends on the nuclear positions, because $\hat{U}_{en}|\Psi_e\rangle \neq 0$ and the nuclei-nuclei potential energy U_{nn} is a constant but unique for given arrangement of nuclei. Varying positions of nuclei as a function of E_e maps the potential energy surface (PES) of the system of interest.

Decoupling of nuclear and electronic wavefunctions (and assuming $\hat{T}_n = 0$) leads to negligence of coupling between different electronic states and thus prevents crossings between electronic states. For this reason the BO approximation is also known as the adiabatic approximation. For the most part, BO is a valid approximation, but for degenerate or near-degenerate solutions for electronic SE, the coupling between electronic states can be substantial.[123]

5.2 Electronic Wavefunctions – Basis Sets

The quantum state of an electron (n, l, m_l, m_s) is defined in terms of its *spatial* and *spin* functions:

$$\psi(n, l, m_l, m_s) = \phi(n, l, m_l)\sigma(m_s) \tag{5.4}$$

where ψ is known as a *spin-orbital* - the product of spatial wavefunction ϕ and spin function σ, which is either "spin-up" (α) or "spin-down" (β). For an atom, the spatial wavefunction (atomic orbital, $\phi \equiv \chi(n, l, m_l)$), is a product of a radial function ($R_{n,l}$) and a spherical harmonic function (Y_{l,m_l}):

$$\chi(n, l, m_l) = R_{n,l} \times Y_{l,m_l} \tag{5.5}$$

The atomic orbitals can be approximated with atom-centered atomic orbitals, such as *hydrogenic* orbitals (Schrödinger orbitals), Slater-type orbitals (STOs), or Gaussian-type orbitals (GTOs). The difference between these orbitals is the different ways of approximating the radial part of the orbital function. Of these, the Schrödinger orbitals are most accurate, as they properly treat the nuclear cusp region and allow radial nodes for the wavefunction. The STOs take into account the nuclear cusp but do not describe the radial nodes, while the Gaussian-type functions describe neither. Nevertheless, GTOs are often chosen as the atomic orbital basis, because the nuclear cusp region can be approximated

by a linear combination of primitive Gaussian-functions, and the GTOs have an attractive property, the "Gaussian product rule", which means that a product of Gaussians is another Gaussian. The latter greatly simplifies and speeds up various integrals in electronic structure calculations, and is the reason GTOs outperform other radial functions.

For molecular systems, the spatial wavefunction is often constructed using the *linear combinations of atomic orbitals - molecular orbitals* (LCAO-MO) method. In this method the spatial wavefunction is a weighted linear combination of multiple atomic orbitals:

$$\phi_i = \sum_{\mu}^{M_{\text{basis}}} c_{\mu i}\chi_\mu \tag{5.6}$$

where $c_{\mu i}$ are the orbital expansion coefficients, χ_μ are the atomic orbitals (fixed one-electron basis functions), and M_{basis} is the total number of χ_μ terms and defines the size of the **basis set**. The size of M_{basis} is generally larger than the number of electrons, so a basis set defines N occupied spin-orbitals and $M_{\text{basis}} - N$ unoccupied/virtual orbitals. The larger the basis set, the more accurate the results of electronic structure calculations are, but simultaneously the calculations become more time-consuming.

As electrons are fermions, they cannot occupy identical quantum states, as per the *Pauli exclusion principle*. This entails that a total electronic wavefunction describing a collection of electrons has to satisfy the *antisymmetry principle*, meaning that the wavefunction has to be antisymmetric with respect to any permutation of pair of electrons. This condition can be satisfied by constructing complete linear combination of all permutations of spin-orbitals and electrons. This linear combination can be written in a determinantal form, known as a Slater determinant (SD, $|\Phi\rangle$),[124] which for general N-electron $(e_1, e_2, ..., e_N)$ case is:

$$|\Psi\rangle \approx |\Phi\rangle = \frac{1}{\sqrt{N!}} \begin{vmatrix} \psi_1(e_1) & \psi_2(e_1) & \cdots & \psi_N(e_1) \\ \psi_1(e_2) & \psi_2(e_2) & \cdots & \psi_N(e_2) \\ \vdots & \vdots & \ddots & \vdots \\ \psi_1(e_N) & \psi_2(e_N) & \cdots & \psi_N(e_N) \end{vmatrix} \tag{5.7}$$

The determinants can be constructed under two assumptions: 1) each spatial orbital ϕ is used twice for pairs of α and β electron, which corresponds to restricted determinant, or 2) spatial orbitals for α and β electron pairs are allowed to be different in unrestricted determinant. However, relaxing the spatial orbitals for α and β electrons separately leads to spin contamination, which means that the spin state of the system is no longer

precisely determined, but a mixture of spin states. The use of determinants have also a drawback that a single determinant is not guaranteed to describe a pure spin state – the determinant is not an eigenstate of $\hat{S}^2$ operator. On the other hand, linear combinations of determinants can be used to construct pure spin states, which are also known as configuration state functions (CSFs).

5.3 Hartree-Fock Approximation

Approximate solutions for electronic energies may obtained by using the Hartree-Fock (HF) method.[125–128] The HF method assumes that the ground state wavefunction of the system can be approximated as a single Slater determinant, Φ, constructed from an orthonormal set of spin-orbitals, $\{\psi\}$. The Slater determinant corresponding to the lowest energy (E_{HF}) is obtained by variational minimization of the energy expectation value (eqn 5.8), while constraining the spin-orbitals to remain orthonormal.

$$E_{HF} = \min_{\Phi} \langle \Phi | \hat{\mathcal{H}} | \Phi \rangle \tag{5.8}$$

A stationary solution of the variation is satisfied by solving a set of equations known as the Hartree-Fock equations, which state that the energy corresponding to each spin-orbital depends on an average electrostatic field caused by all the other electrons (mean-field approximation), i.e., the optimal solution for each spin-orbital depends on the other spin-orbitals. Consequently, the lowest-energy solution for the spin-orbital energies is obtained iteratively, using the self-consistent field (SCF) method.[125] In a LCAO basis (eqn 5.6), the variables are the orbital expansion coefficients $\{c_{\mu i}\}$, and the method is known as the Roothaan-Hall method for solving Hartree-Fock equations.[129,130] The final, self-consistent solution is a set of Hartree-Fock spin-orbitals, $\{\psi^{HF}\}$, corresponding to a Slater determinant with lowest possible energy – the Hartree-Fock determinant, Φ_{HF}.

5.4 Electron Correlation

The single determinant approximation, which leads to the mean-field treatment of electronic interactions, means that there is no distinction between the various types of interactions between the electrons other than that enforced by the antisymmetry of the determinant. In the HF method, the electrons are spatially confined in their respective

spin-orbitals, which restricts their movement and neglects longer range interactions, such as dispersion. In reality, the electrons are not strictly confined, thus the exact wavefunction allows the electrons to exist in other regions than the spin-orbitals that they are confined in the HF method. However, if the ground electronic state of the system can be qualitatively described with a single Slater determinant, then $\{\psi^{HF}\}$ is a reasonable basis for describing the individual electronic interactions that the mean-field approximation fails to capture.

The exact wavefunction is more relaxed in terms of electron-electron repulsions than the Hartree-Fock wavefunction, and thus corresponds to a lower energy than E_{HF}. The energy difference of the exact energy and E_{HF} is known as the electron correlation energy E_{corr}:[131,132]

$$E_{\mathrm{exact}} = E_{\mathrm{HF}} + E_{\mathrm{corr}} \tag{5.9}$$

Multiple methods exist that aim to solve this correlation energy by using different approaches to describe explicit electron-electron interactions. In this section, three methods will be reviewed: configuration interaction, coupled cluster method, and many body perturbation theory. These methods are called post-Hartree-Fock (post-HF) or single-reference methods, because E_{corr} is estimated in terms of $\{\psi^{\mathrm{HF}}\}$, which is not reoptimized in the post-HF methods.

$$E_{\mathrm{exact}} \approx E[\{\psi^{\mathrm{HF}}\}] = E_{\mathrm{HF}}[\{\psi^{\mathrm{HF}}\}] + E_{\mathrm{corr}}[\{\psi^{\mathrm{HF}}\}] \tag{5.10}$$

The accuracy and applicability of the post-HF methods depend on how well a single determinant describes the ground state wavefunction of the system of interest. For certain systems, the single determinant approximation does not hold, and a different approaches are needed. These methods are reviewed in section 5.5.

5.4.1 Configuration Interaction

In the configuration interaction (CI) method,[132,133] the electron-electron interactions are treated by interactions between electron configurations. These configurations are generated from the Φ_{HF} by "moving" electrons from occupied orbitals to unoccupied orbitals, in a process called CI substitution. The CI wavefunction is constructed by linear expansion of the interacting electron configurations. If all possible determinants generated from

Φ_{HF}, within the limits of M_{basis}, are considered, the resulting wavefunction corresponds to full configuration interaction (FCI) wavefunction, which is an exact solution to the electronic SE for the chosen basis set:

$$|\Psi_{\mathrm{FCI}}\rangle = C_0\,|\Phi_{\mathrm{HF}}\rangle + \sum_i C_i\,|\Phi_i^a\rangle + \sum_{ij} C_{ij}\,|\Phi_{ij}^{ab}\rangle + ... + \sum_{ij...N} C_{ij...N}\,|\Phi_{ij...N}^{ab...M}\rangle \qquad (5.11)$$

where i,j...N are indices of occupied ψ, and a,b...M are indices of virtual orbitals, M = $\mathrm{M_{basis}}$-N. The first term is the Hartree-Fock determinant multiplied by its CI-coefficient (the capital C's), the first sum term collects all single substitutions from Φ_{HF}, the second sum term collects all double substitutions, and so on all the way to the N-electron substitutions in the last term. While the FCI yields the exact energy, it is practically unattainable for many-electron systems. The total number of Slater determinants in the CI expansion scales with the total spin, number of electrons, and the size of the basis set as:

$$SDs = \binom{M_{\mathrm{basis}}}{\frac{N}{2}+S}\binom{M_{\mathrm{basis}}}{\frac{N}{2}-S}$$

In practice, the CI-expansions are restricted in some fashion. This is done by either restricting the interaction space and/or truncating the expansion order. Interaction space restriction means that certain orbitals are not substituted at all. This is often applied for core electrons and their virtual counterparts, which is known as "frozen core and frozen virtual approximation".[134] Expansion order truncation means that only substitutions up to certain order are considered. Example of a such method is to include only one- and two-electron substitutions in the CI-expansion (CISD, CI singles and doubles).[135] These systematically truncated methods are attractive in the sense that the truncation is unambiguous, but the truncation has an unfortunate side-effect that it leads to non-size-extensivity and size-inconsistency.[b] A third way for restricting the size of the CI-expansion is to carry out the substitutions only in a subspace of the total orbital space. The subspace can be chosen such that full CI-expansion can be done within that space, and thus the resulting wavefunction is both size-extensive and size-consistent. Such a method is known as the complete active space CI (CASCI).[136] An apparent difficulty in CASCI in contrast to expansion truncation is that the choice of interaction space is not unique and some choices are better than others.

[b] Size-inconsistency entails that $E(A+B) \neq E(A)+E(B)$, i.e., energy of supermolecular system is not a sum of its components in the limit of no interaction. Size-extensive methods exhibit linear scaling of the energy with respect to the number of electrons.

With truncated CI methods the wavefunction corresponding to the lowest energy can be obtained using the variational method, similarly to HF, except that variables are the CI-coefficients instead of the orbital coefficients. The optimized CI-coefficients, which show how much a given determinant contributes to the overall state, provide a valuable tool for estimating the quality of the Hartree-Fock approximation. For non-degenerate electronic states, the CI coefficient of the Hartree-Fock state is often much larger than any other CI coefficient, which suggests that the overall state is mostly of HF-kind. For degenerate or near-degenerate states, other electron configurations have sizable contributions to the overall state as well. As a result, the HF approximation is less accurate, hence the $\{\psi^{\mathrm{HF}}\}$ are a less accurate basis.

5.4.2 Coupled Cluster Method

Coupled cluster is a method closely related to CI in that the total wavefunction is generated from the Φ_{HF} by the use of substitution operators $\hat{\mathcal{T}}$, which generate determinants from the Φ_{HF} up to N-electron substitutions ($\hat{\mathcal{T}} = \hat{\mathcal{T}}_1 + \hat{\mathcal{T}}_2 + ... + \hat{\mathcal{T}}_N$).[137–139] However, the total wavefunction (Ψ_{CC}) is expressed in terms of an exponential of the substitution operator acting on the Φ_{HF}:

$$|\Psi_{\mathrm{CC}}\rangle = e^{\hat{\mathcal{T}}} |\Phi_{\mathrm{HF}}\rangle \tag{5.12}$$

The exponential is approximated with a power series expansion:

$$e^{\hat{\mathcal{T}}} = 1 + \hat{\mathcal{T}} + \frac{1}{2}\hat{\mathcal{T}}^2 + \frac{1}{6}\hat{\mathcal{T}}^3 + ... + \frac{1}{k!}\hat{\mathcal{T}}^k$$

The $\hat{\mathcal{T}}$ is often truncated to second order, and when that is inserted into the power series and terms of similar excitation order are grouped together, the exponential has the form:

$$e^{\hat{\mathcal{T}}_1+\hat{\mathcal{T}}_2} = 1_{\mathbf{0}} + (\hat{\mathcal{T}}_1)_{\mathbf{1}} + (\hat{\mathcal{T}}_2 + \frac{1}{2}\hat{\mathcal{T}}_1^2)_{\mathbf{2}} + (\frac{1}{6}\hat{\mathcal{T}}_1^3 + \hat{\mathcal{T}}_1\hat{\mathcal{T}}_2)_{\mathbf{3}} + (\frac{1}{2}\hat{\mathcal{T}}_2^2 + \frac{1}{2}\hat{\mathcal{T}}_2\hat{\mathcal{T}}_1^2 + \frac{1}{24}\hat{\mathcal{T}}_1^4)_{\mathbf{4}} + ...$$

Even though only one- and two-electron substitution operators are included explicitly, the power series yields product operators of higher order, up to N-electron substitutions.[c] These operators are called the connected operators, that directly generate substitutions of given order (such as $\hat{\mathcal{T}}_1$ and $\hat{\mathcal{T}}_2$), and disconnected product operators, such as $\hat{\mathcal{T}}_1^2$ and $\hat{\mathcal{T}}_1\hat{\mathcal{T}}_2$. The disconnected operators, which arise from the exponential ansatz, ensure that the Ψ_{CC} is size-extensive in any truncation order.

[c] Power series is infinite, but only operator terms up to N-electron substitutions are effective.

The coupled cluster energy is not usually solved variationally, because the disconnected operators generate all determinants up to N-electron substitutions, and the variational solution scales similarly to FCI. Instead, the coupled cluster SE is projected onto the Hartree-Fock determinant, yielding an expression for the coupled cluster energy (E_{CC}):

$$\langle \Phi_{HF}|\hat{\mathcal{H}}|\Psi_{CC}\rangle = E_{CC}\,\langle \Phi_{HF}|\Psi_{CC}\rangle = E_{CC} \tag{5.13}$$

Expressing the left-hand side in terms of the substitution operator, the energy equation reduces to:

$$E_{CC} = E_{HF} + \sum_{i,j}\{(t_{ij}^{ab} + t_i^a t_j^b - t_i^b t_j^a)(\langle\psi_i\psi_j|\psi_a\psi_b\rangle - \langle\psi_i\psi_j|\psi_b\psi_a\rangle)\} \tag{5.14}$$

where the t_i^a and t_{ij}^{ab} are called the single and double substitution cluster amplitudes, respectively. These are similar to the CI-coefficients in that a large cluster amplitude corresponds to a large weight of the respective substituted determinant in the total coupled cluster wavefunction. The E_{CC} directly depends only on the single and double substitution amplitudes, but the amplitudes themselves depend on other amplitudes of the same order as well as on higher terms. Consequently, the coupled cluster energy can be improved by taking into account higher order substitutions. The amplitudes are solved by projecting onto determinants of the corresponding substitution order, which yields a set of equations that are solved to self-consistency.

Amplitudes of higher than second-order substitutions are extremely time-consuming to solve iteratively, because of the higher number of substituted determinants compared to singles and doubles. While full iterative methods, such as CCSDT (all amplitudes iterated up to triples),[140] may be applied for small systems, other approximations for solving high order amplitudes are usually used. The CCSD(T) method,[141] which is widely regarded as the "gold-standard" method of quantum chemistry, solves the singles and doubles amplitudes iteratively, while the triples are obtained with perturbation theory.

5.4.3 Many-Body Perturbation Theory

Many-body perturbation theory is based on the assumption that the exact solution to the SE can be approached by improving a known approximate solution with an external perturbation.[142] The exact Hamiltonian is expressed as a sum of the known approximate Hamiltonian $\hat{\mathcal{H}}^{(0)}$ and a perturbation operator $\lambda\hat{\mathcal{V}}$. Similarly, the exact wavefunctions

and their eigenvalues are expressed as corrections to the known approximate solutions. Importantly, the higher order corrections to the wavefunctions are expressed in the basis of the known approximate solutions, $\{\psi^{(0)}\}$. The solution to the perturbed SE is an infinite set of equations of increasing order of corrections. In practical applications, the corrections are truncated, most often to the second order, where the energy corrected to second order (E_{PT2}) is:

$$E_{PT2} = E_n^{(0)} + E_n^{(1)} + E_n^{(2)} = \langle\psi_n^{(0)}|\hat{\mathcal{H}}^0|\psi_n^{(0)}\rangle + \langle\psi_n^{(0)}|\hat{\mathcal{V}}|\psi_n^{(0)}\rangle + \sum_{n\neq k} \frac{|\langle\psi_n^{(0)}|\hat{\mathcal{V}}|\psi_k^{(0)}\rangle|^2}{E_n^{(0)} - E_k^{(0)}} \quad (5.15)$$

Electron correlation can be assessed with Møller-Plesset (MP) perturbation theory.[143] In this method, the unperturbed Hamiltonian is defined as the Fock-operator $\hat{\mathcal{F}}$, whose eigenfunctions are the Hartree-Fock spin-orbitals $\{\psi^{HF}\}$, and eigenvalues the spin-orbital energies ε. The perturbation operator is defined as the difference between the Born-Oppenheimer Hamiltonian and the Fock-operator, $\hat{\mathcal{V}} \equiv \hat{\mathcal{H}} - \hat{\mathcal{F}}$. Applying the perturbational corrections to the Φ_{HF} state, the second-order energy (MP2) reduces equation to:

$$E_{MP2} = E_{HF} + \sum_{i,j,a,b} \frac{|\langle\Phi_{HF}|\hat{\mathcal{V}}|\Phi_{ij}^{ab}\rangle|^2}{\varepsilon_i + \varepsilon_j - \varepsilon_a - \varepsilon_b} \quad (5.16)$$

The second-order correction to the energy involves a denominator term of orbital energy differences, which shows that the method is not directly applicable for quasi-degenerate electronic states, as for such cases some denominators would approach zero and correction term would approach infinity. Higher than second-order energy correction terms also involve denominators of energy differences between virtual orbitals, and these can yield highly divergent correction terms, especially in calculations employing diffuse basis sets.[144] Like coupled cluster method, all the MPn methods are size-extensive, but the energies are solved by projection instead of using the variational method, so the higher level corrections to energy do not systematically converge towards the exact energy.

5.5 Multi-Configurational Self-Consistent Field Method (MCSCF)

So far the discussed electron correlation methods have been based on the assumption that the ground electronic state can be approximated with the Hartree-Fock determinant, i.e., the ground state is dominated by one electron configuration. In several situations, such as during formation or dissociation of chemical bonds, and for quasi-degenerate electronic states, the single determinant assumption no longer holds and consequently the Hartree-Fock spin-orbitals are an inadequate basis for the electron correlation.

To illustrate the necessity of multiple electron configurations, consider a homolytic dissociation of a covalent chemical bond in a closed-shell molecule in a singlet state (Fig. 5.1). At the equilibrium structure, the bonding orbital σ is doubly occupied and the overall electronic state is dominated by one electron configuration (Φ_0) and the HF approximation is valid. However, the homolysis of the bond leads to formation of two radical fragments, where one of the bonding electrons moves to the corresponding antibonding orbital σ^*, resulting in an electron configuration with two singly occupied orbitals (Φ_1 and Φ_2). A single determinant with two singly occupied orbitals does not correspond to a pure singlet electronic state. To retain the spin purity, a linear combination of the two open-shell determinants (configuration state function, CSF) have to be used to describe the wavefunction (Φ_{1-2}), so at the dissociation limit the qualitative description of the electronic state requires two determinants. Moreover, between these two extrema the electronic state is a combination of all these determinants, and all of them may have a large contribution to the overall state.

The optimal wavefunction describing a collection of configurations,[d] can be constructed by combining the orbital optimization from Hartree-Fock theory (SCF) with the CI-expansion in the configuration basis. These methods are called multi-configurational self-consistent field (MCSCF) methods.[145,146] In MCSCF methods, the energy expectation value of the CI wavefunction is variationally minimized, and the variational parameters are both the CI-coefficients $\{C_i\}$ of the contributing configurations as well as the orbital coefficients $\{c_{\mu i}\}$ of the basis set.

[d] Without loss of generality, the term configuration used here instead of specifying either determinant or CSF.

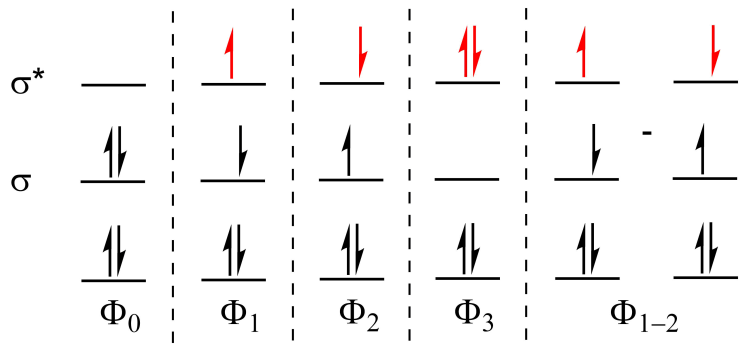

Fig. 5.1: Electron configurations involved in homolytic dissociation of a fictitious chemical bond. At equilibrium structure, the electronic state is Φ_0, where the bonding orbital σ is doubly occupied. At dissociation limit, both the σ and σ^* are singly occupied, and the electronic state is Φ_{1-2}.

In the MCSCF procedure, configurations with large C_i have individually large contributions to the overall electronic state, and consequently affect the $\{c_{\mu i}\}$. Such configurations are called strongly or statically correlated configurations, and the purpose of MCSCF is to account for at least these configurations. Configurations with small C_i have a negligible effect on $\{c_{\mu i}\}$, but these configurations are far greater in number and collectively have a large contribution to the energy. These configurations are called dynamically correlated configurations.

The $\{C_i\}$ and $\{c_{\mu i}\}$ are usually not optimized simultaneously but with an alternating scheme where the CI energy is first minimized by varying the $\{C_i\}$, and afterwards the energy is minimized with respect to the $\{c_{\mu i}\}$ with the obtained $\{C_i\}$, repeated until self-consistency.[147] Even though this decoupling of variational parameters is done, the $\{C_i\}$ and $\{c_{\mu i}\}$ can be strongly coupled for statically correlated configurations, which leads to slow trailing convergence of the MCSCF procedure. The convergence can be forced by using second-order variation methods,[148,149] but these are more costly due to energy Hessian calculations, and these methods may converge into a local minimum instead of a global energy minimum. Often MCSCF solvers begin with the cheaper first order variation methods until certain energy convergence threshold is reached and then switch into second-order variation to reach tighter convergence if necessary.

The MCSCF energy can be minimized using two ansätze, first of which is called the single-state/state-specific MCSCF (SS-MCSCF method), where the $\{c_{\mu i}\}$ are optimized

to minimize the energy of a single selected CI state. Another possibility is to minimize the energy with respect to a weighted combination of multiple states, but then the resulting orbitals are not a lowest-energy solution to any of the states individually, but a compromise between all of them. This approach is called a state-averaged MCSCF (SA-MCSCF).[145,150] The SA-MCSCF methods are beneficial for estimating excitation processes, because the SA orbitals are equally representative for all of the involved states. For targeted properties of a given electronic state, the SS-MCSCF methods are more accurate, and these were solely used in the research underlying this thesis.

As discussed in Section 5.4.1, the CI expansions are truncated to obtain computationally tractable solutions. For MCSCF wavefunctions, the need for truncations is even more evident, because the variational space is larger due to the orbital optimization; however, the number of statically correlated configurations is small and these often differ only at the occupations of the frontier orbitals of the chemical reaction of interest, or at the valence orbitals around the HOMO-LUMO gap for quasi-degenerate states. These configurations can be generated by carrying out the CI-expansion in the subspace of these orbitals. Furthermore, the size non-extensivity problem of truncated CI methods can be bypassed, if the subspace of orbitals defining the static correlation is small enough such that FCI within this subspace of orbitals can be carried out, as in the related CASCI method. The combination of the CASCI expansion with the SCF procedure is known as the complete active space self-consistent field (CASSCF) method,[151–153] which is the most often used method in MCSCF calculations.

The CASSCF method systematically generates all configurations from the subspace-FCI (hereinafter complete active space, CAS), which is ideally chosen such that each statically correlated configuration arises from the CAS expansion. The CAS method also yields configurations with small CI coefficients, so both the static correlation and some amount of the dynamic correlation are solved simultaneously, depending on the size of the CAS. The orbitals that are not within the active space, are either doubly occupied or unoccupied in all configurations, i.e., inactive internal orbitals and inactive virtual orbitals, respectively (Fig. 5.2). The inactive orbitals are essentially of HF quality, as these orbitals have same occupations in each configuration in the MCSCF procedure. The choice and size of the CAS is ambiguous, but it should include at least all the orbitals that qualitatively define the electronic state – the statically correlated orbitals. Inclu-

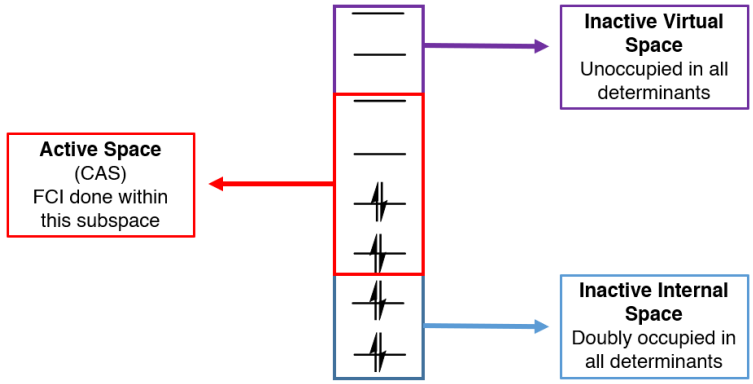

Fig. 5.2: Scheme of CAS expansion of a wavefunction.

sion of more orbitals adds more degrees of freedom to the variational solution and always corresponds to lower and hence more accurate energy, but at a rapidly increasing computational cost. The number of CSFs in the CASSCF wavefunction defined by distributing n electrons among m orbitals, notated as CASSCF(n,m), can be calculated using the Weyl's dimension formula:[154]

$$\#\text{ of CSF in CASSCF}(n,m) = \frac{2S+1}{m+1}\binom{m+1}{m-\frac{1}{2}n-S}\binom{m+1}{\frac{1}{2}n-S} \tag{5.17}$$

The scaling of the number of CSFs in terms of CAS size is illustrated in Table 5.1.

Table 5.1: The number of configuration state functions with various CAS and spin states.

Singlet, S=0		Doublet, S=0.5		Triplet, S=1	
CAS(n,m)	# CSF	CAS(n,m)	# CSF	CAS(n,m)	# CSF
CAS(2,2)	3	CAS(3,2)	2	CAS(2,2)	1
CAS(4,4)	20	CAS(5,4)	20	CAS(4,4)	15
CAS(6,6)	175	CAS(7,6)	210	CAS(6,6)	189
CAS(8,8)	1764	CAS(9,8)	2352	CAS(8,8)	2352
CAS(10,10)	19404	CAS(11,10)	27720	CAS(10,10)	29700
CAS(12,12)	226512	CAS(13,12)	339768	CAS(12,12)	382239
CAS(14,14)	2760615	CAS(15,14)	4294290	CAS(14,14)	5010005
CAS(16,16)	34763300	CAS(17,16)	55621280	CAS(16,16)	42474432

There are plethora of other widely used MCSCF methods such as restricted active space SCF (RASSCF),[155] generalized active space SCF (GASSCF),[156] and adaptive sam-

pling configuration interaction SCF (ASCI-SCF).[157,158] The RASSCF and GASSCF methods are similar to CASSCF, but the active space is further partitioned into subspaces. In RASSCF, the active space is partitioned to three parts: RAS1 corresponds to occupied orbital space, from which a predefined maximum number of substitutions are allowed, RAS2 is analogous to CAS such that FCI is carried out within it, and RAS3 is an unoccupied virtual orbital space that allows for predefined maximum number of electrons within it. GASSCF differs from RASSCF only in that the number and types of subspaces are arbitrary and chosen at will. The purpose of RAS and GAS expansions is to tackle larger active spaces, while avoiding the exponential scaling of the full CAS. In the ASCI method the CI solution is calculated with a predefined CAS, but the adaptive sampling only keeps configurations with coefficients larger than given threshold value, so the method can be tuned to account either only for strongly correlated configurations or for additional dynamically correlated configurations as long as the solution is computationally tractable.

5.6 Electron Correlation Methods for Multiconfigurational Wavefunctions

The MCSCF wavefunction accounts for more configurations than the Hartree-Fock wavefunction, but it does not necessarily yield much improved electronic energies or other molecular properties, because the dynamic electron correlation is largely not accounted for. For a multiconfigurational state, the dynamic correlation can also be solved with perturbation theory, configuration interaction, and coupled cluster methods. Examples of such methods (multireference methods, MR) will be discussed in more detail below.

The research underlying this thesis made excessive use of various MR methods, such as complete active space second-order perturbation theory (CASPT2),[159,160] its ionization potential - electronic affinity (IPEA) shifted variant (CASPT2-IPEA),[161] and N-electron valence state second-order perturbation theory (NEVPT2).[162–164] Other used MR methods were extended multiconfigurational quasi-degenerate second-order perturbation theory (XMC-QDPT2)[165] and multireference configuration interaction (MRCI).[166–168] The XMC-QDPT2 method was used solely in its state-specific form, which is exactly equivalent to the multireference second-order Møller-Plesset method (MR-MP2),[169] which will be briefly introduced along the more detailed discussion of the CASPT2 method. The

multi-state XMC-QDPT2 theory and MRCI methods will not be discussed in detail.

5.6.1 First-Order Interacting Space, FOIS

A concept central to all MR methods is the definition of a first-order interacting space (FOIS) – the multiconfigurational reference state and all configurations that have non-vanishing Hamiltonian matrix elements with the reference.[170] The FOIS can be defined *a priori* from the results of the single-reference correlation theories. As an example, the first-order wavefunction required for the second-order energy in perturbation theory depends only on the Hamiltonian matrix elements of the reference state and doubly substituted configurations. The substituted configurations can be expressed in terms of either uncontracted configurations (UC) or internally contracted configurations (IC).[166,171] Consider the nth root of a CAS-type MCSCF wavefunction $\{\Psi_n^{(0)}\}$ as the reference state:

$$|\Psi_n^{(0)}\rangle = \sum_r^{CAS} C_{rn} |\Phi_r\rangle \tag{5.18}$$

which is a linear combination of all the configurations (Φ_r) arising from the CAS expansion multiplied by their respective CI-coefficients $\{C_{rn}\}$ for the nth state. The FOIS is formed by generating the substituted configurations by applying substitution operator $\hat{E}$ of appropriate order to the $|\Psi_n^{(0)}\rangle$. In the UC scheme, the substitutions are carried out for all the constituent configurations individually ($\hat{E}|\Phi_r\rangle$), and in the IC scheme the substitution operator acts directly on the reference state as a whole ($\hat{E}|\Psi_n^{(0)}\rangle$). Furthermore, if all types of substitutions are carried out using the IC scheme, the method is referred to as fully internally contracted (FIC),[172] and if some substitutions are uncontracted, then the method is partially contracted (PC).[173] Internal contractions are computationally much more efficient, but less flexible variationally than uncontracted methods. Moreover, FIC methods are closer to size-consistency, because the FIC scheme spans the FOIS exactly, while uncontracted and partially contraction schemes include functions outside the FOIS.[174]

5.6.2 Multireference Perturbation Theory

The CASPT2, CASPT2-IPEA, and NEVPT2 methods are briefly presented. These methods follow so-called "diagonalize then perturb" procedure, where the zeroth-order reference wavefunction is first obtained with CASSCF procedure, and then the solution is per-

turbed to calculate the dynamic correlation. The CASPT2, CASPT2-IPEA, and NEVPT2 methods are presented below only at their state-specific formalism, details of their state-averaged extensions, MS-CASPT2, QD-NEVPT2, can be found elsewhere.[175,176]

CASPT2

The premise of the CASPT2 method is to generalize the second-order Møller-Plesset (MP2) theory for multiconfigurational reference state: the zeroth-order Hamiltonian $\hat{\mathcal{H}}_0$ is defined as a one-electron Fock-type operator, the perturbation operator $\hat{\mathcal{V}}$ defined as the difference between BO Hamiltonian and $\hat{\mathcal{H}}_0$ ($\hat{\mathcal{V}} \equiv \hat{\mathcal{H}} - \hat{\mathcal{H}}_0$), and the higher-order corrections to the wavefunction are constructed from the zeroth-order basis. The energy corrections up to second-order are

$$E_n^{(0)} + E_n^{(1)} = \langle \Psi_n^{(0)} | \hat{\mathcal{H}}_0 | \Psi_n^{(0)} \rangle + \langle \Psi_n^{(0)} | \hat{\mathcal{V}} | \Psi_n^{(0)} \rangle \qquad \text{and} \qquad E_n^{(2)} = \sum_{m \neq n} \frac{| \langle \Psi_n^{(0)} | \hat{\mathcal{V}} | \Psi_m^{(0)} \rangle |^2}{E_n^{(0)} - E_m^{(0)}} \tag{5.19}$$

where $\{\Psi_m^{(0)}\}$ are doubly substituted configurations. Any of the CI-states $\{\Psi_n^{(0)}\}$ from the CAS may be chosen as the reference. CASPT2 employs internally contracted FOIS, while related MR-MP2 uses fully uncontracted FOIS, otherwise the methods are equivalent. The FOIS required for second-order energy correction is divided into three subspaces $V_n, V_K,$ and V_{SD}, which are the reference CAS state $|\Psi_n^{(0)}\rangle = V_n$, all the other roots of the CASSCF solution $\sum_{k \neq n} |\Psi_k^{(0)}\rangle \in V_K \perp V_n$, and the singly and doubly substituted configurations from the reference state $\in V_{SD}$.[e] The V_{SD} subspace is further divided into eight double substitution classes, which are shown in Fig. 5.3. The MP2 theory cannot be extended directly to MR case, because multiconfigurational wavefunctions are not eigenfunctions of the one-electron $\hat{\mathcal{F}}$ operator,[177] which defines the $\hat{\mathcal{H}}_0$ in MP2. In CASPT2 and MR-MP2, the zeroth-order Hamiltonian is redefined such that the reference state and all the interacting states are simultaneous eigenstates of the $\hat{\mathcal{H}}_0$. This is done by projecting the $\hat{\mathcal{F}}$ onto the reference state and to all the other interacting states:

$$\hat{\mathcal{H}}_0^{MR-MP2} \equiv \hat{\mathcal{P}}_n \hat{\mathcal{F}} \hat{\mathcal{P}}_n + \hat{\mathcal{P}}_k \hat{\mathcal{F}} \hat{\mathcal{P}}_k + \hat{\mathcal{P}}_{SD} \hat{\mathcal{F}} \hat{\mathcal{P}}_{SD}, \qquad \hat{\mathcal{P}}_i = \sum_i |\Psi_i\rangle \langle \Psi_i| \tag{5.20}$$

[e] If the orbitals involved in the substitution are all active orbitals, the substitution belongs to V_k instead of V_{SD}

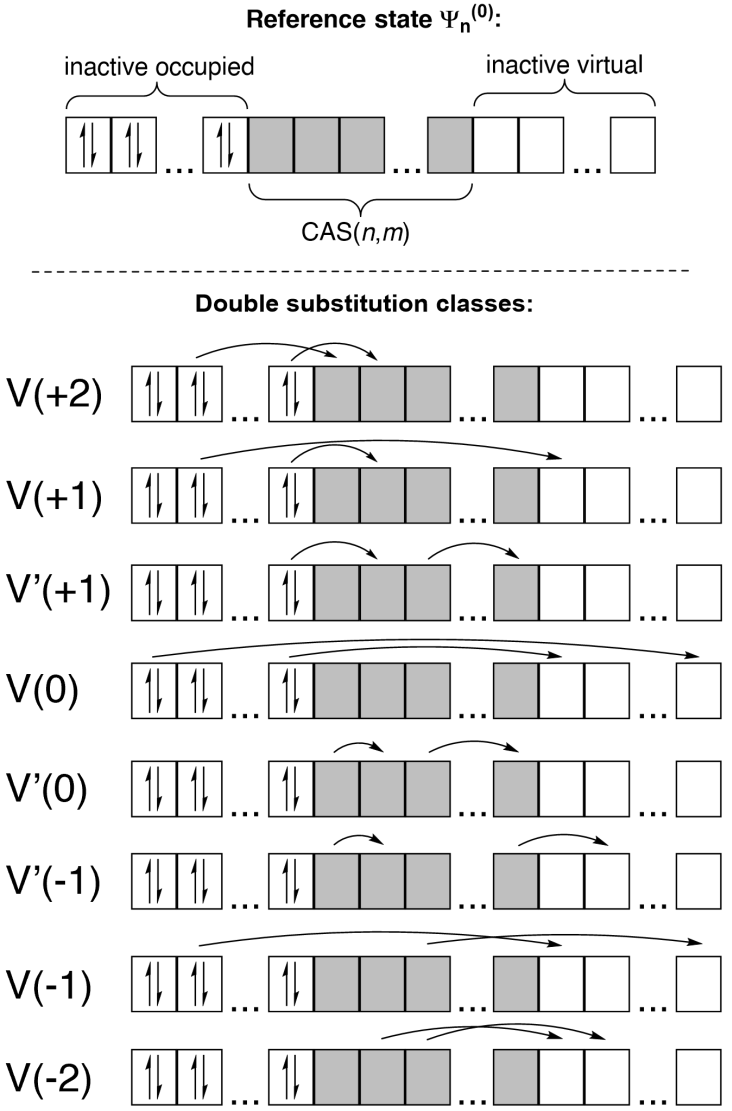

Fig. 5.3: First-order interaction space in multireference second-order perturbation theory. The values in brackets show how many electrons are introduced/removed from the active space in the substitution, primed classes (V') involve substitutions within the active space.

If the reference state is a single configuration, the $\hat{\mathcal{H}}_0$ reduces to the MP Hamiltonian, and the single-reference MP method is obtained.

The second-order energy correction terms (eqn 5.19) in non-degenerate perturbation theories are sensitive to so-called intruder states, which arise when another state becomes close in energy with the reference state. In such cases the energy denominator $\Delta E_{nk} = E_n^{(0)} - E_k^{(0)}$ approaches zero, and the second-order energy correction approaches singularity. There are various techniques to avoid the intruder states, the easiest way (if affordable) would be to incorporate the intruder states into the reference function, so the intruding energy denominators do not emerge at all.[178] Another way to avoid small denominators is by using level-shifting techniques,[179,180] where an additional term is added to the denominator, such that even for degenerate states the denominator is non-zero. There are two kinds of level shifts: a real level shift,[179] which adds a constant parameter ε to each evaluated denominator, and a so-called imaginary level shift $\varepsilon^2/\Delta E_{nk}$,[180] which is inversely proportional to the unshifted energy denominator. Real level shifts systematically lead to overestimated energy corrections, while imaginary shifts only have sizable effect for quasi-degenerate denominators, such that the overall perturbational energy correction is less affected by the shift.

As mentioned before, the multiconfigurational wavefunction is not an eigenfunction of a one-electron operator, because the CAS space is bielectronic, i.e., active space orbitals are eigenfunctions of a two-electron operator. The inactive orbitals of the MC-SCF wavefunction (always doubly occupied + virtual unoccupied) are eigenfunctions of the Fock-operator. When a substitution is done either into or from partially occupied orbital (active space orbital), the corresponding energy denominator involves both inactive/virtual orbital energies and CAS orbital energies, which is ill-defined. The poorly defined denominators reduce the accuracy of absolute energies, but relative energies can be accurate due to error-cancellation. However, the error-cancellation only applies if the static correlation does not change drastically during the simulated process. For processes where the static correlation changes, such as during bond homolysis, CASPT2 is not suitable.[181] CASPT2 has been found to yield atomization energies and homolytic dissociation energies that are systematically too low in comparison to experimental values. Moreover, the underestimation scales by 2–5 kcal mol^{-1} for each emerging unpaired electron in the dissociation process,[181] so other methods should be used for studying nonisogyric reac-

tions.

CASPT2-IPEA

A variant of CASPT2, known as CASPT2-IPEA was developed to reproduce more accurate homolytic dissociation energies.[161] The IPEA term stems from the generalized Koopmans' theorem,[182,183] which states that the diagonal elements of the generalized Fock matrix (orbital energies) correspond to negative ionization potentials (IP) for occupied orbitals and to negative electron affinities (EA) for virtual orbitals. In this framework, the CAS orbital energies are weighted averages of IP and EA, because these orbitals are neither fully occupied nor empty. The purpose of CASPT2-IPEA method is to shift the CAS orbital energies away from the average towards EA, when a substitution introduces an electron in an active orbital, and towards IP, when the substitution is from an active orbital, such that the interpretation of the CAS orbital energies are more consistent with the Koopmans' theorem, and the related denominator terms are consequently less erroneous. The orbital energy shifting is done by introducing a parameter, which depends on the energy difference IP-EA shift. The definition of individual IP and EA values for the CAS orbitals is not clear, so the CASPT2-IPEA method employs a single shift value for all denominators involving CAS orbitals. The optimal shift value is purely empirical, and varies for different reactions, and should be benchmarked against either experimental or more accurate theoretical values, if possible.[184] The IPEA shift also alleviates intruder state problems present in CASPT2, although it is not its original purpose.[178]

NEVPT2

In NEVPT2 method, the zeroth-order Hamiltonian with respect to the active orbital space is redefined such that its two-electronic structure is taken into account. This is done by Dyall's partitioning of the Hamiltonian:[185]

$$\hat{\mathcal{H}}_0^D = \hat{\mathcal{H}}_i^D + \hat{\mathcal{H}}_a^D + \hat{\mathcal{H}}_v^D \tag{5.21}$$

where the first and last terms are one-electron Fock-type operators that interact with the inactive and virtual orbitals respectively, and the $\hat{\mathcal{H}}_a^D$ term is an exact two-electron Hamiltonian for the active subspace. In the full-active space limit, this term is equal to the FCI Hamiltonian. A multiconfigurational wavefunction is also a true eigenfunction of the

Dyall Hamiltonian ($\hat{\mathcal{H}}_0^D$), meaning that it does not need to be projected onto the MCSCF state and its interaction space separately. Apart from the definition of $\hat{\mathcal{H}}_0$, CASPT2 and NEVPT2 methods are very similar, both relying on internally contracted FOIS.

The benefit of NEVPT2 over CASPT2 and all its variants, is that it is completely free of parameters, and far less susceptible for intruder state problems. In general, NEVPT2 and CASPT2-IPEA yield comparable dissociation energies and excitation energies,[186,187] and the latter can be tuned with the IPEA shift.

5.7 Density Functional Theory

The wavefunction theory states that all information of a quantum system is described by its wavefunction. However, according to the first Hohenberg-Kohn (HK) theorem, all information pertaining to ground electronic states are also contained in the electron density function ρ.[188] The second HK theorem states that the minimum of the energy density functional $E[\rho]$ corresponds to the true ground state electron density, and that a variationally obtained minimum of the energy functional is an upper-bound to the exact energy. These two theorems are the basis of the density functional theory (DFT). One way to obtain solutions for $E[\rho]$ is by using the Kohn-Sham method (KS-DFT),[189] where the electron density function is approximated with a determinant of non-interacting one-electron spin-orbitals $\{\psi_i\}$ that have the same electron density as the true system of interacting electrons.[f] In KS-DFT framework, the exact energy functional is

$$E[\rho] = T_{KS}[\rho] + U_{ne}[\rho] + J_{ee}[\rho] + V_{xc}[\rho], \qquad \text{where} \qquad \rho = \sum_i^N n_i |\psi_i|^2 \tag{5.22}$$

where the $T_{KS}[\rho]$ term is the kinetic energy of the non-interacting particles, $U_{ne}[\rho]$ the nuclei-electron attraction potential, $J_{ee}[\rho]$ the Coulombic self-interaction of the electron density, and $V_{xc}[\rho]$ the exchange-correlation term. The first three terms are trivially solvable, but the exact form of the $V_{xc}[\rho]$ term is not known. This term ideally corrects for all approximations made in the kinetic energy term, electron-electron self-interaction, and in exchange interactions. In contrast to wavefunction methods, there is no systematic way of approaching the exact functional in KS-DFT, even though justified improvements on the exchange-correlation term can be made.

[f] These orbitals are identical to the spin-orbitals used in wavefunction methods, both methodologies can use the same basis sets.

The various DFT methods, known as DFT functionals, are otherwise identical but have different ways for approximating the $V_{xc}[\rho]$ term. Popular DFT functional types include generalized gradient approximation (GGA) functionals,[190,191] meta generalized gradient approximation (meta-GGA) functionals,[192,193] global hybrid GGA and meta-GGA functionals,[194,195] and range-separated hydrid functionals.[196] The GGA methods approximate the $V_{xc}[\rho]$ term as a function of the ρ and its gradient $\nabla\rho$,[190] which accounts for the non-uniformity of the electron density in molecular systems. The meta-GGA methods include also the Laplacians of the electron density $\nabla^2\rho$. In global hybrid methods, a fixed fraction of the exchange energy is calculated with Hartree-Fock instead of DFT exchange. In range-separated hybrid methods, the amount of HF-exchange is distance dependent. At short distance, the exchange is more DFT-like, but the HF-exchange contribution increases with distance.

The DFT functionals include short-range dynamic electron correlation by design, but long-range correlation effects are neglected. These effects can be accounted for by using empirical dispersion corrections,[197,198] which enable more accurate description of weakly bound systems, such as intermolecular complexes. Due to the partial inclusion of electron correlation at a fraction of the computational cost of post-HF methods, DFT methods are great for calculating ground-state structures and properties, whenever suitable. However, the KS-DFT is a single determinant approximation for the ground state electron density, and has similar limitations for its applicability as the HF method, i.e., is not suitable for strongly correlated systems, for which the multiconfigurational methods are required. There are also multiconfigurational variants of DFT methods, such as multiconfigurational pair-density functional theory (MC-PDFT),[199] where the MCSCF method is used for assessing the static correlation and DFT is used for the dynamic correlation.

In the research underlying this thesis, DFT methods were used to obtain initial molecular structures for further calculations, like single-reference electron correlation calculations or multireference calculations. The DFT methods most extensively used in this thesis work were B3LYP,[200,201] M06-2X,[202] and ωB97X-D3,[203] which are hybrid-GGA, hybrid meta-GGA, and range-separated hybrid functionals, respectively.

5.8 Thermodynamics and Kinetics

In computational studies of chemical reactions, the most valuable results of electronic structure calculations are the nuclear energies and electronic energies, which are used to map the PES of the reactions. These surfaces can be used to estimate qualitatively, whether certain chemical reactions are feasible or not. However, even at absolute zero temperature, the total energies of molecular systems depend on their vibrational energy structure. Furthermore, at finite temperature, also rotational and translational energies contribute to the energy; therefore, to describe any real reaction system theoretically, the aforementioned contributions to the total energy need to be accounted for.

5.8.1 Molecular Vibrations and Thermochemical Analysis

At the stationary points on the molecular PES, where the gradient of the potential energy is zero, the molecular vibrations can be treated with the quantum harmonic oscillator model, where the vibrational energies are obtained from the molecular Hessian – the second derivative matrix of the potential energy as a function of the $3N$ Cartesian nuclear coordinates. Thereafter, the Hessian is mass-weighted with respect to the nuclear masses of the system and diagonalized to obtain $3N$ orthogonal eigenvectors. Of these vectors, 6 (5 for linear molecules) describe the translational and rotational degrees of freedom, while the rest are known as the vibrational normal modes, whose eigenvalues are proportional to the vibrational energies. The energy of the lowest vibrational state is known as the zero-point vibrational energy (ZPVE). The sum of ZPVEs and the nuclear energy and electronic energy of the system (E+ZPVE) defines the lowest possible internal energy of the system.

At finite (i.e., non-zero) temperatures, thermal contributions by vibrations, rotations, and translations are calculated with statistical mechanics. The rotations are usually treated with the rigid-rotor model, and translations with the ideal gas model. The usual vibrational and rotational models (rigid-rotor harmonic oscillator, RRHO) can be improved if the corresponding fine-structure is of particular interest. This can be done for example by accounting for the anharmonicity of the vibrations, or motions that resemble rotations with free or hindered rotor models. The internal energies (U), enthalpies (H), entropies (S), and Gibbs energies (G) obtained with statistical mechanics are used to

predict the spontaneity of chemical reactions and are essential in the study of theoretical chemical reaction kinetics.

5.8.2 Reaction Kinetics

The rates of chemical reactions can be estimated with the thermodynamically corrected reaction potential surfaces. The kinetic rate laws relate the reaction specific rate coefficients and the concentrations of the participating reactants with the rate of the chemical reaction. The rate coefficient depends on the available thermal energy of the reacting molecules and the thermodynamical features of the reaction potential surface.

A simple, but often used approximation for calculating the rate coefficients, is the transition state theory (TST),[204–206] which estimates the rate coefficients as a product of an encounter frequency, which depends, e.g., on the temperature and the reaction molecularity, and an exponential Boltzmann factor, which describes the fraction of the reaction system that is able to attain energy equal to energy state E_i with respect to a lower energy reference state E_j. In TST, the reference energy E_j corresponds to the energy level of the reactants, and the E_i to the energy of a saddle-point that connects the reactants to products, so the energy difference $E_i - E_j$ is the minimum energy required for the reaction to occur ($\Delta E^\ddagger$), and the Boltzmann factor describes the probability of this event. It is convenient to express the Boltzmann factor in terms of Gibbs energies (G) instead of electronic energies (E), because then the TST rate coefficient equation does not explicitly depend on partition functions:

$$k(T) = \kappa \frac{k_B T}{h} \times (\rho^\ominus)^{1-M} \times \exp\left(-\frac{\Delta G^\ddagger}{k_B T}\right), \text{where} \qquad \rho^\ominus = \frac{p^\ominus}{k_B T} \tag{5.23}$$

where $k(T)$ is the temperature (T) dependent rate coefficient, κ the transmission coefficient, k_B Boltzmann's constant, h Planck's constant, $\rho^\ominus$ the volumetric number density of ideal gas at a reference pressure $p^\ominus$, M the reaction molecularity, and $\Delta G^\ddagger$ the quasi-thermodynamic Gibbs energy of activation.[g] The value of the transmission coefficient is usually assumed as unity, except for reactions where reaction barrier widths are narrow enough for quantum tunnelling to enhance the reaction rates. This condition usually only applies for dissociation or isomerization reactions involving hydrogen atoms. The tunnelling coefficients can be estimated with various tunnelling models, such as Eckart

[g]Quasi-thermodynamic means that the motion corresponding to the reaction coordinate is excluded.

potential approximation.[207]

Apparent limitations of the TST approach is that it is well defined only for reactions with saddle points in the Gibbs energy surface ($\Delta G^{\ddagger} > 0$), and the exponential part of the rate coefficient equation assumes that whenever the system has energy larger than $\Delta G^{\ddagger}$, the reaction is certain to occur, which is not true. Even if the value of $\Delta G^{\ddagger}$ is exactly correct, the rate coefficient is larger than in reality; therefore, the TST rate coefficient should be regarded as an upper-limit. To estimate rate coefficients for barrierless reactions, more sophisticated methods, such as variational TST,[208–210] are required to obtain reliable results.

Chapter 6

Practical Guidelines for Carrying Out Multireference Calculations

6.1 Do you really need to use MR methods?

If the answer to the question above turns out to be no, then you probably should not use multireference methods, because acquiring good results with them often requires a lot of trial and error, and you might even obtain more accurate results with other methods that are considerably easier to use. There are multiple ways to diagnose the electronic structure of the system of interest before doing any sort of multireference treatments. Many of these diagnostics rely on comparing the accuracy or weight of the one-determinant reference approximation to the magnitude of post-HF corrections. The larger these corrections are, the worse the single-determinant approximation is. Simple diagnostics such as the $\mathcal{T}_1$, $\mathcal{D}_1$, and $\%\mathrm{TAE}_e[(\mathrm{T})]$ diagnostics,[211–213] can be obtained using the output of a few CCSD(T) calculations.

The $\mathcal{T}_1$ diagnostic is based on the magnitude of the t_1 amplitudes, which in turn express how much singly substituted configurations contribute on average to a total CC wavefunction. These amplitudes can be obtained from any CC calculation of at least CCSD quality. The $\mathcal{T}_1$ is defined as the Frobenius norm of the t_1 amplitudes divided by the square-root of the total number of electrons that are substituted in the CCSD expansion. Generally, $\mathcal{T}_1$ values smaller than 0.02 demonstrate that the Hartree-Fock reference is qualitatively appropriate and that the corrections provided by the CCSD expansion are minor. Larger values mean that singly-substituted configurations have a

substantial contribution to the overall state, and that the electronic state may be strongly correlated. The $\mathcal{D}_1$ value is defined as the maximum of the matrix 2-norm of the t_1 amplitude-matrix. Large $\mathcal{D}_1$ value (≥ 0.02) means that there are some singly-substituted configurations that are very strongly correlated with the reference, again suggesting for static correlation. Similar diagnostics also exist for double-substitution amplitudes,[214] and the recommended threshold values for these are bit more forgiving, because double-substitutions tend to have larger contributions to the CC wavefunctions than single-substitutions. It is important to emphasize that the mentioned limit values are based on empirical observations, so blindly following these thresholds is not necessarily a great idea.

The %TAE[(T)] diagnostic, i.e., the perturbative triples contribution to the total electronic atomization energy is another way for assessing the need for multireference methods. The %TAE[(T)] value requires CCSD and CCSD(T) energies for the system of interest as well as for its constituent atoms:

$$\%\mathrm{TAE_e[(T)]} = \frac{\mathrm{TAE_e[CCSD(T)]} - \mathrm{TAE_e[CCSD]}}{\mathrm{TAE_e[CCSD(T)]}} \times 100 \tag{6.1}$$

where the TAE_e are calculated from the atomization energies at the corresponding level of theory. For example, the total atomization energy for $C_xH_yO_z$ molecule is defined as:

$$\mathrm{TAE_e(C_xH_yO_z)} = \mathrm{xE_e(C)} + \mathrm{yE_e(H)} + \mathrm{zE_e(O)} - \mathrm{E_e(C_xH_yO_z)} \tag{6.2}$$

It has been shown that the size of the %TAE[(T)] values are proportional to the magnitudes of t_4 and t_5 amplitudes.[213] For electronic states dominated by a single electron configuration, the correlation energy is usually almost converged already at the (T) level. However, %TAE[(T)] values larger than 2% suggest the opposite, which means that the electronic state is statically correlated and converging the correlation energy would require either multiconfigurational expansion of the reference state or energy contributions from higher than third-order CC substitutions, which are practically unobtainable for other than very small systems. In other words, "moderately multireference" systems can be treated with single-reference coupled-cluster calculations, if these higher-order terms, or approximations to these terms, are computationally feasible to obtain.

The $\mathcal{T}_1$, $\mathcal{D}_1$ and $\%\mathrm{TAE}_e$[(T)] diagnostics provide numbers that can be used to assess the need for multireference methods, but they do not easily demonstrate how the electronic

state is correlated; however, the strongly correlated areas of the molecule can be visualized by plotting the fractional occupation number weighted electron density (FOD),[215] which can be obtained with finite-temperature DFT calculations. Details of the finite-temperature DFT methods are beyond the scope of this work, further information is provided elsewhere.[216]

If all or some of the diagnostics discussed above indicate that using multireference methods would be beneficial or necessary, the next two sections discuss general guidelines for where to start and how to solve some of the issues that will inevitably occur with these methods.

6.2 Constructing the Multiconfigurational Reference Wavefunction

The selection of the configuration space is likely the most time-consuming part of multireference calculation workflow, but arguably the most important. The CASSCF method can be recommended as a default approach, due to its ease of use and robustness. The CASSCF method involves the construction of the CAS, which in practice is formed by selecting a set of orbitals most representative to the studied problem. For studying chemical reactions, where bonds are formed or broken, this orbital set should include at least all the bonding and antibonding orbitals of the chemical bonds relevant for the reaction. For simulating excitation processes, the orbitals involved are often those around the HOMO-LUMO gap.

Usually, the CASSCF calculations are preceded by calculations with another method, such as KS-DFT, that is used to generate preliminary orbitals that can be visualized to aid in the selection of the CAS. These calculations yield canonical molecular orbitals, which are delocalized across the whole body of the molecule, and therefore offer little guidance in CAS selection; however, these orbitals can be transformed into natural orbitals (NOs), which are localized around specific bonds or non-bonding lone pairs of the system. The NOs are similar to the valence-bond theory representation of molecular electronic structure, which is more familiar to chemists. Another benefit of the NOs is that their eigenvalues correspond to electron occupation numbers, which becomes very useful in interpreting the results of a CASSCF calculations, as will be discussed shortly.

The programs that carry out CASSCF calculations usually require that the active orbitals are ordered in a sequence around the HOMO-LUMO gap. As an illustrative example, consider a CAS(4e,4o) calculation for a singlet state. The program initially considers that the orbitals of the preceding calculation represent a closed-shell structure, therefore the 4 electrons in 4 orbitals requirement is fulfilled by choosing the HOMO and HOMO-1 as doubly occupied orbitals (2 orbitals, 4 electrons) with LUMO and LUMO+1 as unoccupied orbitals (2 orbitals, 0 electrons). However, these orbitals may not be the orbitals desired to be included in the CAS, so the actual active orbitals must be moved or "rotated" into these specific orbital indices before the CASSCF procedure. After the CASSCF optimization, the natural orbitals corresponding to the active orbitals should be inspected again to verify that they are indeed the orbitals that were selected.

Like mentioned, the eigenvalues of the NOs are electron occupation numbers. For usual HF or DFT calculations these are integer values of either 0, 1, or 2, depending on whether the orbitals are unoccupied, singly occupied, or fully occupied. The natural orbitals corresponding to optimized CAS orbitals have non-integer occupation numbers. These values are useful in deciding whether the orbitals included in the active space contribute to the static correlation or not. If the value is close to an integer, it means that in the configurations that have large contribution to the total CASSCF wavefunction, the occupation of the specific natural orbital is almost always the same, and consequently, almost same wavefunction could be obtained by having that orbital in the inactive space instead. Such orbitals are called weakly correlated orbitals. As a general guideline, orbitals with natural orbital occupations of 0.02–1.98 demonstrate substantial contribution to the static correlation,[217] and these should be included into the active space, if feasible.

6.3 Stability of the Multiconfigurational Reference Wavefunction

For studying chemical reactions, the method for generating the reference wavefunction should be deterministic, meaning that the electron configurations included are always the same, independent of the geometry of the system. This ensures that all the obtained points in the reaction potential surface are comparable and that the potential is continuous. Unfortunately, it is quite common that the active space composition changes during

the simulated processes. This can be verified by inspecting the NOs and realizing that some of the orbitals in the active space are not the ones that should be in there. The changes that occur in the active space composition are related to the CASSCF energy optimization problem. In the CASSCF method, the orbital coefficients and the CI coefficients are constantly being reoptimized throughout the calculations to reach the lowest energy solution. Sometimes it occurs that an orbital that was statically correlated in the beginning, becomes weakly correlated during the simulated process. As a result, the optimization algorithm decides to exchange that orbital with another orbital from the inactive orbital space, aiming to reach a lower energy solution. An example of a process where this behaviour can be observed is the hydrogen abstraction reactions by O_2, where the O_2 forms HO_2. The change in the static correlation, i.e., in the occupation numbers of the frontier orbitals of $O_2 \longrightarrow HO_2$ process is illustrated in Fig. 6.1. In this reaction, the hydrogen atom interacts with one of the π^*-orbitals of O_2 to form a bond, which is observed as the change of occupation number from 1.04 to 1.98. Consequently, the corresponding π-orbital of O_2 localizes on one oxygen atom and transforms into a p-type lonepair. During the bond-formation process, this localization causes the orbital to become weakly correlated, and ultimately it exchanges with an s-type inactive orbital (not shown in Fig. 6.1), leading to the transformation of the active space.

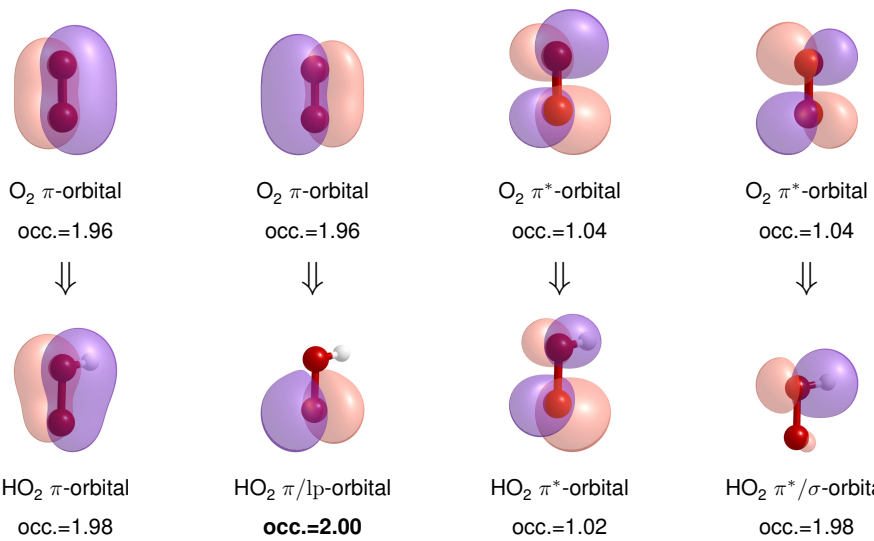

Fig. 6.1: Evolution of the static correlation in the frontier orbitals of $O_2 \longrightarrow HO_2$ reaction.

Fortunately, there are strategies to prevent or reduce these unwanted transformations.

After obtaining the wanted active space, the energies of the internal inactive orbitals can be shifted down in energy with respect to the lowest energy active orbital, or the virtual inactive orbitals can be shifted up with respect to the highest energy active orbital. These level-shifts create an energy separation between the inactive-active-virtual spaces, which helps to preserve the active space composition; however, level shifts should be used cautiously, because they often enforce convergence also with bad or ill-defined active spaces. Sometimes not being able to reach reasonable energy convergence with a certain active space composition is a sign of a poor active space design.

Another way to get around the orbital-rotations is to include the orbitals that cause the unwanted rotations into the active space. This naturally increases the active space size, and makes the calculation more expensive, but also makes the resulting wavefunction more accurate. Lastly, it is noteworthy to mention that rotations within the different orbital subspaces do not change the CASSCF wavefunction or affect the dynamic correlation energies calculated with any state-specific method, such as CASPT2 or NEVPT2. However, certain state-averaged dynamical correlation methods, such as MS-CASPT2 and MC-QDPT are not invariant with respect to orbital-rotations within the active space, but their newer "extended" versions (XMS-CASPT2 and XMC-QDPT) do not suffer from this problem.[218]

Chapter 7

Results and Discussion

7.1 Publication I

The premise of the publication **I** was that the theoretical modeling of the reaction pathways connecting the peroxyl radicals to the tetroxide intermediate and further to the experimentally observed products had proven extremely difficult and unsolved problem for quantum chemistry.[219] This is because both the association reaction and the decomposition reactions involve open-shell electronic structures (Fig. 7.1), whose accurate description requires multireference electronic structure methods. This requirement was first realized back in 2003 in a study by Ghigo et al.[79], where they investigated the self-reaction of methylperoxyl radicals using CASSCF and CASPT2 methods (see Sections 5.5 and 5.6.2 for details of these methods). The same study was also the first to suggest that an intersystem crossing (ISC) in the decomposing tetroxide ($RO \cdots O_2 \cdots OR'$) is required to facilitate the formation of the ROOR' products and ground state carbonyl compounds in the HAT reactions between the alkoxyl radicals. These ISC processes and related product formation reactions have been studied in detail in our research group (publications **IV**, **V**, **VI**, and **IX**).

In publication **I**, we studied the association and decomposition reactions with a larger selection of atmospherically relevant model compounds (Fig. 7.3) using multireference methods. For the most part, we adopted the methodology from Ghigo et al.,[79] such that the stationary structures along the reaction potentials were obtained using the CASSCF method, using the same CAS(10,8) active space (Fig. 7.2), but the dynamical electron correlation at the relevant stationary structures was addressed with XMC-QDPT2 method

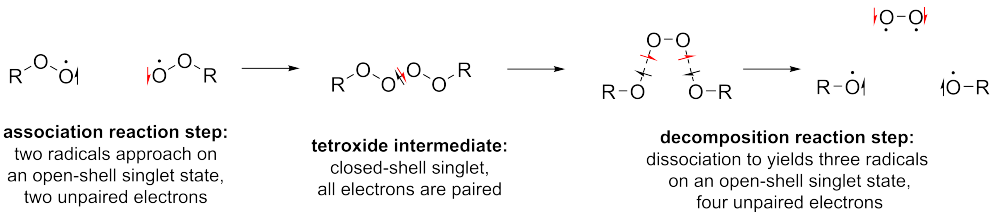

Fig. 7.1: Schematic of the electronic structures involved in the formation and decomposition of the tetroxide intermediate, black and red arrows represent electrons with opposite spins.

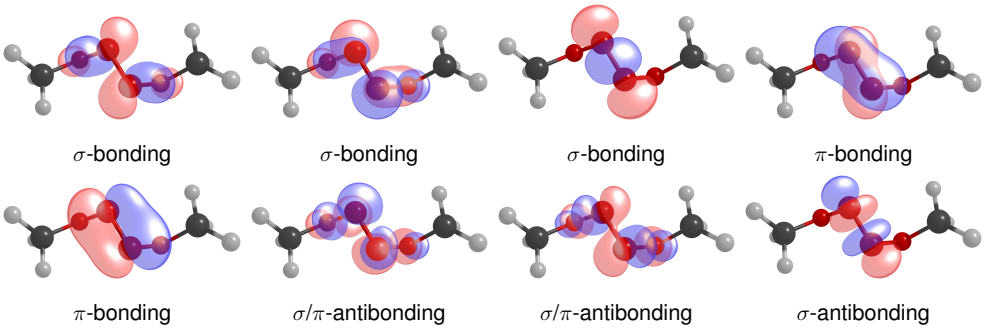

Fig. 7.2: Natural orbitals corresponding to the optimized CAS(10,8) orbitals, $[CH_3O\cdots O_2\cdots OCH_3]$ decomposition transition state structure.

instead of CASPT2. The CASSCF and XMC-QDPT2 calculations were done using Firefly software version 8.20.[220]

One of the key results from the study was that while the CASSCF(10,8) method can be used to produce qualitatively correct electronic structures, both the molecular structures and absolute energies are strongly affected by dynamical correlation. This was manifested in the relative energy differences of the stationary points when comparing CASSCF energies and XMC-QDPT2 single-point corrections on the CASSCF stationary points (Table 7.1). For example, the XMC-QDPT2 results show that for some systems the formation and decomposition transition states are below the tetroxide intermediate in energy. However, the most alarming discrepancies between CASSCF and XMC-QDPT2 were the relative energy differences of the tetroxide intermediate, the reactants, and the dissociation products. CASSCF results suggested that the decomposition is exoergic with respect to the tetroxide by 12–24 kcal mol^{-1}, depending on the system, while the XMC-QDPT2 single-point corrected CASSCF stationary points show that the dissociation products are systematically above the tetroxide in electronic energy, with the largest

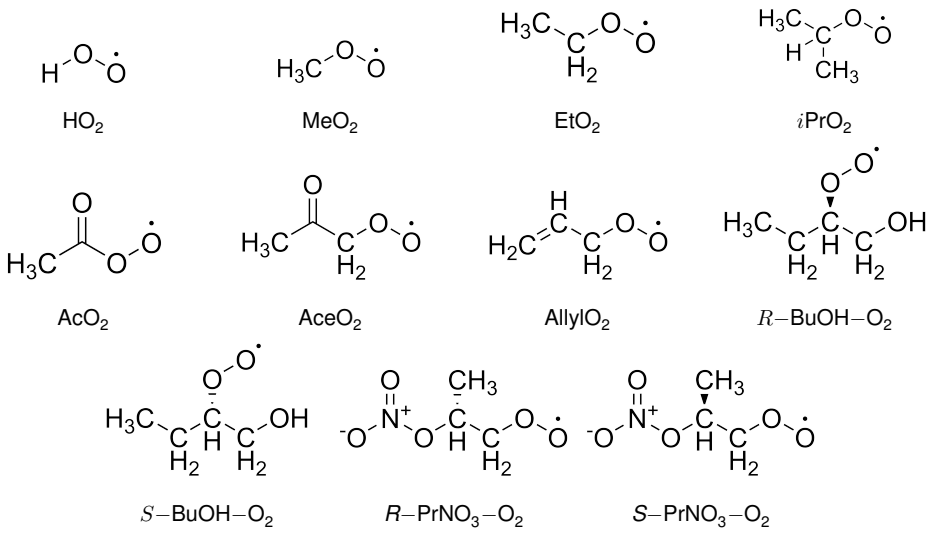

Fig. 7.3: The peroxyl radicals studied in publication **I**.

deviation between CASSCF and XMC-QDPT2 relative energies being more than 70 kcal mol^{-1} (R=R'=*R*-PrNO$_3$−O$_2$, in Table 7.1). Similar deviations were observed also in the relative energies of the reactant peroxyl radicals with respect to the tetroxide, albeit these were not as pathological.

Nevertheless, these discrepancies led us to believe that the CASSCF optimized geometries for the stationary structures are likely quite far off from what XMC-QDPT2 level geometry optimizations would yield, and this was further verified by comparing the CASSCF optimized stationary structures for the $MeO_2 + MeO_2$ system with XMC-QDPT2 optimized structures from **IV**. Unfortunately, at the time of the study, we could not perform geometry optimizations at the full XMC-QDPT2 level for the other studied reactions.

However, we realized that the isolated reactants, the tetroxide intermediate, and the isolated products could also be investigated using single-reference methods, so we did DFT geometry optimizations at ωB97X-D/aug-cc-pVTZ level of theory and calculated single-point corrections at CCSD(T)-F12/cc-pVDZ-F12 level of theory to obtain more accurate relative energies for these systems (Table 3 in publication **I**). These relative energies were much more in line with the XMC-QDPT2 energies than with the CASSCF energies, but still far from quantitative agreement. The DFT calculations were carried out using Gaussian16 software,[221] and the coupled cluster calculations were done with Molpro

Table 7.1: CASSCF(10,8)/6-311++G(d,p) and XMC-QDPT2//CASSCF energies of the stationary points along the total reaction path $RO_2 + R'O_2 \longrightarrow RO....O_2...R'O$, energies relative to the RO_4R' intermediate, in kcal mol^{-1}.[a]

R	R'	$RO_2 + R'O_2$	$RO_2...R'O_2$	$[ROO\cdots OOR']^{\ddagger}$	RO_4R'	$RO\cdots O_2\cdots OR'$	$RO\ldots O_2\ldots R'O$
H	H	3.92 (8.42)	-0.32 (2.95)	4.19 (4.13)	0.00	2.71 (1.71)	-12.46 (9.57)
Me	H	3.09 (10.88)	-1.23 (4.06)	3.87 (4.65)	0.00	1.21 (1.03)	-16.63 (12.62)
Me	Me	0.88 (3.72)	-1.27 (-0.56)	1.40 (-3.00)	0.00	2.31 (-3.42)	-17.41 (3.98)
Et	Et	0.69 (10.71)	-1.73 (5.38)	1.53 (-0.30)	0.00	1.21 (-0.74)	-18.37 (13.64)
*i*Pr	*i*Pr	-0.47 (6.98)	-2.92 (1.23)	1.06 (-3.69)	0.00	2.97 (-5.40)	-17.17 (12.08)
Ac	Me	7.48 (19.37)	4.66 (15.82)	-	0.00	1.09 (-0.44)	-20.33 (14.30)
Ac	Ac	12.23 (32.04)	8.66 (26.33)	-	0.00	0.05 (-0.99)	-23.94 (16.59)
Allyl	Allyl	1.31 (14.30)	-1.06 (10.41)	2.73 (3.67)	0.00	0.71 (0.32)	-20.17 (18.02)
Ace	Ace	2.36 (19.65)	-0.73 (14.24)	3.41 (5.10)	0.00	0.91 (0.72)	-22.92 (18.66)
Ace	*S*-BuOH	3.67 (21.28)	-1.64 (13.48)	3.26 (3.58)	0.00	1.35 (-2.82)	-21.49 (45.69)
R-BuOH	*R*-BuOH	3.02 (21.55)	-2.40 (13.45)	6.64 (6.76)	0.00	1.11 (-3.25)	-21.86 (47.58)
R-BuOH	*S*-BuOH	3.57 (20.00)	-1.57 (14.26)	3.52 (2.52)	0.00	1.36 (-3.65)	-20.87 (18.70)
R-$PrNO_3$	*R*-$PrNO_3$	3.44 (28.03)	-1.82 (18.61)	3.72 (5.08)	0.00	1.46 (-5.11)	-22.52 (50.56)
R-$PrNO_3$	*S*-$PrNO_3$	4.02 (28.40)	-1.32 (17.50)	2.73 (2.14)	0.00	2.18 (-4.59)	-21.65 (25.09)

[a] The values outside brackets are CASSCF(10,8)/6-311++G(d,p) relative energies, values inside the brackets are XMC-QDPT2(10,8)/6-311++G(d,p) energies calculated at the CASSCF optimized stationary points.

software version 2019.2,[222,223] except for the DLPNO-CCSD(T) calculations, which were done with ORCA software version 4.2.1.[224,225]

One thing where the CASSCF and XMC-QDPT2 descriptions did agree was that for the most part the barrier heights for the formation reactions were higher than for the decomposition reactions, suggesting that the association step is the rate-limiting step in the total reaction, which is in agreement with what has been found in earlier studies.[80,82]

7.2 Publication II

In publication **II**, we continued the work started in publication **I**. One of the major shortcomings in the methodology that was used in the previous work was that the CASSCF method yielded reaction potential energy surfaces that were not quantitatively representative for the studied reactions, even when the energies were corrected with the XMC-QDPT2 method. Also, it was shown that the CASSCF and XMC-QDPT2//CASSCF

relative energies did not agree with the relative energies obtained at CCSD(T)//DFT level of theory.

It is important to clarify why it is beneficial if not crucial that the relative energies calculated with a multireference methods should ideally agree with the relative energies obtained at CCSD(T) or higher single-reference methods. The ground electronic states of individual peroxyl radicals, tetroxides, alkoxyl radicals, and molecular oxygen can be described with a single determinant reference wavefunction. This enables the use of single-reference dynamic electron correlation methods, such as CCSD(T), in the calculation of more accurate absolute energies for these molecules. These absolute energies can then be used to construct the relative energy picture in the $RO_2 + R'O_2 \longrightarrow RO_4R' \longrightarrow RO + R'O + O_2$ total reaction (Fig. 7.4). For systems that require multiconfigurational reference wavefunctions, such as the open-shell reaction potentials that connect these molecules in the reaction above, reaching comparable accuracy for the dynamic electron correlation simply is not computationally feasible due to much steeper computational scaling of these methods. In other words, computationally tractable multireference methods are more approximated than the corresponding single-reference correlation methods; hence, whenever single-reference methods can be used to describe the system or property of interest, they should be used instead of multireference methods.

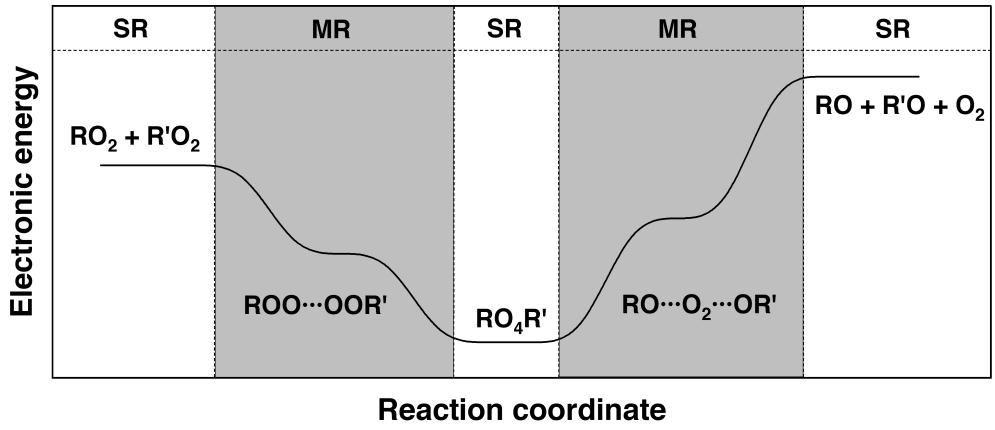

Fig. 7.4: Schematic of the potential energy curve of the $RO_2 + R'O_2 \longrightarrow RO_4R' \longrightarrow RO + R'O + O_2$ total reaction. SR entails that the corresponding structures and energies may be solved with single-reference methods, while the MR sections of the reaction surface require multireference methods.

In this work, we limited the study to the $MeO_2 + MeO_2 \longrightarrow MeO_4Me \longrightarrow MeO + MeO + O_2$ model reaction. This was done because this reaction system is small enough in size that very high accuracy single-reference methods can be used to calculate the absolute energies of the related species. We used three single-reference approaches: complete basis set limit (CBS) extrapolated CCSD(T) as well as W2X and W3X-L composite methods.[226] The CCSD(T)/CBS calculations were done with ORCA version 5.0.3,[227] while the W2X and W3X-L calculations were done using Molpro version 2022.3,[228,229] and MRCC softwares.[230] In CBS extrapolation, successive calculations of the energy are carried out using correlation-consistent basis sets, then the convergence of the absolute energies with respect to increasing basis set size is used to extrapolate to the energy value at infinite basis set size. The W2X composite method is an all-electron relativistic approximation to CCSD(T)/CBS, where in addition to the CCSD(T)/CBS calculation for valence electrons, all-electron effects are accounted with core-valence correlation calculations and scalar-relativistic approximations. The W3X-L composite builds upon the W2X method by adding correlation contributions from CCSDT and CCSDT(Q) calculations with smaller basis sets. Of the three used methods, W3X-L is by far computationally the most demanding but yields extremely accurate energies. Currently, computationally tractable W3X-L single-point energy calculations are limited to systems with six or less heavy atoms.

Then, with the goal to reach accuracy similar to the single-reference methods, we explored multiple variables underlying calculations with multireference methods: different active space compositions, basis sets, and different approaches for assessing the dynamic electron correlation, both as single-point energy corrections and already at geometry optimization level. All multireference calculations were done with the ORCA software version 5.0.3.[227]

Using the CASSCF method, we carried out geometry optimizations for the MeO_4Me intermediate, as well as for supermolecular systems of the reactants ($MeO_2 + MeO_2$) and the decomposition products ($MeO + MeO + O_2$), where all the species were separated by 30 Å such that there is no interaction between the molecules. This ensures that the energy of the supermolecular system is equal to the sum of energies of the isolated molecules, given that the method is fully size consistent [E(A+B) = E(A) + E(B)], and thus directly comparable to the relative energies obtained with the single-reference methods. The

CASSCF calculations were done with three active spaces: CAS(6e,6o), CAS(10e,8o), and CAS(22e,14o). The CAS(6e,6o) includes all oxygen-oxygen σ-bonding and antibonding orbitals, and is the smallest complete active space that qualitatively describes the formation and dissociation of the various O-O bonds in the total reaction. CAS(10e,8o) adds two lonepair/π-type orbitals of the two terminal peroxyl oxygen atoms. Addition of these to the CAS yields better description of the static correlation between the π and π^*orbitals in the molecular oxygen that forms during the decomposition. This CAS(10e,8o) is identical to the one used in publication **I**. The CAS(22e,14o) active includes all oxygen valence orbitals and electrons, except for the C-O σ and σ^* orbitals.

Then, we used CASPT2 and CASPT2-IPEA methods to calculate single-point energy corrections (see details of these methods in sections 5.6.2 and 5.6.2) for the obtained stationary points. These corrections only gave reasonable relative energies with the CAS(22e,14o) active space. CASPT2 method systematically underestimated the energies of the open-shell structures, which manifested as too small relative energy differences in comparison to the CCSD(T)/CBS and W3X-L results. The CASPT2-IPEA method, which is designed to account for these underestimations, yielded relative energies that were in excellent agreement with the single-reference energies. Various IPEA-shift values were tried, with the optimal value being 0.20 a.u. We further optimized the geometries of the stationary points with CASPT2 and found that for calculating the relative energies of the isolated species, both CASSCF(22e,14o) and CASPT2(22e,14o) geometry optimizations yield similar results, when the energies are corrected with CASPT2-IPEA.

Lastly, we investigated the reaction potentials of both the association and the decomposition reactions with CASSCF and CASPT2 geometry optimizations, to address possible saddle points corresponding to the bond formation or bond breaking transition states (Fig. 7.5). While the reaction potentials for the association reaction are quite similar with both approaches (Fig. 7.5a), for the decomposition reactions it turned to out matter quite a lot, whether the geometries are optimized with CASSCF or CASPT2. CASSCF optimized reaction potential shows a clear saddle point for the decomposition and a post-reaction complex, while in the CASPT2 optimized surface the saddle point does not exist when the CASPT2-IPEA corrections are applied (Fig. 7.5b). It appears that both the tetroxide formation and decomposition reactions occur on a barrierless potential energy surface, at least for the studied reaction system. Moreover, the CASPT2(22e,14o)-IPEA

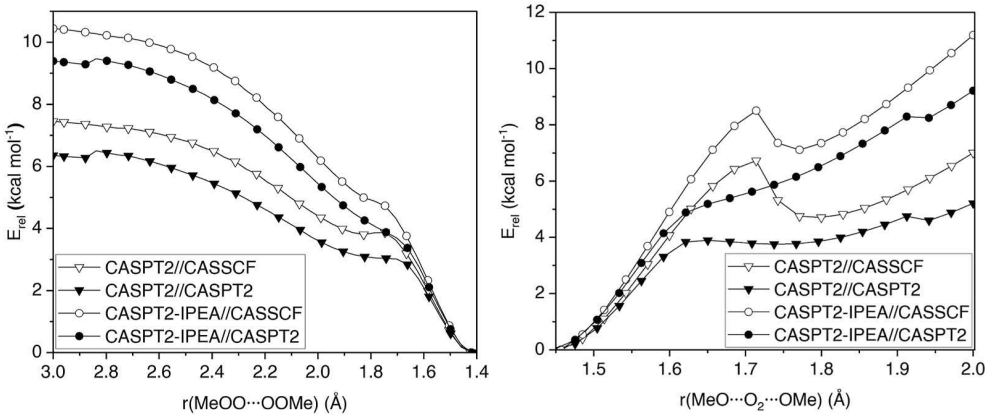

Fig. 7.5: The reaction potential energy curves of the association (a) and decomposition (b) reactions. CASPT2 (▽) and CASPT2-IPEA (○) single-point energy corrections on geometries optimized with either CASSCF(22e,14o) (hollow) or CASPT2(22e,14o) (solid), with cc-pVTZ basis set. Reprinted (adapted) with permission from *J. Phys. Chem. A* **2024**, 128, 10, 1825–1836. Copyright 2024 American Chemical Society.

method is able to reproduce the relative energies obtained at high level single-reference methods, meaning that this method can be recommended for future studies of the various product formation pathways that occur after the initial decomposition (cf. Fig. 3.3). However, the CASPT2-IPEA method has its limitations. The optimal value for the IPEA shift depends on the studied reaction, and while the shift value of 0.20 a.u. was found to work nicely for the reactions studied in this work, this result is not universal. Here, we were able to carry out very expensive single-reference calculations to obtain relative energies to benchmark against, but for larger systems, these calculations would not be feasible. Thus, other methods that would yield results comparable accuracy without relying on empirical parameters are highly desirable for the study of reactions involving open-shell electronic structures. Also, to obtain accurate information about the reaction mechanism pertaining to the decomposition reaction, CASPT2-level geometry optimizations had to done. CASPT2 geometry optimizations are resource-heavy calculations to carry out, and with the currently available computational capabilities, these optimizations are limited to relatively small systems, so cheaper alternatives are desired for investigating larger molecular systems.

7.3 Manuscript III

The manuscript **III** deals with the atmospheric oxidation of ammonia. More specifically, it is concerned with the reaction of aminyl radical (NH_2) with molecular oxygen, a reaction that has been assumed insignificant in atmospheric conditions. Aminyl radicals are formed when ammonia reacts with the OH radicals or Cl radicals by HAT reaction. Current consensus is that further reactions of the NH_2 radical in atmospheric conditions are bimolecular reactions with NO, NO_2, and O_3, which differs from what is known for the reactions of carbon- and sulfur-centered radicals that readily add molecular oxygen to yield the corresponding peroxyl radicals.

The motivation to study the $NH_2 + O_2$ reaction specifically is twofold: First, results from previous theoretical studies of this reaction are inconclusive. While the studies agree, that the reaction yields aminoperoxyl radical (NH_2O_2), some studies report that its formation is highly endothermic, while others suggest that it is exothermic. The past studies have been done using methods that either are not suitable at all for studying reactions between radicals, or have been correctly done using multireference methods, but the accuracy of the specific methods has been insufficient to make any credible estimates of the thermodynamics or kinetics of the reaction. Multiconfigurational methods are required, because NH_2 is a doublet and molecular oxygen a triplet, so the reaction occurs on an electronic state consisting of three unpaired electrons. Second, the currently accepted bimolecular reaction rate coefficient for the $NH_2 + O_2$ reaction, which is about 10^{-21} cm^3 $molecule^{-1}$ s^{-1}, appears extraordinarily small for a reaction between two radicals. Thus, we wanted to study, what is the underlying reason for such a slow observed reactivity.

We began the study by calculating the potential energy surface of the association reaction $NH_2 + O_2 \longrightarrow NH_2O_2$ using NEVPT2/aug-cc-pVTZ level of theory and found out that the bond formation reaction is exothermic, but considerably less than carbon-centered radical + O_2 reactions. This means that NH_2O_2 is relatively unstable with respect to dissociation back to NH_2 and O_2. We were able to find a saddle-point corresponding to the bond-formation, which enabled the use of transition state theory (TST) for estimating the rate coefficients for both the formation and dissociation reactions. All calculations done in this work were carried out using ORCA version 5.0.3.[227]

The calculated rate coefficient for the NH_2O_2 formation reaction was 3.5×10^{-13} cm^3 $molecule^{-1}$ s^{-1} at 298 K, which is much more in line with what is known for similar

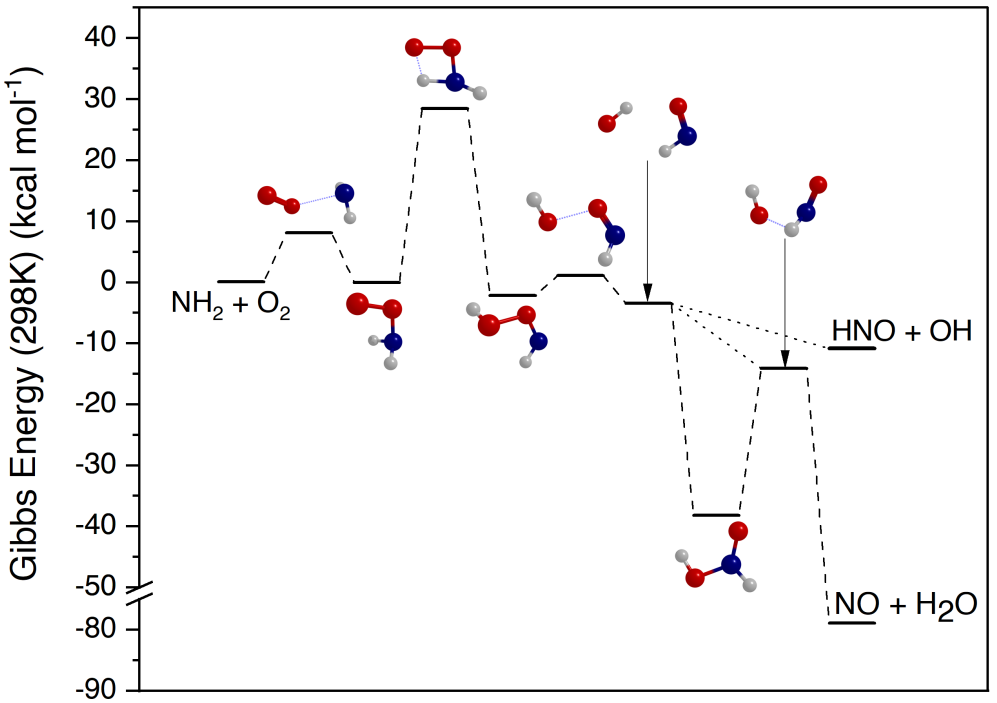

Fig. 7.6: Free energy reaction potential surface of the total reaction from $NH_2 + O_2$ to HNO and NO, at 298 K and 760 Torr, red=oxygen, blue=nitrogen, gray=hydrogen.

reactions. This raised a question of why the currently suggested rate coefficient differs by eight orders of magnitude from the value obtained in our calculations. It turned out that the current estimate is from a study that assumes that NO and HNO would form as the end products in the $NH_2 + O_2$ reaction, and the suggested rate coefficient is an upper bound for the formation of these compounds. Therefore, we calculated the full reaction pathway from the reactants all the way to the NO and HNO (Fig. 7.6). We found that the rate-limiting step in the total reaction is the isomerization of NH_2O_2 to HNOOH, and that the calculated bimolecular rate coefficient corresponding to the formation of NO and HNO is 10^{-24} cm^3 $molecule^{-1}$ s^{-1} at 298 K, which is even smaller than the upper bound estimate. In conclusion, the $NH_2 + O_2$ reaction does not yield NO and HNO in atmospheric reaction conditions, but the initial association reaction between $NH_2 + O_2$ is rapid and may compete with other bimolecular reactions available to NH_2.

Whether the $NH_2 + O_2$ reaction has any relevance in atmospheric conditions, depends on three factors: 1) the rate at which the NH_2O_2 is formed in comparison to the other

bimolecular reactions of NH_2, 2) the stability of the NH_2O_2 radical, and 3) the rate at which the NH_2O_2 reacts further. The last factor was not explicitly studied in this work, but the bimolecular reaction rates of NH_2O_2 are likely similar to those of other peroxyl radicals.

The competition between the various bimolecular reactions of the NH_2 radical can be estimated by comparing the corresponding pseudo-first-order rate coefficients, which depend on the bimolecular rate coefficients and the concentrations of the reacting species: NO, NO_2, O_3, and O_2. The atmospheric concentration of oxygen is always at least five orders of magnitude higher than the other compounds, which means that even if the bimolecular rate coefficient of the $NH_2 + O_2$ reaction was five orders of magnitude smaller than for the other reactions, it would still be competitive reaction pathway. Our results suggest that the $NH_2 + O_2$ reaction rate coefficient is similar to that of $NH_2 + O_3$ and only two orders of magnitude smaller than those for reactions with NO and NO_2. So the rate at which NH_2 and O_2 react in atmospheric conditions greatly exceed the rates of the competing reactions.

Because the $NH_2 + O_2 \longrightarrow NH_2O_2$ reaction occurs with a much higher rate than the other possible reactions, it can be assumed that the association and dissociation reactions reach equilibrium before the other reactions can occur. The relative concentrations of free NH_2 and NH_2O_2 at equilibrium can be estimated from the equilibrium constant of the $NH_2 + O_2 \rightleftharpoons NH_2O_2$ reaction, which in turn depend on the rate coefficients of the association and dissociation reactions, and the concentration of O_2. It is important to note that rate coefficients calculated with transition state theory can be larger than in reality, but because both the association and dissociation reactions were studied with TST, the possible overestimation is cancelled in the formulation of the equilibrium constant.

Finally, we proceeded to model the equilibrium in different temperatures and pressures, as well as a function of altitude (Fig. 7.7).[a] We found that the fraction of NH_2O_2 is surprisingly large in various atmospherically relevant conditions, especially at low temperature and high pressure, and is the dominant species in these conditions. These results suggest that large fraction of ammonia oxidation proceeds through the NH_2O_2 radical, which greatly changes the current understanding of how ammonia oxidation affects the

[a]The temperatures and pressures at the varying altitudes were calculated with the barometric formula, see section S5 in the Supporting Information of Manuscript **III** for details.

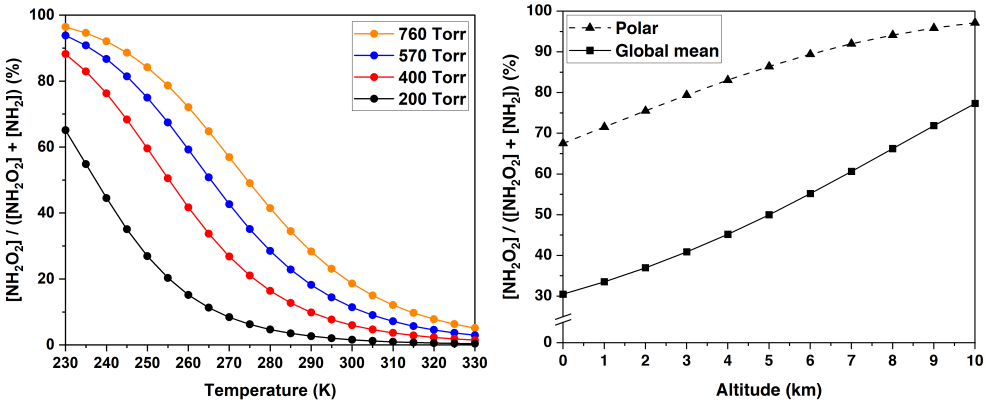

(a) (b)

Fig. 7.7: Fraction of NH_2O_2 at typical tropospheric conditions, and 21% O_2 percentage. (a) At total pressures of 200 Torr (**black**), 400 Torr (**red**), 570 Torr (**blue**), and 760 Torr (**orange**), in temperature range of 230–330 K, and (b) as a function of altitude 0–10 km, the square symbols represent global mean surface temperature of 288 K, and dashed curve with triangle symbols corresponds to polar surface temperature of 263 K.

global NO_x-cycle (cf. Fig. 4.2 and Fig. 4.3).

Chapter 8

Conclusions and Future Outlook

In the beginning of this thesis, three main objectives were introduced: 1) find and optimize computational methodologies required for accurate descriptions of chemical reactions occurring on complex electronic states, 2) apply these methods to further the knowledge of reactions relevant for the atmosphere, and 3) promote the use of multireference electronic structure methods as a tool for studying chemical reactions.

The first two objectives have been a central theme in all the original publications of this thesis, and these goals have been improved in each successive publication. This progress highlights that the methodologies chosen for carrying out the research have turned out to be successful. The last objective has also been an integral part of the research and publications, but even more so some kind of personal goal that I wanted to use this thesis to convey. In my experience, the multireference methods are praised and recognized in the computational chemistry community, but not many people know how to use them properly, and many tend to steer away from them. I also had no idea how to use them when I began my PhD studies. I hope that this thesis reduces the intimidation associated with the use of these methods, and enables them for a wider audience.

One of the original research questions, that my PhD studies began with, was to develop a methodology, with which the chemistry between peroxyl radicals can be comprehensively studied. The research done for this dissertation has successfully solved a part of this problem, but important aspects are yet to be explored. For example, the studies of the various product formation reactions with these methods remains largely unfinished. These reactions are just as central as all the processes that this dissertation specifically dealt with. However, potential tools for studying these have now been identified, and their

applicability remains to be determined in future work.

The reactions selected as topics for this dissertation are just a few examples of important reactions in the atmosphere. Now that methods suitable for their description have been found in this dissertation, the natural next step is to continue to study other relevant reaction systems, for which the current understanding is limited. However, one clear limitation of the methods used in this research work is that at the present moment they are only readily applicable for small systems. Therefore, there is a clear call for new methods that are able to handle larger systems with similar accuracy, or alternatively, the computational scalability and parallelizability of the existing methods should be improved.

I conclude this thesis with a personal anecdote of this entire doctoral journey. The day I started doing my PhD, my supervisor set me out with words that were equally encouraging and depressing: "This is a very high risk–high reward project. It is very likely that we will not solve this problem at all during your PhD, but if we find something, even just a little, it will be a big thing." So naturally I, who had close to zero experience in computational chemistry and equally much ability to judge how difficult it would be, accepted the task, because what I did have was all the healthy self-confidence to fool myself into it. I had become aware and interested in computational chemistry already some time earlier after attending a seminar, where the speaker proclaimed that "...computational chemistry, yeah the theory of it is hard, but you can do all the cool simulations first, and learn the theory later." Now that I am reflecting back to the days I started this PhD, I feel I followed this instruction too much to the letter. If only I had known then what I know now: I can wholeheartedly recommend anyone adopting multireference methods to their toolkit to do some research into the underlying theory before running extensive sets of calculations. I know it sounds like a pain, but you can thank me later.

Bibliography

[1] Schumann, U.; Huntrieser, H. The Global Lightning-Induced Nitrogen Oxides Source. *Atmospheric Chemistry and Physics* **2007**, *7*, 3823–3907.

[2] Dickerson, R. R.; Stedman, D. H.; Delany, A. C. Direct Measurements of Ozone and Nitrogen Dioxide Photolysis Rates in the Troposphere. *Journal of Geophysical Research: Oceans* **1982**, *87*, 4933–4946.

[3] Wayne, R. P. *Chemistry of Atmospheres*; Oxford University Press; 3rd edition, 2000.

[4] Stark, H.; Lerner, B.; Schmitt, R.; Jakoubek, R.; Williams, E.; Ryerson, T.; Sueper, D.; Parrish, D.; Fehsenfeld, F. Atmospheric In Situ Measurement of Nitrate Radical (NO_3) and Other Photolysis Rates Using Spectroradiometry and Filter Radiometry. *Journal of Geophysical Research: Atmospheres* **2007**, *112*, D10S04.

[5] Hudson, R. Absorption Cross Sections of Stratospheric Molecules. *Canadian Journal of Chemistry* **1974**, *52*, 1465–1478.

[6] Matsumi, Y.; Kawasaki, M. Photolysis of Atmospheric Ozone in the Ultraviolet Region. *Chemical Reviews* **2003**, *103*, 4767–4782.

[7] Hewitt, C.; Harrison, R. M. Tropospheric Concentrations of the Hydroxyl Radical—A Review. *Atmospheric Environment* **1985**, *19*, 545–554.

[8] Stone, D.; Whalley, L. K.; Heard, D. E. Tropospheric OH and HO_2 Radicals: Field Measurements and Model Comparisons. *Chemical Society Reviews* **2012**, *41*, 6348–6404.

[9] Atkinson, R. Gas-Phase Tropospheric Chemistry of Volatile Organic Compounds: 1. Alkanes and Alkenes. *Journal of Physical and Chemical Reference Data* **1997**, *26*, 215–290.

[10] Atkinson, R. Kinetics and Mechanisms of the Gas-Phase Reactions of the Hydroxyl Radical With Organic Compounds Under Atmospheric Conditions. *Chemical Reviews* **1986**, *86*, 69–201.

[11] Ehhalt, D.; Dorn, H.-P.; Poppe, D. The Chemistry of the Hydroxyl Radical in the Troposphere. *Proceedings of the Royal Society of Edinburgh, Section B: Biological Sciences* **1990**, *97*, 17–34.

[12] Platt, U.; LeBras, G.; Poulet, G.; Burrows, J.; Moortgat, G. Peroxy Radicals From Night-Time Reaction of NO_3 With Organic Compounds. *Nature* **1990**, *348*, 147–149.

[13] Wayne, R. P.; Barnes, I.; Biggs, P.; Burrows, J.; Canosa-Mas, C.; Hjorth, J.; Le Bras, G.; Moortgat, G.; Perner, D.; Poulet, G.; others The Nitrate Radical: Physics, Chemistry, and the Atmosphere. *Atmospheric Environment. Part A. General Topics* **1991**, *25*, 1–203.

[14] Skov, H.; Benter, T.; Schindler, R.; Hjorth, J.; Restelli, G. Epoxide Formation in the Reactions of the Nitrate Radical with 2,3-Dimethyl-2-Butene, Cis- and Trans-2-Butene and Isoprene. *Atmospheric Environment* **1994**, *28*, 1583–1592.

[15] Vereecken, L.; Peeters, J. H-Atom Abstraction by OH-Radicals From (Biogenic) (Poly)alkenes: C–H Bond Strengths and Abstraction Rates. *Chemical Physics Letters* **2001**, *333*, 162–168.

[16] Peeters, J.; Vereecken, L.; Fantechi, G. The Detailed Mechanism of the OH-Initiated Atmospheric Oxidation of α-Pinene: A Theoretical Study. *Physical Chemistry Chemical Physics* **2001**, *3*, 5489–5504.

[17] Lelieveld, J.; Crutzen, P. J.; Dentener, F. J. Changing concentration, Lifetime and Climate Forcing of Atmospheric Methane. *Tellus B* **1998**, *50*, 128–150.

[18] Atkinson, R. Atmospheric Chemistry of VOCs and NO_x. *Atmospheric Environment* **2000**, *34*, 2063–2101.

[19] Johnson, D.; Marston, G. The Gas-Phase Ozonolysis of Unsaturated Volatile Organic Compounds in the Troposphere. *Chemical Society Reviews* **2008**, *37*, 699–716.

[20] Chuong, B.; Zhang, J.; Donahue, N. M. Cycloalkene Ozonolysis: Collisionally Mediated Mechanistic Branching. *Journal of the American Chemical Society* **2004**, *126*, 12363–12373.

[21] Horie, O.; Moortgat, G. Decomposition Pathways of the Excited Criegee Intermediates in the Ozonolysis of Simple Alkenes. *Atmospheric Environment. Part A. General Topics* **1991**, *25*, 1881–1896.

[22] Vereecken, L.; Francisco, J. S. Theoretical Studies of Atmospheric Reaction Mechanisms in the Troposphere. *Chemical Society Reviews* **2012**, *41*, 6259–6293.

[23] Kurtén, T.; Donahue, N. M. MRCISD Studies of the Dissociation of Vinylhydroperoxide, CH_2CHOOH: There is a Saddle Point. *The Journal of Physical Chemistry A* **2012**, *116*, 6823–6830.

[24] Mentel, T.; Springer, M.; Ehn, M.; Kleist, E.; Pullinen, I.; Kurtén, T.; Rissanen, M.; Wahner, A.; Wildt, J. Formation of Highly Oxidized Multifunctional Compounds: Autoxidation of Peroxy Radicals Formed in the Ozonolysis of Alkenes–Deduced From Structure–Product Relationships. *Atmospheric Chemistry and Physics* **2015**, *15*, 6745–6765.

[25] Madronich, S.; Calvert, J. G. Permutation Reactions of Organic Peroxy Radicals in the Troposphere. *Journal of Geophysical Research: Atmospheres* **1990**, *95*, 5697–5715.

[26] Lightfoot, P. D.; Cox, R.; Crowley, J.; Destriau, M.; Hayman, G.; Jenkin, M.; Moortgat, G.; Zabel, F. Organic Peroxy Radicals: Kinetics, Spectroscopy and Tropospheric Chemistry. *Atmospheric Environment. Part A. General Topics* **1992**, *26*, 1805–1961.

[27] Orlando, J. J.; Tyndall, G. S. Laboratory Studies of Organic Peroxy Radical Chemistry: An Overview With Emphasis on Recent Issues of Atmospheric Significance. *Chemical Society Reviews* **2012**, *41*, 6294–6317.

[28] Glowacki, D. R.; Pilling, M. J. Unimolecular Reactions of Peroxy Radicals in Atmospheric Chemistry and Combustion. *ChemPhysChem* **2010**, *11*, 3836–3843.

[29] Simic, M. G. Free Radical Mechanisms in Autoxidation Processes. *Journal of Chemical Education* **1981**, *58*, 125–131.

[30] Crounse, J. D.; Nielsen, L. B.; Jørgensen, S.; Kjaergaard, H. G.; Wennberg, P. O. Autoxidation of Organic Compounds in the Atmosphere. *The Journal of Physical Chemistry Letters* **2013**, *4*, 3513–3520.

[31] Calvert, J. G.; Orlando, J. J.; Stockwell, W. R.; Wallington, T. J. *The Mechanisms of Reactions Influencing Atmospheric Ozone*; Oxford University Press, 2015; pp 315–347.

[32] Zhao, Y.; Houk, K.; Olson, L. P. Mechanisms of Peroxynitrous Acid and Methyl Peroxynitrite, ROONO (R = H, Me), Rearrangements: A Conformation-Dependent Homolytic Dissociation. *The Journal of Physical Chemistry A* **2004**, *108*, 5864–5871.

[33] Zhang, J.; Dransfield, T.; Donahue, N. M. On the Mechanism for Nitrate Formation via the Peroxy Radical + NO Reaction. *The Journal of Physical Chemistry A* **2004**, *108*, 9082–9095.

[34] Arey, J.; Aschmann, S. M.; Kwok, E. S.; Atkinson, R. Alkyl Nitrate, Hydroxyalkyl Nitrate, and Hydroxycarbonyl Formation from the NO_x-Air Photooxidations of C_5-C_8 *n*-Alkanes. *The Journal of Physical Chemistry A* **2001**, *105*, 1020–1027.

[35] Kirchner, F.; Mayer-Figge, A.; Zabel, F.; Becker, K. Thermal Stability of Peroxynitrates. *International Journal of Chemical Kinetics* **1999**, *31*, 127–144.

[36] Singh, H. B.; Salas, L. J.; Viezee, W. Global Distribution of Peroxyacetyl Nitrate. *Nature* **1986**, *321*, 588–591.

[37] LaFranchi, B.; Wolfe, G.; Thornton, J.; Harrold, S.; Browne, E.; Min, K.; Wooldridge, P.; Gilman, J.; Kuster, W.; Goldan, P.; others Closing the Peroxy Acetyl Nitrate Budget: Observations of Acyl Peroxy Nitrates (PAN, PPN, and MPAN) During BEARPEX 2007. *Atmospheric Chemistry and Physics* **2009**, *9*, 7623–7641.

[38] Hou, H.; Wang, B. A Systematic Computational Study on the Reactions of HO_2 With RO_2: The HO_2 + CH_3O_2 (CD_3O_2) and HO_2 + CH_2FO_2 Reactions. *The Journal of Physical Chemistry A* **2005**, *109*, 451–460.

[39] Hasson, A. S.; Kuwata, K. T.; Arroyo, M. C.; Petersen, E. B. Theoretical Studies of the Reaction of Hydroperoxy Radicals (HO_2) With Ethyl Peroxy ($CH_3CH_2O_2$), Acetyl Peroxy ($CH_3C(O)O_2$), and Acetonyl Peroxy ($CH_3C(O)CH_2O_2$) Radicals. *Journal of Photochemistry and Photobiology A: Chemistry* **2005**, *176*, 218–230.

[40] Russell, G. A. Deuterium-Isotope Effects in the Autoxidation of Aralkyl Hydrocarbons. Mechanism of the Interaction of Peroxy Radicals[1]. *Journal of the American Chemical Society* **1957**, *79*, 3871–3877.

[41] Ingold, K. U. Peroxy Radicals. *Accounts of Chemical Research* **1969**, *2*, 1–9.

[42] Ziemann, P. J. Evidence for Low-Volatility Diacyl Peroxides as a Nucleating Agent and Major Component of Aerosol Formed From Reactions of O_3 With Cyclohexene and Homologous Compounds. *The Journal of Physical Chemistry A* **2002**, *106*, 4390–4402.

[43] Berndt, T.; Scholz, W.; Mentler, B.; Fischer, L.; Herrmann, H.; Kulmala, M.; Hansel, A. Accretion Product Formation From Self- and Cross-Reactions of RO_2 Radicals in the Atmosphere. *Angewandte Chemie International Edition* **2018**, *57*, 3820–3824.

[44] Ehn, M.; Thornton, J. A.; Kleist, E.; Sipilä, M.; Junninen, H.; Pullinen, I.; Springer, M.; Rubach, F.; Tillmann, R.; Lee, B.; others A Large Source of Low-Volatility Secondary Organic Aerosol. *Nature* **2014**, *506*, 476–479.

[45] Da Silva, G.; Graham, C.; Wang, Z.-F. Unimolecular β-Hydroxyperoxy Radical Decomposition With OH Recycling in the Photochemical Oxidation of Isoprene. *Environmental Science & Technology* **2009**, *44*, 250–256.

[46] Peeters, J.; Nguyen, T. L.; Vereecken, L. HO_x Radical Regeneration in the Oxidation of Isoprene. *Physical Chemistry Chemical Physics* **2009**, *11*, 5935–5939.

[47] Crounse, J. D.; Paulot, F.; Kjaergaard, H. G.; Wennberg, P. O. Peroxy Radical Isomerization in the Oxidation of Isoprene. *Physical Chemistry Chemical Physics* **2011**, *13*, 13607–13613.

[48] Crounse, J. D.; Knap, H. C.; Ørnsø, K. B.; Jørgensen, S.; Paulot, F.; Kjaergaard, H. G.; Wennberg, P. O. Atmospheric Fate of Methacrolein. 1. Peroxy Radical Isomerization Following Addition of OH and O_2. *The Journal of Physical Chemistry A* **2012**, *116*, 5756–5762.

[49] Praske, E.; Otkjær, R. V.; Crounse, J. D.; Hethcox, J. C.; Stoltz, B. M.; Kjaergaard, H. G.; Wennberg, P. O. Intramolecular Hydrogen Shift Chemistry of Hydroperoxy-Substituted Peroxy Radicals. *The Journal of Physical Chemistry A* **2018**, *123*, 590–600.

[50] Otkjær, R. V.; Jakobsen, H. H.; Tram, C. M.; Kjaergaard, H. G. Calculated Hydrogen Shift Rate Constants in Substituted Alkyl Peroxy Radicals. *The Journal of Physical Chemistry A* **2018**, *122*, 8665–8673.

[51] Richters, S.; Pfeifle, M.; Olzmann, M.; Berndt, T. Endo-Cyclization of Unsaturated RO_2 Radicals From the Gas-Phase Ozonolysis of Cyclohexadienes. *Chemical Communications* **2017**, *53*, 4132–4135.

[52] Xu, L.; Møller, K. H.; Crounse, J. D.; Otkjær, R. V.; Kjaergaard, H. G.; Wennberg, P. O. Unimolecular Reactions of Peroxy Radicals Formed in the Oxidation of α-Pinene and β-Pinene by Hydroxyl Radicals. *The Journal of Physical Chemistry A* **2019**, *123*, 1661–1674.

[53] Møller, K. H.; Otkjær, R. V.; Chen, J.; Kjaergaard, H. G. Double Bonds are key to Fast Unimolecular Reactivity in First-Generation Monoterpene Hydroxy Peroxy Radicals. *The Journal of Physical Chemistry A* **2020**, *124*, 2885–2896.

[54] Iyer, S.; Rissanen, M. P.; Valiev, R.; Barua, S.; Krechmer, J. E.; Thornton, J.; Ehn, M.; Kurtén, T. Molecular Mechanism for Rapid Autoxidation in α-Pinene Ozonolysis. *Nature Communications* **2021**, *12*, 878.

[55] Bianchi, F. et al. Highly Oxygenated Organic Molecules (HOM) From Gas-Phase

Autoxidation Involving Peroxy Radicals: A Key Contributor to Atmospheric Aerosol. *Chemical Reviews* **2019**, *119*, 3472–3509.

[56] Rissanen, M. Anthropogenic Volatile Organic Compound (AVOC) Autoxidation as a Source of Highly Oxygenated Organic Molecules (HOM). *The Journal of Physical Chemistry A* **2021**, *125*, 9027–9039.

[57] Savee, J. D.; Papajak, E.; Rotavera, B.; Huang, H.; Eskola, A. J.; Welz, O.; Sheps, L.; Taatjes, C. A.; Zádor, J.; Osborn, D. L. Direct Observation and Kinetics of a Hydroperoxyalkyl Radical (QOOH). *Science* **2015**, *347*, 643–646.

[58] Paulot, F.; Crounse, J. D.; Kjaergaard, H. G.; Kürten, A.; St. Clair, J. M.; Seinfeld, J. H.; Wennberg, P. O. Unexpected Epoxide Formation in the Gas-Phase Photooxidation of Isoprene. *Science* **2009**, *325*, 730–733.

[59] Møller, K. H.; Kurtén, T.; Bates, K. H.; Thornton, J. A.; Kjaergaard, H. G. Thermalized Epoxide Formation in the Atmosphere. *The Journal of Physical Chemistry A* **2019**, *123*, 10620–10630.

[60] Atkinson, R. Atmospheric Reactions of Alkoxy and β-Hydroxyalkoxy Radicals. *International Journal of Chemical Kinetics* **1997**, *29*, 99–111.

[61] Atkinson, R. Rate Constants for the Atmospheric Reactions of Alkoxy Radicals: An Updated Estimation Method. *Atmospheric Environment* **2007**, *41*, 8468–8485.

[62] Davis, A. C.; Francisco, J. S. Reactivity Trends Within Alkoxy Radical Reactions Responsible for Chain Branching. *Journal of the American Chemical Society* **2011**, *133*, 18208–18219.

[63] Orlando, J. J.; Tyndall, G. S.; Vereecken, L.; Peeters, J. The Atmospheric Chemistry of the Acetonoxy Radical. *The Journal of Physical Chemistry A* **2000**, *104*, 11578–11588.

[64] Fittschen, C.; Hippler, H.; Viskolcz, B. The β C–C Bond Scission in Alkoxy radicals: Thermal Unimolecular Decomposition of t-Butoxy Radicals. *Physical Chemistry Chemical Physics* **2000**, *2*, 1677–1683.

[65] Zabarnick, S.; Heicklen, J. Reactions of Alkoxy Radicals With O_2. I. C_2H_5O Radicals. *International Journal of Chemical Kinetics* **1985**, *17*, 455–476.

[66] Zabarnick, S.; Heicklen, J. The Reactions of Alkoxy Radicals With O_2. II. n-C_3H_7O Radicals. *International Journal of Chemical Kinetics* **1985**, *17*, 477–501.

[67] Zabarnick, S.; Heicklen, J. Reactions of Alkoxy Radicals With O_2. III. i-C_4H_9O Radicals. *International Journal of Chemical Kinetics* **1985**, *17*, 503–524.

[68] Pope, F. D.; Smith, C. A.; Davis, P. R.; Shallcross, D. E.; Ashfold, M. N.; Orr-Ewing, A. J. Photochemistry of Formaldehyde Under Tropospheric Conditions. *Faraday Discussions* **2005**, *130*, 59–72.

[69] Bartlett, P. D.; Traylor, T. G. Oxygen-18 Tracer Studies of Alkylperoxy Radicals. I. The Cumylperoxy Radical and Chain Termination in the Autoxidation of Cumene. *Journal of the American Chemical Society* **1963**, *85*, 2407–2410.

[70] Bennett, J.; Howard, J. Bimolecular Self-Reaction of Peroxy Radicals. Oxygen-18 Isotope Study. *Journal of the American Chemical Society* **1973**, *95*, 4008–4010.

[71] Ase, P.; Bock, W.; Snelson, A. Alkylperoxy and Alkyl Radicals. 1. Infrared Spectra of CH_3O_2 and $CH_3O_4CH_3$ and the Ultraviolet Photolysis of CH_3O_2 in Argon + Oxygen Matrixes. *The Journal of Physical Chemistry* **1986**, *90*, 2099–2109.

[72] Chettur, G.; Snelson, A. Alkylperoxy and Alkyl radicals. 4. Matrix IR Spectra and UV Photolysis of Ethylperoxy and Ethyl Radicals. *Journal of Physical Chemistry* **1987**, *91*, 3483–3488.

[73] Adamic, K.; Howard, J.; Ingold, K. Di-t-Alkyl Tetroxides. *Journal of the Chemical Society D: Chemical Communications* **1969**, 505–506.

[74] Bartlett, P. D.; Guaraldi, G. Di-tert-Butyl Trioxide and Di-tert-Butyl Tetroxide. *Journal of the American Chemical Society* **1967**, *89*, 4799–4801.

[75] Lee, R.; Gryn'Ova, G.; Ingold, K.; Coote, M. L. Why Are Sec-Alkylperoxyl Bimolecular Self-Reactions Orders of Magnitude Faster Than the Analogous Reactions of tert-Alkylperoxyls? The Unanticipated Role of CH Hydrogen Bond Donation. *Physical Chemistry Chemical Physics* **2016**, *18*, 23673–23679.

[76] Belyakov, V.; Vassil'ev, R. Chemiluminescence in Hydrocarbon Oxidation in Solution. A Quantitative Study of the Excitation and Emission Steps. *Photochemistry and Photobiology* **1970**, *11*, 179–192.

[77] Fedorova, G. F.; Trofimov, A. V.; Vasil'ev, R. F.; Veprintsev, T. L. Peroxy-Radical-Mediated Chemiluminescence: Mechanistic Diversity and Fundamentals for Antioxidant Assay. *Arkivoc* **2007**, *8*, 163–215.

[78] Mendenhall, G.; Quinga, E. Deuterium Isotope Cage Effects in the Dismutation of Alkoxyl Radicals. Significance for the Mode of Alkylperoxyl Termination. *International Journal of Chemical Kinetics* **1985**, *17*, 1187–1190.

[79] Ghigo, G.; Maranzana, A.; Tonachini, G. Combustion and Atmospheric Oxidation of Hydrocarbons: Theoretical Study of the Methyl Peroxyl Self-Reaction. *The Journal of Chemical Physics* **2003**, *118*, 10575–10583.

[80] Shallcross, D. E.; Raventos-Duran, M. T.; Bardwell, M. W.; Bacak, A.; Solman, Z.; Percival, C. J. A Semi-Empirical Correlation for the Rate Coefficients for Cross- and Self-Reactions of Peroxy Radicals in the Gas-Phase. *Atmospheric Environment* **2005**, *39*, 763–771.

[81] Daub, C. D.; Zakai, I.; Valiev, R.; Salo, V.-T.; Gerber, R. B.; Kurtén, T. Energy Transfer, Pre-Reactive Complex Formation and Recombination Reactions During the Collision of Peroxy Radicals. *Physical Chemistry Chemical Physics* **2022**, *24*, 10033–10043.

[82] Daub, C. D.; Valiev, R.; Salo, V.-T.; Zakai, I.; Gerber, R. B.; Kurtén, T. Computed Pre-reactive Complex Association Lifetimes Explain Trends in Experimental Reaction Rates for Peroxy Radical Recombinations. *ACS Earth and Space Chemistry* **2022**, *6*, 2446–2452.

[83] Daub, C. D.; Skog, R.; Kurtén, T. Lifetimes of Pre-Reactive Complexes of Peroxy Radicals Revisited: Thermostat Effects, Temperature Dependence and Highly Oxygenated Molecules. *Environmental Science: Atmospheres* **2024**,

[84] Hasan, G.; Salo, V.-T.; Valiev, R. R.; Kubecka, J.; Kurtén, T. Comparing Reaction

Routes for ^{3}(RO$\cdots$OR') Intermediates Formed in Peroxy Radical Self- and Cross-Reactions. *The Journal of Physical Chemistry A* **2020**, *124*, 8305–8320.

[85] Hasan, G.; Salo, V.-T.; Golin Almeida, T.; Valiev, R. R.; Kurtén, T. Computational Investigation of Substituent Effects on the Alcohol + Carbonyl Channel of Peroxy Radical Self -and Cross-Reactions. *The Journal of Physical Chemistry A* **2023**, *127*, 1686–1696.

[86] Franzon, L. Simple Physical Model for the Estimation of Irreversible Dissociation Rates for Bimolecular Complexes. *The Journal of Physical Chemistry A* **2023**, *127*, 5956–5966.

[87] Perakylä, O.; Berndt, T.; Franzon, L.; Hasan, G.; Meder, M.; Valiev, R. R.; Daub, C. D.; Varelas, J. G.; Geiger, F. M.; Thomson, R. J.; Rissanen, M.; Kurtén, T.; Ehn, M. Large Gas-Phase Source of Esters and Other Accretion Products in the Atmosphere. *Journal of the American Chemical Society* **2023**, *145*, 7780–7790.

[88] Kenseth, C. M.; Hafeman, N. J.; Rezgui, S. P.; Chen, J.; Huang, Y.; Dalleska, N. F.; Kjaergaard, H. G.; Stoltz, B. M.; Seinfeld, J. H.; Wennberg, P. O. Particle-Phase Accretion Forms Dimer Esters in Pinene Secondary Organic Aerosol. *Science* **2023**, *382*, 787–792.

[89] Franzon, L. J.; Camredon, M.; Valorso, R.; Aumont, B.; Kurtén, T. C. Ether and Ester Formation From Peroxy Radical Recombination: A Qualitative Reaction Channel Analysis. *EGUsphere* **2024**, *2024*, 1–35.

[90] Valiev, R. R.; Hasan, G.; Salo, V.-T.; Kubečka, J.; Kurtén, T. Intersystem Crossings Drive Atmospheric Gas-Phase Dimer Formation. *The Journal of Physical Chemistry A* **2019**, *123*, 6596–6604.

[91] Jenkin, M. E.; Valorso, R.; Aumont, B.; Rickard, A. R. Estimation of Rate Coefficients and Branching Ratios for Reactions of Organic Peroxy Radicals for use in Automated Mechanism Construction. *Atmospheric Chemistry and Physics* **2019**, *19*, 7691–7717.

[92] Murphy, S. E.; Crounse, J. D.; Møller, K. H.; Rezgui, S. P.; Hafeman, N. J.; Park, J.; Kjaergaard, H. G.; Stoltz, B. M.; Wennberg, P. O. Accretion Product Formation in the Self-Reaction of Ethene-Derived Hydroxy Peroxy Radicals. *Environmental Science: Atmospheres* **2023**, *3*, 882–893.

[93] Atkinson, R.; Baulch, D. L.; Cox, R. A.; Crowley, J. N.; Hampson, R. F.; Hynes, R. G.; Jenkin, M. E.; Rossi, M. J.; Troe, J.; Subcommittee, I. Evaluated Kinetic and Photochemical Data for Atmospheric Chemistry: Volume II–Gas Phase Reactions of Organic Species. *Atmospheric Chemistry and Physics* **2006**, *6*, 3625–4055.

[94] Tyndall, G.; Wallington, T.; Ball, J. FTIR Product Study of the Reactions CH_3O_2+ CH_3O_2 and $CH_3O_2 + O_3$. *The Journal of Physical Chemistry A* **1998**, *102*, 2547–2554.

[95] Horie, O.; Crowley, J.; Moortgat, G. Methylperoxy Self-Reaction: Products and Branching Ratio Between 223 and 333 K. *Journal of Physical Chemistry* **1990**, *94*, 8198–8203.

[96] Lightfoot, P.; Lesclaux, R.; Veyret, B. Flash Photolysis Study of the Methylperoxy + Methylperoxy Reaction: Rate Constants and Branching Ratios From 248 to 573 K. *Journal of Physical Chemistry* **1990**, *94*, 700–707.

[97] Shamas, M.; Assali, M.; Zhang, C.; Tang, X.; Zhang, W.; Pillier, L.; Schoemaecker, C.; Fittschen, C. Rate Constant and Branching Ratio for the Reactions of the Ethyl Peroxy Radical With Itself and With the Ethoxy Radical. *ACS Earth and Space Chemistry* **2021**, *6*, 181–188.

[98] Noell, A.; Alconcel, L.; Robichaud, D.; Okumura, M.; Sander, S. Near-Infrared Kinetic Spectroscopy of the HO_2 and $C_2H_5O_2$ Self-Reactions and Cross Reactions. *The Journal of Physical Chemistry A* **2010**, *114*, 6983–6995.

[99] Sander, S.; Friedl, R.; Golden, D.; Kurylo, M.; Moortgat, G.; Wine, P.; Ravishankara, A.; Kolb, C.; Molina, M.; Finlayson-Pitts, B.; Huie, R.; Orkin, V.; Keller-Rudek, H. *Chemical Kinetics and Photochemical Data for Use in Atmospheric Studies Evaluation Number 15*; 2006.

[100] Adachi, H.; Basco, N. Spectra of Propylperoxy Radicals and Rate Constants for Mutual Interaction. *International Journal of Chemical Kinetics* **1982**, *14*, 1125–1138.

[101] Boyd, A.; Villenave, E.; Lesclaux, R. Structure–Reactivity Relationships for the Self-Reactions of Linear Secondary Alkylperoxy Radicals: An Experimental Investigation. *International Journal of Chemical Kinetics* **1999**, *31*, 37–46.

[102] Kirsch, L. J.; Parkes, D. A.; Waddington, D. J.; Woolley, A. Reactions of Oxygenated Radicals in the Gas Phase. Part 6.– Reactions of Isopropylperoxy and Isopropoxy Radicals. *Journal of the Chemical Society, Faraday Transactions 1: Physical Chemistry in Condensed Phases* **1979**, *75*, 2678–2687.

[103] Cowley, L. T.; Waddington, D. J.; Wooley, A. Reactions of Oxygenated Radicals in the Gas Phase. Part 9.–Self-Reactions of Isopropylperoxy Radicals. *Journal of the Chemical Society, Faraday Transactions 1: Physical Chemistry in Condensed Phases* **1982**, *78*, 2535–2546.

[104] Osborne, D. A.; Waddington, D. J. Reactions of Oxygenated Radicals in the Gas Phase. Part 14. Reactions of t-Butylperoxyl Radicals. *Journal of the Chemical Society, Perkin Transactions 2* **1984**, 1861–1867.

[105] Kirsch, L. J.; Parkes, D. A. Recombination of Tertiary Butyl Peroxy Radicals. Part 1. Product Yields Between 298 and 373 K. *Journal of the Chemical Society, Faraday Transactions 1: Physical Chemistry in Condensed Phases* **1981**, *77*, 293–307.

[106] Boyd, A. A.; Lesclaux, R. The Temperature Dependence of the Rate Coefficients for β-Hydroxyperoxy Radical Self Reactions. *International Journal of Chemical Kinetics* **1997**, *29*, 323–331.

[107] Boyd, A. A.; Villenave, E.; Lesclaux, R. Self- and Cross-Reactions of β-Hydroxyperoxy Radicals of Relevance to Tropospheric Monoterpene Oxidation: Structure–Activity Relationships for Rate Coefficients. *Atmospheric Environment* **2003**, *37*, 2751–2760.

[108] Zuraski, K.; Grieman, F. J.; Hui, A. O.; Cowen, J.; Winiberg, F. A.; Percival, C. J.; Okumura, M.; Sander, S. P. Acetonyl Peroxy and Hydroperoxy Self-and Cross-

Reactions: Temperature-Dependent Kinetic Parameters, Branching Fractions, and Chaperone Effects. *The Journal of Physical Chemistry A* **2023**, *127*, 7772–7792.

[109] Assali, M.; Fittschen, C. Self-Reaction of Acetonyl Peroxy Radicals and Their Reaction With Cl Atoms. *The Journal of Physical Chemistry A* **2022**, *126*, 4585–4597.

[110] Zuraski, K.; Hui, A. O.; Grieman, F. J.; Darby, E.; Møller, K. H.; Winiberg, F. A.; Percival, C. J.; Smarte, M. D.; Okumura, M.; Kjaergaard, H. G.; Sander, S. P. Acetonyl Peroxy and Hydro Peroxy Self- and Cross-Reactions: Kinetics, Mechanism, and Chaperone Enhancement From the Perspective of the Hydroxyl Radical Product. *The Journal of Physical Chemistry A* **2020**, *124*, 8128–8143.

[111] Bridier, I.; Veyret, B.; Lesclaux, R.; Jenkin, M. E. Flash Photolysis Study of the UV Spectrum and Kinetics of Reactions of the Acetonylperoxy Radical. *Journal of the Chemical Society, Faraday Transactions* **1993**, *89*, 2993–2997.

[112] Assali, M.; Fittschen, C. Rate Constants and Branching Ratios for the Self-Reaction of Acetyl Peroxy ($CH_3C(O)O_2^{\cdot}$) and Its Reaction with CH_3O_2. *Atmosphere* **2022**, *13*, 186.

[113] Roehl, C. M.; Bauer, D.; Moortgat, G. K. Absorption Spectrum and Kinetics of the Acetylperoxy Radical. *The Journal of Physical Chemistry* **1996**, *100*, 4038–4047.

[114] Moortgat, G.; Veyret, B.; Lesclaux, R. Absorption Spectrum and Kinetics of Reactions of the Acetylperoxy Radical. *The Journal of Physical Chemistry* **1989**, *93*, 2362–2368.

[115] Le Crâne, J.-P.; Villenave, E.; Hurley, M. D.; Wallington, T. J.; Ball, J. C. Atmospheric Chemistry of Propionaldehyde: Kinetics and Mechanisms of Reactions With OH Radicals and Cl Atoms, UV Spectrum, and Self-Reaction Kinetics of $CH_3CH_2C(O)O_2$ Radicals at 298 K. *The Journal of Physical Chemistry A* **2005**, *109*, 11837–11850.

[116] Tomas, A.; Lesclaux, R. Self-Reaction Kinetics of the $(CH_3)_2CHC(O)O_2$ and $(CH_3)_3CC(O)O_2$ Acylperoxy Radicals Between 275 and 363 K. *Chemical Physics Letters* **2000**, *319*, 521–528.

[117] Tang, Y.; Nielsen, C. J. Theoretical Study on the Formation and Photolysis of Nitrosamines (CH_3CH_2NHNO and $(CH_3CH_2)_2NNO$) Under Atmospheric Conditions. *The Journal of Physical Chemistry A* **2013**, *117*, 126–132.

[118] Melius, C.; Binkley, J. Energetics of the Reaction Pathways for $NH_2 + NO \rightarrow$ Products and $NH + NO \rightarrow$ Products. Symposium (International) on Combustion. 1985; pp 575–583.

[119] Atakan, B.; Jacobs, A.; Wahl, M.; Weller, R.; Wolfrum, J. Kinetic Measurements and Product Branching Ratio for the Reaction NH_2 + NO at 294–1027 K. *Chemical Physics Letters* **1989**, *155*, 609–613.

[120] Mebel, A.; Hsu, C.-C.; Lin, M.-C.; Morokuma, K. An Ab Initio Molecular Orbital Study of Potential Energy Surface of the NH_2 + NO_2 reaction. *The Journal of Chemical Physics* **1995**, *103*, 5640–5649.

[121] Lindholm, N.; Hershberger, J. F. Product Branching Ratios of the NH_2 (X^2B_1) + NO_2 Reaction. *The Journal of Physical Chemistry A* **1997**, *101*, 4991–4995.

[122] Peiró-García, J.; Nebot-Gil, I.; Merchán, M. An Ab Initio Study on the Mechanism of the Atmospheric Reaction $NH_2 + O_3 \longrightarrow H_2NO + O_2$. *ChemPhysChem* **2003**, *4*, 366–372.

[123] Yonehara, T.; Hanasaki, K.; Takatsuka, K. Fundamental Approaches to Nonadiabaticity: Toward a Chemical Theory Beyond the Born–Oppenheimer Paradigm. *Chemical Reviews* **2012**, *112*, 499–542.

[124] Slater, J. C. The Theory of Complex Spectra. *Physical Review* **1929**, *34*, 1293–1322.

[125] Hartree, D. R. The Wave Mechanics of an Atom With a Non-Coulomb Central Field. Part II. Some Results and Discussion. Mathematical Proceedings of the Cambridge Philosophical Society. 1928; pp 111–132.

[126] Slater, J. C. Note on Hartree's Method. *Physical Review* **1930**, *35*, 210.

[127] Fock, V. Näherungsmethode zur Lösung des Quantenmechanischen Mehrkörperproblems. *Zeitschrift für Physik* **1930**, *61*, 126–148.

[128] Hartree, D. R.; Hartree, W. Self-Consistent Field, With Exchange, for Beryllium. *Proceedings of the Royal Society of London. Series A-Mathematical and Physical Sciences* **1935**, *150*, 9–33.

[129] Roothaan, C. C. J. New Developments in Molecular Orbital Theory. *Reviews of Modern Physics* **1951**, *23*, 69–89.

[130] Hall, G. G. The Molecular Orbital Theory of Chemical Valency VIII. A Method of Calculating Ionization Potentials. *Proceedings of the Royal Society of London. Series A. Mathematical and Physical Sciences* **1951**, *205*, 541–552.

[131] Wigner, E. On the Interaction of Electrons in Metals. *Physical Review* **1934**, *46*, 1002–1011.

[132] Löwdin, P.-O. Quantum Theory of Many-Particle Systems. I. Physical Interpretations by Means of Density Matrices, Natural Spin-Orbitals, and Convergence Problems in the Method of Configurational Interaction. *Physical Review* **1955**, *97*, 1474–1489.

[133] Craig, D. P. Configurational Interaction in Molecular Orbital Theory. A Higher Approximation in the Non-Empirical Method. *Proceedings of the Royal Society of London. Series A. Mathematical and Physical Sciences* **1950**, *200*, 474–486.

[134] Hinze, J. An Overview of Computational Methods for Large Molecules. *Advances in Chemical Physics* **1974**, *26*, 213–263.

[135] Pople, J. A.; Seeger, R.; Krishnan, R. Variational Configuration Interaction Methods and Comparison With Perturbation Theory. *International Journal of Quantum Chemistry* **1977**, *12*, 149–163.

[136] Levine, B. G.; Durden, A. S.; Esch, M. P.; Liang, F.; Shu, Y. CAS Without SCF–Why to Use CASCI and Where to Get the Orbitals. *The Journal of Chemical Physics* **2021**, *154*, 090902.

[137] Sinanoğlu, O. Many-Electron Theory of Atoms and Molecules. I. Shells, Electron Pairs vs Many-Electron Correlations. *The Journal of Chemical Physics* **1962**, *36*, 706–717.

[138] Čížek, J. On the Correlation Problem in Atomic and Molecular Systems. Calculation of Wavefunction Components in Ursell-Type Expansion Using Quantum-Field Theoretical Methods. *The Journal of Chemical Physics* **1966**, *45*, 4256–4266.

[139] Paldus, J.; Čížek, J.; Shavitt, I. Correlation Problems in Atomic and Molecular Systems. IV. Extended Coupled-Pair Many-Electron Theory and Its Application to the BH_3 Molecule. *Physical Review A* **1972**, *5*, 50–67.

[140] Noga, J.; Bartlett, R. J. The Full CCSDT Model for Molecular Electronic Structure. *The Journal of Chemical Physics* **1987**, *86*, 7041–7050.

[141] Raghavachari, K.; Trucks, G. W.; Pople, J. A.; Head-Gordon, M. A Fifth-Order Perturbation Comparison of Electron Correlation Theories. *Chemical Physics Letters* **1989**, *157*, 479–483.

[142] Goldstone, J. Derivation of the Brueckner Many-Body Theory. *Proceedings of the Royal Society of London. Series A. Mathematical and Physical Sciences* **1957**, *239*, 267–279.

[143] Møller, C.; Plesset, M. S. Note on an Approximation Treatment for Many-Electron Systems. *Physical Review* **1934**, *46*, 618–622.

[144] Olsen, J.; Christiansen, O.; Koch, H.; Jørgensen, P. Surprising Cases of Divergent Behavior in Møller–Plesset Perturbation Theory. *The Journal of Chemical Physics* **1996**, *105*, 5082–5090.

[145] Docken, K. K.; Hinze, J. LiH Potential Curves and Wavefunctions for X $^1\Sigma^+$, A $^1\Sigma^+$, B $^1\Pi$, $^3\Sigma^+$, and $^3\Pi$. *The Journal of Chemical Physics* **1972**, *57*, 4928–4936.

[146] Hinze, J. MC-SCF. I. The Multi-Configuration Self-Consistent-Field Method. *The Journal of Chemical Physics* **1973**, *59*, 6424–6432.

[147] Olsen, J.; Yeager, D. L.; Jørgensen, P. Optimization and Characterization of a Multiconfigurational Self-Consistent Field (MCSCF) State. *Advances in Chemical Physics* **1983**, 1–176.

[148] Dalgaard, E.; Jo/rgensen, P. Optimization of Orbitals for Multiconfigurational Reference States. *The Journal of Chemical Physics* **1978**, *69*, 3833–3844.

[149] Siegbahn, P.; Heiberg, A.; Roos, B.; Levy, B. A Comparison of the Super-CI and the Newton-Raphson Scheme in the Complete Active Space SCF Method. *Physica Scripta* **1980**, *21*, 323–327.

[150] Werner, H.-J.; Meyer, W. A Quadratically Convergent MCSCF Method for the Simultaneous Optimization of Several States. *The Journal of Chemical Physics* **1981**, *74*, 5794–5801.

[151] Roos, B. O.; Taylor, P. R.; Siegbahn, P. E. A Complete Active Space SCF Method (CASSCF) Using a Density Matrix Formulated Super-CI Approach. *Chemical Physics* **1980**, *48*, 157–173.

[152] Roos, B. O.; others The Complete Active Space Self-Consistent Field Method and its Applications in Electronic Structure Calculations. *Advances in Chemical Physics* **2007**, *69*, 399–445.

[153] Olsen, J. The CASSCF Method: A Perspective and Commentary. *International Journal of Quantum Chemistry* **2011**, *111*, 3267–3272.

[154] Paldus, J. Group Theoretical Approach to the Configuration Interaction and Perturbation Theory Calculations for Atomic and Molecular Systems. *The Journal of Chemical Physics* **1974**, *61*, 5321–5330.

[155] Malmqvist, P. Å.; Rendell, A.; Roos, B. O. The Restricted Active Space Self-Consistent-Field Method, Implemented With a Split Graph Unitary Group Approach. *Journal of Physical Chemistry* **1990**, *94*, 5477–5482.

[156] Ma, D.; Li Manni, G.; Gagliardi, L. The Generalized Active Space Concept in Multiconfigurational Self-Consistent Field Methods. *The Journal of Chemical Physics* **2011**, *135*, 044128.

[157] Tubman, N. M.; Lee, J.; Takeshita, T. Y.; Head-Gordon, M.; Whaley, K. B. A Deterministic Alternative to the Full Configuration Interaction Quantum Monte Carlo Method. *The Journal of Chemical Physics* **2016**, *145*, 044112.

[158] Levine, D. S.; Hait, D.; Tubman, N. M.; Lehtola, S.; Whaley, K. B.; Head-Gordon, M. CASSCF With Extremely Large Active Spaces Using the Adaptive

Sampling Configuration Interaction Method. *Journal of Chemical Theory and Computation* **2020**, *16*, 2340–2354.

[159] Roos, B. O.; Linse, P.; Siegbahn, P. E.; Blomberg, M. R. A Simple Method for the Evaluation of the Second-Order-Perturbation Energy From External Double-Excitations With a CASSCF Reference Wavefunction. *Chemical Physics* **1982**, *66*, 197–207.

[160] Andersson, K.; Malmqvist, P.-Å.; Roos, B. O. Second-Order Perturbation Theory With a Complete Active Space Self-Consistent Field Reference Function. *The Journal of Chemical Physics* **1992**, *96*, 1218–1226.

[161] Ghigo, G.; Roos, B. O.; Malmqvist, P.-Å. A Modified Definition of the Zeroth-Order Hamiltonian in Multiconfigurational Perturbation Theory (CASPT2). *Chemical Physics Letters* **2004**, *396*, 142–149.

[162] Angeli, C.; Cimiraglia, R.; Evangelisti, S.; Leininger, T.; Malrieu, J.-P. Introduction of N-Electron Valence States for Multireference Perturbation Theory. *The Journal of Chemical Physics* **2001**, *114*, 10252–10264.

[163] Angeli, C.; Cimiraglia, R.; Malrieu, J.-P. N-Electron Valence State Perturbation Theory: A Fast Implementation of the Strongly Contracted Variant. *Chemical Physics Letters* **2001**, *350*, 297–305.

[164] Angeli, C.; Cimiraglia, R.; Malrieu, J.-P. N-Electron Valence State Perturbation Theory: A Spinless Formulation and an Efficient Implementation of the Strongly Contracted and of the Partially Contracted Variants. *The Journal of Chemical Physics* **2002**, *117*, 9138–9153.

[165] Granovsky, A. A. Extended Multi-Configuration Quasi-Degenerate Perturbation Theory: The New Approach to Multi-State Multi-Reference Perturbation Theory. *The Journal of Chemical Physics* **2011**, *134*, 214113.

[166] Siegbahn, P. E. Direct Configuration Interaction With a Reference State Composed of Many Reference Configurations. *International Journal of Quantum Chemistry* **1980**, *18*, 1229–1242.

[167] Werner, H.-J.; Reinsch, E.-A. The Self-Consistent Electron Pairs Method for Multiconfiguration Reference State Functions. *The Journal of Chemical Physics* **1982**, *76*, 3144–3156.

[168] Werner, H.-J.; Knowles, P. J. An Efficient Internally Contracted Multiconfiguration–Reference Configuration Interaction Method. *The Journal of Chemical Physics* **1988**, *89*, 5803–5814.

[169] Hirao, K. Multireference Møller–Plesset method. *Chemical Physics Letters* **1992**, *190*, 374–380.

[170] McLean, A.; Liu, B. Classification of Configurations and the Determination of Interacting and Noninteracting Spaces in Configuration Interaction. *The Journal of Chemical Physics* **1973**, *58*, 1066–1078.

[171] Meyer, W. *Methods of Electronic Structure Theory*; Springer, 1977; pp 413–446.

[172] Sivalingam, K.; Krupicka, M.; Auer, A. A.; Neese, F. Comparison of Fully Internally and Strongly Contracted Multireference Configuration Interaction Procedures. *The Journal of Chemical Physics* **2016**, *145*, 054104.

[173] Celani, P.; Werner, H.-J. Multireference Perturbation Theory for Large Restricted and Selected Active Space Reference Wave Functions. *The Journal of Chemical Physics* **2000**, *112*, 5546–5557.

[174] Rintelman, J. M.; Adamovic, I.; Varganov, S.; Gordon, M. S. Multireference Second-Order Perturbation Theory: How Size Consistent is "Almost Size Consistent". *The Journal of Chemical Physics* **2005**, *122*, 044105.

[175] Finley, J.; Malmqvist, P.-Å.; Roos, B. O.; Serrano-Andrés, L. The Multi-State CASPT2 Method. *Chemical Physics Letters* **1998**, *288*, 299–306.

[176] Angeli, C.; Borini, S.; Cestari, M.; Cimiraglia, R. A Quasidegenerate Formulation of the Second Order N-Electron Valence State Perturbation Theory Approach. *The Journal of Chemical Physics* **2004**, *121*, 4043–4049.

[177] Roos, B. O.; Andersson, K.; Fülscher, M. P.; Malmqvist, P.-Å.; Serrano-Andrés, L.; Pierloot, K.; Merchán, M. Multiconfigurational Perturbation Theory: Applications

in Electronic Spectroscopy. *Advances in Chemical Physics: New Methods in Computational Quantum Mechanics* **1996**, *93*, 219–331.

[178] Battaglia, S.; Fransén, L.; Fdez. Galván, I.; Lindh, R. Regularized CASPT2: An Intruder-State-Free Approach. *Journal of Chemical Theory and Computation* **2022**, *18*, 4814–4825.

[179] Roos, B. O.; Andersson, K. Multiconfigurational Perturbation Theory With Level Shift—The Cr_2 Potential Revisited. *Chemical Physics Letters* **1995**, *245*, 215–223.

[180] Forsberg, N.; Malmqvist, P.-Å. Multiconfiguration Perturbation Theory With Imaginary Level Shift. *Chemical Physics Letters* **1997**, *274*, 196–204.

[181] Andersson, K.; Roos, B. O. Multiconfigurational Second-Order Perturbation Theory: A Test of Geometries and Binding Energies. *International Journal of Quantum Chemistry* **1993**, *45*, 591–607.

[182] Day, O. W.; Smith, D. W.; Garrod, C. A Generalization of the Hartree-Fock One-Particle Potential. *International Journal of Quantum Chemistry* **1974**, *8*, 501–509.

[183] Morrell, M. M.; Parr, R. G.; Levy, M. Calculation of Ionization Potentials From Density Matrices and Natural Functions, and the Long-Range Behavior of Natural Orbitals and Electron Density. *The Journal of Chemical Physics* **1975**, *62*, 549–554.

[184] Zobel, J. P.; Nogueira, J. J.; González, L. The IPEA Dilemma in CASPT2. *Chemical Science* **2017**, *8*, 1482–1499.

[185] Dyall, K. G. The Choice of a Zeroth-Order Hamiltonian for Second-Order Perturbation Theory With a Complete Active Space Self-Consistent-Field Reference Function. *The Journal of Chemical Physics* **1995**, *102*, 4909–4918.

[186] Kollmar, C.; Sivalingam, K.; Neese, F. An Alternative Choice of the Zeroth-Order Hamiltonian in CASPT2 Theory. *The Journal of Chemical Physics* **2020**, *152*.

[187] Sarkar, R.; Loos, P.-F.; Boggio-Pasqua, M.; Jacquemin, D. Assessing the Performances of CASPT2 and NEVPT2 for Vertical Excitation Energies. *Journal of Chemical Theory and Computation* **2022**, *18*, 2418–2436.

[188] Hohenberg, P.; Kohn, W. Inhomogeneous Electron Gas. *Physical Review* **1964**, *136*, B864–B871.

[189] Kohn, W.; Sham, L. J. Self-Consistent Equations Including Exchange and Correlation Effects. *Physical Review* **1965**, *140*, A1133–A1138.

[190] Langreth, D. C.; Mehl, M. Beyond the Local-Density Approximation in Calculations of Ground-State Electronic Properties. *Physical Review B* **1983**, *28*, 1809.

[191] Becke, A. D. Density-Functional Exchange-Energy Approximation With Correct Asymptotic Behavior. *Physical Review A* **1988**, *38*, 3098.

[192] Perdew, J. P. Accurate Density Functional for the Energy: Real-Space Cutoff of the Gradient Expansion for the Exchange Hole. *Physical Review Letters* **1985**, *55*, 1665–1668.

[193] Perdew, J. P.; Tao, J.; Staroverov, V. N.; Scuseria, G. E. Meta-Generalized Gradient Approximation: Explanation of a Realistic Nonempirical Density Functional. *The Journal of Chemical Physics* **2004**, *120*, 6898–6911.

[194] Becke, A. Density-Functional Thermochemistry. III. The Role of Exact Exchange. *The Journal of Chemical Physics* **1993**, *98*, 5648–5652.

[195] Csonka, G. I.; Perdew, J. P.; Ruzsinszky, A. Global Hybrid Functionals: A Look at the Engine Under the Hood. *Journal of Chemical Theory and Computation* **2010**, *6*, 3688–3703.

[196] Gerber, I. C.; Angyán, J. G. Hybrid Functional With Separated Range. *Chemical Physics Letters* **2005**, *415*, 100–105.

[197] Grimme, S.; Antony, J.; Ehrlich, S.; Krieg, H. A Consistent and Accurate Ab Initio Parametrization of Density Functional Dispersion Correction (DFT-D) for the 94 Elements H-Pu. *The Journal of Chemical Physics* **2010**, *132*, 154104.

[198] Grimme, S. Density Functional Theory With London Dispersion Corrections. *Wiley Interdisciplinary Reviews: Computational Molecular Science* **2011**, *1*, 211–228.

[199] Gagliardi, L.; Truhlar, D. G.; Li Manni, G.; Carlson, R. K.; Hoyer, C. E.; Bao, J. L. Multiconfiguration Pair-Density Functional Theory: A New Way to Treat Strongly Correlated Systems. *Accounts of Chemical Research* **2017**, *50*, 66–73.

[200] Becke, A. D. Density-Functional Thermochemistry. I. The Effect of the Exchange-Only Gradient Correction. *The Journal of Chemical Physics* **1992**, *96*, 2155–2160.

[201] Lee, C.; Yang, W.; Parr, R. G. Development of the Colle-Salvetti Correlation-Energy Formula Into a Functional of the Electron Density. *Physical Review B* **1988**, *37*, 785–789.

[202] Zhao, Y.; Truhlar, D. G. The M06 Suite of Density Functionals for Main Group Thermochemistry, Thermochemical Kinetics, Noncovalent Interactions, Excited States, and Transition Elements: Two New Functionals and Systematic Testing of Four M06-class Functionals and 12 Other Functionals. *Theoretical Chemistry Accounts* **2008**, *120*, 215–241.

[203] Chai, J.-D.; Head-Gordon, M. Long-Range Corrected Hybrid Density Functionals With Damped Atom-Atom Dispersion Corrections. *Physical Chemistry Chemical Physics* **2008**, *10*, 6615–6620.

[204] Eyring, H. The Activated Complex in Chemical Reactions. *The Journal of Chemical Physics* **1935**, *3*, 107–115.

[205] Evans, M. G.; Polanyi, M. Some Applications of the Transition State Method to the Calculation of Reaction Velocities, Especially in Solution. *Transactions of the Faraday Society* **1935**, *31*, 875–894.

[206] Laidler, K. J.; King, M. C. The Development of Transition-State Theory. *The Journal of Physical Chemistry* **1983**, *87*, 2657–2664.

[207] Brown, R. L. A Method of Calculating Tunneling Corrections for Eckart Potential Barriers. *Journal of Research of the National Bureau of Standards* **1981**, *86*, 357–359.

[208] Truhlar, D. G.; Garrett, B. C. Variational Transition-State Theory. *Accounts of Chemical Research* **1980**, *13*, 440–448.

[209] Georgievskii, Y.; Klippenstein, S. J. Variable Reaction Coordinate Transition State Theory: Analytic Results and Application to the $C_2H_3 + H \longrightarrow C_2H_4$ Reaction. *The Journal of Chemical Physics* **2003**, *118*, 5442–5455.

[210] Bao, J. L.; Truhlar, D. G. Variational Transition State Theory: Theoretical Framework and Recent Developments. *Chemical Society Reviews* **2017**, *46*, 7548–7596.

[211] Janssen, C. L.; Nielsen, I. M. New Diagnostics for Coupled-Cluster and Møller–Plesset Perturbation Theory. *Chemical Physics Letters* **1998**, *290*, 423–430.

[212] Lee, T. J. Comparison of the T_1 and D_1 Diagnostics for Electronic Structure Theory: A New Definition for the Open-Shell D_1 Diagnostic. *Chemical Physics Letters* **2003**, *372*, 362–367.

[213] Karton, A.; Rabinovich, E.; Martin, J. M.; Ruscic, B. W4 Theory for Computational Thermochemistry: In Pursuit of Confident sub-kJ/mol Predictions. *The Journal of Chemical Physics* **2006**, *125*, 144108.

[214] Nielsen, I. M. B.; Janssen, C. L. Double-Substitution-Based Diagnostics for Coupled-Cluster and Møller–Plesset Perturbation Theory. *Chemical Physics Letters* **1999**, *310*, 568–576.

[215] Bauer, C. A.; Hansen, A.; Grimme, S. The Fractional Occupation Number Weighted Density as a Versatile Analysis Tool for Molecules With a Complicated Electronic Structure. *Chemistry–A European Journal* **2017**, *23*, 6150–6164.

[216] Mermin, N. D. Thermal Properties of the Inhomogeneous Electron Gas. *Physical Review* **1965**, *137*, A1441–A1443.

[217] Veryazov, V.; Malmqvist, P. Å.; Roos, B. O. How to Select Active Space for Multiconfigurational Quantum Chemistry? *International Journal of Quantum Chemistry* **2011**, *111*, 3329–3338.

[218] Battaglia, S.; Galván, I. F.; Lindh, R. *Theoretical and Computational Photochemistry*; Elsevier, 2023; pp 135–162.

[219] Dibble, T. S. Failures and Limitations of Quantum Chemistry for Two Key Problems in the Atmospheric Chemistry of Peroxy Radicals. *Atmospheric Environment* **2008**, *42*, 5837–5848.

[220] Granovsky, A. A. Firefly version 8.20. `http://classic.chem.msu.su/gran/gamess/index.html`.

[221] Frisch, M. J. et al. Gaussian16 Revision C.01. 2016; Gaussian Inc. Wallingford CT.

[222] Werner, H.-J.; Knowles, P. J.; Knizia, G.; Manby, F. R.; Schütz, M. Molpro: A General-Purpose Quantum Chemistry Program Package. *Wiley Interdisciplinary Reviews: Computational Molecular Science* **2012**, *2*, 242–253.

[223] Werner, H.-J. et al. Molpro version 2019.2, A Package of Ab Initio Programs. `https://www.molpro.net/`.

[224] Neese, F. The ORCA Program System. *Wiley Interdisciplinary Reviews: Computational Molecular Science* **2012**, *2*, 73–78.

[225] Neese, F. Software Update: The ORCA Program System, Version 4.0. *Wiley Interdisciplinary Reviews: Computational Molecular Science* **2018**, *8*, e1327.

[226] Chan, B.; Radom, L. W2X and W3X-L: Cost-Effective Approximations to W2 and W4 With kJ mol^{-1} Accuracy. *Journal of Chemical Theory and Computation* **2015**, *11*, 2109–2119.

[227] Neese, F. Software Update: The ORCA Program System—Version 5.0. *Wiley Interdisciplinary Reviews: Computational Molecular Science* **2022**, *12*, e1606.

[228] Werner, H.-J. et al. MOLPRO, 2022.3 , A Package of Ab Initio Programs. `https://www.molpro.net/`, (accessed Sep 20, 2024).

[229] Werner, H.-J. et al. The Molpro Quantum Chemistry Package. *The Journal of Chemical Physics* **2020**, *152*, 144107.

[230] Kállay, M. et al. The MRCC Program System: Accurate Quantum Chemistry From Water to Proteins. *The Journal of Chemical Physics* **2020**, *152*, 074107.